COARSENINO OF CEMETITE PARTICLES IN Fe–0.74 C–0.37 Si ALLOY

A Thesis Submitted
In Partial Fulfilment of the Requirements
for the Degree of
MASTER OF TECHNOLOGY

By
A. SARANGI

to the

INTERDEPARTMENTAL PROGRAMME IN MATERIAL SCIENCE
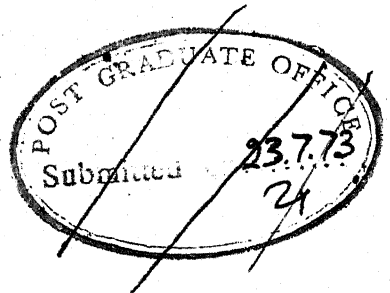INDIAN INSTITUTE OF TECHNOLOGY KANPUR
JULY 1973

CERTIFICATE

This is to certify that this work on

"Coarsening of Cementite Particles in Fe - 0.74%C

- 0.37%Si Alloy" has been carried out by

Mr. A. Sarangi, under my supervision and that this

work has not been submitted elsewhere for a degree.

Dr. A.K. JENA

Associate Professor
Department of Metallurgical Engineering
Indian Institute of Technology
Kanpur.

ACKNOWLEDGEMENT

I am very much grateful to Dr. A.K. Jena who introduced me in to this new field of 'Kinetics of Coarsening'. I am very thankful to him for his valuable suggestions and new ideas which he offered to me on various instances.

I am also thankful to Mr. S.P. Bhat and Mr. K.P. Mukherjee for their valuable assistance from time to time.

Last but not least, I thank Mr. R.N. Srivastava for typing this thesis.

A. Sarangi

ABSTRACT

Experiments were conducted to study the effect of 0.37% silicon on the coarsening kinetics of cementite in a 0.74%C steel at 630°C, 660°C, 690°C and 710°C. Coarsening was found to be diffusion controlled. Particle size distribution did not reach a steady state. The coarsening rates of individual particles were calculated from particle size distribution. The activation energy for the coarsening process was 51.03 Kcal/gm-atom. Silicon also decreases the α-Fe/Fe$_3$C interfacial energy. The activation energy during coarsening was found to be between those for carbon diffusion and iron diffusion in ferrite.

CONTENTS

CHAPTER 1

INTRODUCTION

A system of particles of a phase dispersed in a matrix has a tendency to reduce its total surface free energy. Because the surface to volume ratio of smaller particles is larger than that of larger particles, the average particle size increases with time. This phenomenon is called coarsening and is seen in many alloys of interest. Our understanding of the coarsening kinetics has been considerably enhanced by the theoretical and experimental investigations carried out in the last decade. However, much more work has to be done so that clear ideas about coarsening mechanisms may be developed.

A thorough understanding of the coarsening kinetics in steel has practical as well as theoretical importance. The loss of strength of steel during tempering is due to the coarsening of carbides. The sensitivity of mechanical properties to temperature and rate of spheroidisation are controlled by the coarsening mechanism. From the theoretical stand point, the understanding of coarsening mechanism in steels may help us to understand the coarsening behaviour in other systems. Also data on surface energy obtained from coarsening studies are useful in the study of nucleation and growth.

In the work reported here, kinetics of coarsening of cementite in Fe - 0.74% C - 0.37% Si alloy have been investigated as a function of time and temperature.

CHAPTER 2

LITERATURE REVIEW

2.1 Theory of Coarsening:

In a supersaturated solid solution diffusion effects can cause precipitation of a second phase. Three stages of this process can be distinguished. In the first stage, concentration and structural fluctuations produce nuclei of the new phase. In the second stage, growth of nuclei occurs directly from the super saturated medium and the concentration of the solute in the matrix decreases with time. In the third stage, larger particles grow at the expense of the smaller particles. This stage is called 'Coarsening' or 'Ostwald ripening'. The driving force for the process is the tendency of the system to decrease its over all free energy by reducing the total interfacial area.

Consider a precipitate of radius 'r' in the matrix. The pressure difference[1] across the surface of the sphere can be written as

$$P_{pt} - P_{ext} = \frac{2\gamma}{r}$$

$$P_{pt} = P_{ext} + \frac{2\gamma}{r} \qquad \dots (1)$$

where, P_{pt} = Pressure inside the precipitate of radius 'r'.

P_{ext} = Pressure in the matrix.

γ = Surface energy of precipitate.

The above equation is derived assuming that a single average value of γ can be used for the various parts of the surface and that

the shape of the precipitate does not change when the size
changes. If the precipitate consists of only one species and
surface energy and density of precipitate are independent of its
size, than at constant temperature we can write

$$d\mu_r = V_m \, dP \qquad \qquad \ldots \ldots (2)$$

where, μ_r = Chemical potential of precipitate of size 'r'.

V_m = Molar volume of precipitate.

Assuming the compressibility of the solid to be small and using
equation (1) and (2) it can be shown that

$$\mu_r - \mu_\infty = \frac{2\gamma V_m}{r} \qquad \qquad \ldots \ldots (3)$$

where, μ_∞ = Chemical potential of particle of infinite size.

It is seen from equation (3) that the chemical potential
of small particle is larger than that of a large particle. Hence,
it follows that concentration of solute in the matrix in equilli-
brium with smaller particle is larger than for a larger one.

Assuming the matrix to be dilute solution where the
activity of the solute is directly proportional to its concentration,
the precipitates to be incoherent and the precipitate interface
is free from preferential solute adsorption, the following equation
called Gibb's-Thomas equation can be derived

$$C_r = C_\infty \exp \left(\frac{2\gamma V_m}{rRT} \right) \qquad \qquad \ldots \ldots (4)$$

where, C_r = Concentration of solute in the matrix in equillibrium
with particle of radius r.

C_∞ = Concentration of solute in the matrix in equillibrium
with particle of infinite size.

R = Gas constant.

T = Absolute temperature.

Thus in a system consisting of mixed particle sizes concentration gradient exist which leads to the growth of larger particles at the expense of smaller ones.

The steps involved in any coarsening process are as follows:

(1) Dissolution of solute from smaller particles in the matrix i.e., transfer of atoms across the particle-matrix interface.

(2) Diffusion of solute in the matrix from regions near smaller particles to regions near larger one.

(3) Deposition of solute on the larger particles, i.e. transfer of solute atoms across the interface between the matrix and the larger particle.

If the rate of transfer of solute atoms across the interface is much faster than the rate of diffusion of solute in the matrix, the coarsening process is called <u>diffusion controlled</u>. When the rate of matrix diffusion is much faster than the transfer of solute across the interface, the process is called <u>interface controlled coarsening</u>. A third probability arises when most of the particles are situated near the grain boundaries of the matrix and diffusion occurs along the grain boundaries. In such a case the process is termed <u>grain boundary diffusion controlled coarsening</u>. At higher temperatures lattice diffusion is expected to be more important where as at lower temperatures grain boundary diffusion may become more prominent.

2.2 Theory of diffusion controlled coarsening:

Following assumptions are made to derive an expression for the growth rate of a particle[2].

(1) Diffusion of solute in the matrix is controlling the rate

(2) Concentration gradients are independent of time.

(3) Volume fraction of precipitate is very small and the inter particle distance is large.

(4) Volume fraction of particles remain constant.

(5) Local equillibrium exist at the particle matrix interface.

(6) Gibbs-Thomas equation is applicable.

(7) Precipitates have spherical shape and the solute concentration around each particle is spherically symmetrical.

(8) Precipitate consist of only one species.

(9) Diffusion coefficient of solute is independent of concentration of solute.

In the steady state, the rate of change of volume of a precipitate equated to the flux of solute gives,

$$4 \pi r^2 \frac{dr}{dt} = D \, 4 \pi R^2 \frac{dC'}{dR} \qquad \ldots \ldots (5)$$

where, D = Diffusion coefficient of the solute

C' = Concentration of solute in the matrix at a distance R from the precipitate.

At any given time integrating equation (5) from $R = r$ to $R = \infty$ i.e, $C' = C_r$ to $C' = C_\infty$ we obtain

$$\frac{dr}{dt} = -\frac{D}{r} (C_r - C_\infty) \qquad \ldots \ldots (6)$$

where, C_∞ = Concentration of solute in the matrix at a large distance from the particle.

If $2\gamma V_m \ll rRT$ the Gibbs-Thomas equation can be written as

$$C_r = C_e \left[1 + \frac{2V_m \gamma}{rRT} \right] \quad \quad \cdots \cdots (7)$$

Since the volume fraction of the precipitate is constant, in a system of n highly dispersed particles

$$\sum_{i=1}^{n} \frac{dV_i}{dt} = 0 \quad \quad \cdots \cdots (8)$$

Using equation (6), (7) and (8) and substituting $\bar{r}$, the arithmetic average radius for $\sum_{i=1}^{n} r_i/n$ we get

$$\frac{dr}{dt} = \frac{2C_e \gamma V_m D}{rRT} \left(\frac{1}{\bar{r}} - \frac{1}{r} \right) \quad \quad \cdots \cdots (9)$$

Theoretically, coarsening does not occur in a system of particles of the same size. But in practice small thermal or other fluctuations will give rise to concentration gradients and will effect coarsening of some particles. Thus with increasing time, this limited size distribution of particles will become wider. However, the spread will be limited. It can be shown that the growth rate is maximum at $r = 2\bar{r}$. The particles of radius greater than $2\bar{r}$ will grow at a rate smaller than the rate of growth of smaller particles. It follows that particle of radius much greater than $2\bar{r}$ can not exist in the system. It implies that a relatively sharp cut off in the particle size distribution should exist. It may be noted that particles of size $\bar{r}$ neither grow nor shrink. This implies that particles of size greater than $\bar{r}$, grow at the expense of particles of size less than $\bar{r}$. A schematic plot of this is shown in fig. 1.

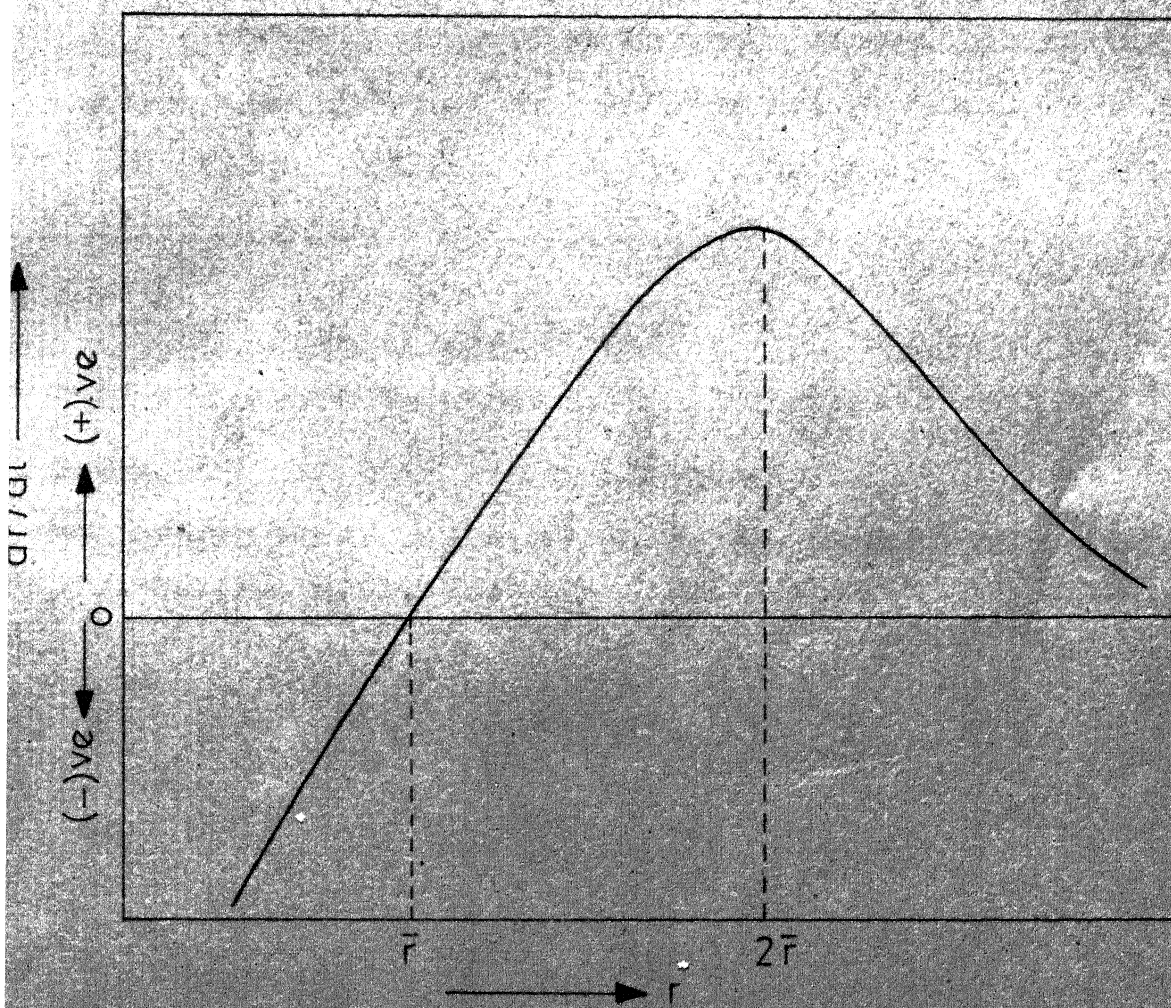An expression for $\bar{r}$ can be derived by putting $r = 2\bar{r}$ in

Fig. 1   Schematic plot of dr/dt vs. r for
diffusion controlled coarsening.

equation (9) and integrating. We get

$$\bar{r}^3 - \bar{r}_0^3 = (\frac{3 \gamma C_e V_m D}{RT})t \qquad \ldots \ldots (10)$$

where, $\bar{r}_0$ = Average radius when coarsening just begins.

A rigorous analysis of diffusion controlled coarsening has been done by Wagner[3] and Liftshiz and Slyozov[4]. This is known as WLS theory. Let $f(r, t)$ be the particle size distribution function such that

$$N = \int_0^\infty f(r, t)\, dr \qquad \ldots \ldots (11)$$

where, N = Number of grains per unit volume.

The unknown function $f(r, t)$ can be determined from the equation of continuity in r space,

$$\frac{\partial f}{\partial t} + \frac{\partial (f, \frac{dr}{dt})}{\partial r} = 0 \qquad \ldots \ldots (12)$$

and the equation for the conservation of matter is

$$Q_0 = C_t + \int_0^\infty \frac{4}{3} r^3 f(r, t)\, dr \qquad \ldots \ldots (13)$$

where, Q_0 = Total amount of solute in the alloy in cm^3/cm^3.

C_t = Average concentration of matrix at any instant t.

Using equation (6), (7) and (13) Wagner and Liftshiz and Slyozov solved the differential equation and showed that the particle size distribution reaches a pseudostatic form. The theory arrives at the following results, where $P = r/\bar{r}$

molar volume of cementite with the formula Fe_3C and C_e is the concentration of carbon in the matrix in equilibrium with precipitate of infinite size.

Moreen[5] has shown that cumulative size distribution function can be approximated by the following expression

$$C(P) = AP^4 \qquad\qquad \dots\dots (17)$$

where

$$C(P) = \int_0^P P^2\, h_1(P)\, dP$$

and   A = Constant.

Markworth[6] has shown the following expression for the variation of size of individual particles with time

$$\left(\frac{3-2P_0}{3-2P}\right)^{5/3} \left(\frac{3+P_0}{3+P}\right)^{4/3} \exp \frac{6(P_0 - P)}{(3-2P_0)} = \frac{t}{t_0} \qquad \dots (18)$$

where,

$$P_0 = \left(\frac{P}{P}\right)_{t=t_0}$$

t_0 = The time when coarsening just begins.

Exnel and Lukas[7] tried to verify WLS distribution of the particle. Ardell[8] studied the cumulative particle size distribution.

In the WLS theory it is assumed that the volume fraction of precipitate is very small and the motion of interface is not obstructed by the solvent atoms, i.e. matrix atoms move much faster than solute atoms. This is valid only in liquid fluid matrix. Hence diffusion coefficient in equation (15) is not merely diffusion coefficient of solute but some effective diffusion coefficient.

Le, Blakely and Feingold[9] have developed a coupled diffusion analysis which considers composition constraint as well as volume constraint. In a coarsening process when the particle consist of more than one component, exchange of matter between the particles will in general be subjected to a composition constraint, requiring that the diffusive fluxes of the components of the dispersed phase be coupled in order to prevent change of composition of any particle. This composition constraint has the form

$$\frac{J_A}{J_B} = \frac{a}{b} \qquad \ldots \ldots (19)$$

where the precipitate has the formula $A_a B_b$ and the matrix consist of metal A.

The volume constraint arises from the fact that it is required to remove a volume of matrix material around a growing particle equal to the volume by which that particle has grown in order to avoid any elastic strain energy in the system. This may be expressed as

$$J_1 V_1 + J_2 V_2 = 0 \qquad \ldots \ldots (20)$$

where J_1 and J_2 are flux of solute and solvent respectively. V_1 is the volume made available by the transfer of one gm. atom of solute from the particle to the matrix and V_2 is the atomic volume of solvent in the matrix Le et al[9] have derived effective diffusion coefficient for such cases. The expression is given below

$$D_{eff} = \frac{C_2 D_1 D_2 V_2 (V_2 + C_1/C_2 \times V_1)}{C_2 D_2 V_2^2 + C_1 D_1 V_1^2} \qquad \ldots \ldots (21)$$

For the iron-carbon system this can be written as

$$D_{eff} = \frac{C_{Fe}\, D_{Fe}\, D_C\, V_{Fe}}{C_{Fe}\, D_{Fe}\, V_{Fe}^2 + C_C\, D_C\, V_C^2} \left(V_{Fe} + \frac{C_C}{C_{Fe}} V_C\right) \quad \dots \text{(22)}$$

where subscript Fe and C stand for iron and carbon respectively. Since $D_{Fe} \ll D_C$ and $\frac{C_C}{C_{Fe}} V_C \ll V_{Fe}$ equation (22) can be written as

$$D_{eff} = \frac{C_{Fe}\, V_{Fe}^2}{C_C\, V_C^2} D_{Fe} \quad \dots \text{(23)}$$

Determination of D and γ :

Rastogi and Ardell[10] and Ardell[11,12] have emphasized the importance of concurrent measurement of $\bar{r}$ and C during coarsening. If such measurements are made γ and D can be known independently. Otherwise to evaluate D we must know the value of γ and vice versa. Since the rate constant after equation (15) is

$$K = \frac{8\, \gamma\, D\, C_e\, V_m}{9RT} \quad \dots \text{(24)}$$

where K is the experimental rate constant for the growth of particles. Ardell[11,12] and Rastogi and Ardell[10] have shown that for matrix composition

$$C - C_e = (K' t)^{-\frac{1}{3}} \quad \dots \text{(25)}$$

where

$$K' = \frac{D(RT)^2}{9\, \gamma^2\, C_e^2\, V_m} \quad \dots \text{(26)}$$

From equation (24) and (26) we get,

$$D_{eff} = \frac{9}{4} \frac{(K^2 K')^{1/3}}{V_m} \qquad \qquad \cdots \cdots (27)$$

and

$$\gamma = \frac{(K/K')^{1/3}}{V_m} \qquad \qquad \cdots \cdots (28)$$

With the help of equations (27) and (28) values of D_{eff} and γ can be obtained. Though it is assumed that in Ostwald ripening the amount of solute in the matrix remains constant, the equation (24) and (26) can still be taken advantage of with reasonable assumption that interface energy γ does not change with composition of the matrix appreciably and also is independent of particle size. This assumption breaks down if the particles are so small that they are coherent with the matrix.

Effect of Volume Fraction on Coarsening Rate:

The theory of diffusion controlled coarsening developed by WIS assume that the volume fraction of precipitate is so small that it does not effect the diffusion passage of solute atoms. Ardell[13] in a recent paper has theoretically considered the effect of volume fraction on particle coarsening. His expression for average radius is given below

$$\bar{r}^3 - \bar{r}_0^3 = \frac{3 \propto D V_m}{\nu(\phi)} t \qquad \qquad \cdots \cdots (29)$$

where

$$\propto = \frac{2}{RT} \frac{C_e V_m}{}$$

$\nu(\phi)$ = A function of volume fraction ϕ

$$\mathcal{V}(\phi) = \frac{P_m^3}{\beta\, P_m^2 + (1 - \beta)P_m - 1} = \frac{3P_m^2}{1 + 2\beta P_m - \beta} \quad \dots \dots (30)$$

$$\beta = \frac{6\phi^{1/3}}{e^{\phi}\,\Gamma(\phi)}$$

where

$\Gamma(\phi)$ is another function of ϕ

$$P_m = \frac{(\beta^2 + \beta + 1)^{1/2} - (1 - \beta)}{\beta} \quad \dots \dots (31)$$

The new parameter P_m is the theoretical relative maximum particle size of the polydispersed assembly. The theoretical distribution of particle size must go to zero when $P \gg P_m$. When $\beta \to 0$, $\mathcal{V}(\phi) \to \frac{27}{4}$ and $P_m \to \frac{3}{2}$ and as $\beta \to \infty$ $(\phi - 1)$ $\mathcal{V}(\phi) \to 0$ and $P_m \to 2$. This analysis shows that the coarsening rate should increase without limit as the volume fraction increases towards unity. Furthermore, the maximum particle size approaches twice the critical size, so that we can expect a broadening of the theoretical particle size distribution as ϕ increases. The complete dependence of $\mathcal{V}$, P_m and ϕ has been reported[13].

2.3 Theory of Interface Controlled Coarsening:

According to Greenwood[20] the rate of interface controlled coarsening of an individual particle is given by

$$\frac{dr}{dt} = D(C_r - C_e) \quad \dots \dots (32)$$

where D is a constant. Using equation (7), (8) and (32) we can write

$$\frac{dr}{dt} = \frac{2\gamma C_e V_m B}{RT} \left(\frac{1}{r^*} - \frac{1}{r}\right) \qquad \ldots \ldots (33)$$

where

$$r^* = \text{Critical radius} = \frac{\int_0^\infty r^2 f(r, t)dr}{\int_0^\infty r\, f(r, t)dr}$$

Wagner[3] has analysed this case in detail using equation (7), (13) and (32), and solved equation (12). His results are

$$f(P, T) = H(t)\, Ph_2(P)$$

$$Ph_2(P) = P\left(\frac{2}{2-P}\right)^5 \exp\left(-\frac{3P}{2-P}\right) \quad \text{for} \quad P \leqslant 2$$

$$Ph_2(P) = 0 \quad \text{for} \quad P > 2 \qquad \ldots \ldots (34)$$

where $\quad P = \dfrac{r}{r^*}$

Wagner also showed that

$$r^* = \frac{9}{8}\bar{r}$$

and

$$\bar{r}^2 - \bar{r}_0^2 = \frac{64\gamma C_e V_m B}{81 RT}\, t \qquad \ldots \ldots (35)$$

Kirchner[14] has shown that the cumulative size distribution of particles due to interface controlled coarsening is given by

$$C(P) = A\, P^{9/4}$$

where $\quad C(P) = \displaystyle\int_0^P Ph_2(P)\, dP \qquad \ldots \ldots (36)$

and $\quad A = \text{Constant}$

Markworth[6] has shown that the variation of individual particle is given by

$$\left(\frac{2-P_0}{2-P}\right)^2 \exp \frac{r(P_0 - P)}{(2-P)(2-P_0)} = \frac{t}{t_0} \quad \cdots (37)$$

where again $P = \frac{r}{r^*}$ and $P_0 = (\frac{r}{r^*})_{t_0}$. The above equation is applicable only for $t < t_0$.

2.4 Theory of Grain Boundary Diffusion Controlled Coarsening:

If all the precipitates are situated near the grain boundaries of the matrix and if it is assumed that the diffusion of solutes occurs only along grain boundaries (not a very good assumption at high temperatures) the kinetics of coarsening is altered. Speight[15] writes the following modified Gibbs-Thomas equation for this case as,

$$C_r = C_{e.g.} \exp\left(\frac{2\gamma V_m}{rRT}\right) \quad \cdots (38)$$

where,

   C_r = Concentration of solute on the grain boundary in equilibrium with particles of radius r.

   $C_{e.g.}$ = Concentration of solute on the grain boundary which is in equilibrium with particles of infinite size.

Using a method similar to that of Greenwood, Speight[15] has derived an expression for the rate of coarsening of grain boundary particles which is given below

$$\frac{dr}{dt} = \frac{2\gamma C_{e.g.} V_m D \delta}{3 a h RT r^2} \left(\frac{1}{r^*} - \frac{1}{r}\right) \quad \cdots (39)$$

where

D_g = Grain boundary diffusion coefficient

W   = Width of the grain boundary

a $= \frac{2}{3} - \frac{\gamma_{g.b.}}{2\gamma} + \frac{1}{3}\left(\frac{\gamma_{g.b.}}{2\gamma}\right)^3$

$\gamma_{g.b.}$ = Surface free energy per unit area of the boundary

h $= \frac{1}{2}\ln\left(\frac{1}{f}\right)$

f   = Fractional area of grain boundary occupied by the particles.

$$\frac{1}{r.w} = \frac{\sum_{i=1}^{N}\frac{1}{r_i}}{N}$$

The variation of average particle size with time is given by

$$\bar{r}^4 - \bar{r}_0^4 = \frac{4\gamma\, V_m\, C_{e.g.}\, D_g\, W}{3\, a\, h\, R\, T}\, t \qquad \ldots \ldots (40)$$

Kirchner[16] has applied WIS type of analysis to the coarsening of grain boundary precipitate. He found that the distribution function reaches a quasi stationary state after long periods of time.

Kirchner[14] has also shown that cumulative distribution function for pseudostatic distribution of grain boundary particle coarsening can be approximated as

$$G(P) = AP^6$$

In a recent paper Ardell[8] has derived cumulative distribution function for the grain boundary precipitate. The effect of volume fraction is also included in the derivation.

Markworth and Glansur[18] following WIS type of analysis have also derived an expression for the asymptotic size distribution function.

Ardell[17] has studied the behaviour of grain boundary precipitate in a modified way. His results also confirm the r^4 law for the growth of grain boundary precipitate, when grain boundary diffusion is rate controlling factor.

2.5 Effect of Alloying Element on Coarsening Mechanism:

The above theories are applicable to binary alloy only. The effect of a third element on Ostwald ripening has been considered in detail in a quantitative manner by Bjorkulend et al[19]. The ternary rate equation derived for Fe-C-X matrix is

$$\frac{dr}{dt} = \frac{2 \gamma V_m D^*}{3RT(1 - K_1)^2 U_X^e} \frac{1}{r} \left(\frac{1}{r_e} - \frac{1}{r}\right) \qquad \ldots \ldots (43)$$

and the rate of coarsening after long time is given by

$$r_e^3 = \frac{8 \gamma V_m D^*}{27RT(1 - K_1)^2 U_X^e} t \qquad \ldots \ldots (44)$$

The ratio of the rate constant for the binary and ternary cases will be

$$\frac{K_{ternary}}{K_{binary}} = \frac{D^*}{3(1 - K_1)^2 D_e U_e^o U_X^o} \qquad \ldots \ldots (45)$$

where

$$K_1 = \frac{U_X^{cem}}{U_X^{\alpha - Fe}}$$

D^* = Diffusion coefficient of element X.

U_X^{cem} = Amount of element X in cementite in gm moles/cm^2

$U_X^{\alpha - Fe}$ = Amount of element X in α-ferrite in gm moles/cm^2

U_X^e = Alloy content at the surface of particle of

   critical radius r_c

U_c^e = Ordinary solubility of cementite in ferrite.

The U parameters are given as

$$U_X = \frac{x_X}{(1 - x_c)} = x_X(1 + U_c)$$

$$U_c = \frac{x_c}{(1 - x_c)} = x_c(1 + U_c) \qquad \ldots \ldots (46)$$

$$U_{Fe} = \frac{x_{Fe}}{(1 - x_c)} = x_{Fe}(1 + U_c)$$

where x stands for mole fraction and the subscripts X, Fe, c
for alloying element, iron and carbon respectively.

2.6 Coarsening in Non-Ferrous Alloys:

Many investigators have studied coarsening in non-ferrous
alloys. The results of these investigations are listed in
table 1.

2.7 Coarsening in Ferrous Alloys:

Day and Badford[38] studied coarsening of cementite in
Fe-0.3%C alloy at 675°C and 720°C. Average particle size was
measured by using Fullman's method for monodispersed system
(i.e. all particles have same size). At 720°C the slope of log
$\bar{r}$ vs log t was nearly zero at small tempering times and at
longer time it approached a value of 0.33. At 675°C they found
a break in the log $\bar{r}$ vs log t plot. At small tempering time the

slope was nearer to 0.33 while at longer tempering time the slope was found to be nearer to 0.25. It was concluded that at 720°C cementite coarsens by a diffusion controlled process, but at 675°C for longer tempering times the grain boundary diffusion appeared to be a rate controlling factor. However Fullman's analysis can be not be applied for a coarsening system since we have a range of particle size.

Heckel and Degregorio[41] studied coarsening of cementite in Fe-0.75%C alloy at 704°C. Particle size distributions were measured by using Dehoff's method. The size distribution were found to be log-normal. Data were analyzed by using Heckel's[40] model, which is similar to WIS model but requires no specification about shape of the particle size distribution curve. However, Heckel's[40] model assumes that number of particles, per unit volume, of different sizes is same. Coarsening of cementite in this steel appeared to obey an interface controlled kinetics.

Vedula and Heckel[39] investigated coarsening of cementite in binary Fe-C alloys, 0.24, 0.42 and 0.79 wt%C at three temperatures 594°C, 649°C and 704°C for times up to 10^6 secs. It was found that particle size distribution did not reach a steady state even after tempering for 10^6 secs. Analysis of data using Heckel's[40] model indicated that coarsening of cementite in these steels is a diffusion controlled process. Plots of $(\bar{r}^3 - \bar{r}_0^3)$ vs t were linear and approached a slope of 1.0 at high temperatures only. Deviations of slope at low temperatures were attributed to nonsteady state distribution.

Gokhale[46] and Verma[47] have also studied the coarsening of cementite in Fe-0.79%C alloy. They found the coarsening mechanism to be diffusion controlled. Mehl et al[42] studied coarsening of cementite in Fe-0.15%C, Fe-0.15%C - 1%Mn, Fe-0.15%C - 1%Ni and Fe-0.15%C - 1%Cr alloys. A series of tempering temperatures between 500°C and 700°C and tempering times of up to 190 hr. were used. Out of these Fe-C-Cr system could not be studied due to precipitation of double carbides. Plots of $\bar{r}^3$ vs t were linear in all other cases but there was some scatter at lower tempering temperatures. Size distributions were much more broader than predicted by WIS theory. It was also found that cold working of samples before tempering did not have any effect on the rate of coarsening. It was observed that nickel did not have much effect on the coarsening rate, but manganese decreases the rate markedly. The value of surface energy of cementite-ferrite interface is expected to lie in the range of 500 to 1000 ergs/cm^2. Exceptionally high values were obtained at lower tempering temperatures. It was suggested that rate of coarsening in these steels is determined primarily by volume diffusion at high temperatures, but the grain boundary diffusion plays an increasingly important role as the tempering temperature is lowered.

Gokhale[46] has studied coarsening of cementite in Fe-0.79%C - 0.49%Si alloy at 690°C. He found the coarsening mechanism to be diffusion controlled. It was also observed that Si decrease the rate of coarsening.

Mukherjee et al[49] investigated kinetics of coarsening of carbides in a series of Fe-0.20%C - Cr alloys at 700°C. It

was found that the coarsening rates of the carbides decrease in the order Fe_3C : M_3C : $M_{23}C_6$: M_7C_3. The kinetics of coarsening in recrystallized steels indicate that the process is diffusion controlled. M_3C and M_7C_3 are shown to coarsen at rates expected if diffusion of chromium is rate controlling, but Fe_3C coarsens too rapidly for the equivalent diffusion of iron to be controlling. In as tempered steels, the dislocation structure of the matrix inherited from martensite leads to coarsening rates greater than the predicted value.

Bannyh[36] et al as quoted by Greenwood[37] were the first investigators to obtain quantitative experimental data in steels. They studied coarsening in a commercial 0.83%C steel. The tempering temperature ranged from 210°C to 710°C and time from 1.5 secs to 20 hrs. The plot of $\bar{r}^3$ vs t was found to be linear at 700°C. At lower temperatures agreement with WIS theory was poor. They concluded that the coarsening was diffusion controlled. They did not study particle size distribution.

Dirnfeld[48] studied the coarsening kinetics of cementite in eutectoid steel, of commercial purity with 0.89%C and 0.28% Al. Their investigation shows that the reaction was diffusion controlled.

Gokhale[46] also studied the coarsening of cementite in eutectoid steel of commercial purity. He found that the coarsening was diffusion controlled.

Wolfi et al[43] have studied dissolution kinetics of cementite in ferrite by resistivity measurements and data were

correlated to average carbon concentration in the matrix. It was concluded that dissolution of cementite in ferrite is entirely an interface controlled process.

Harris et al[44] studied the growth kinetics of graphite in Fe-C-Si system. According to them the graphitisation obeys an equation of the form

$$y = 1 - \exp\left(-\frac{t}{\tau}\right)^n$$

n taking values close to 3.0; y is any parameter for growth rate in graphitisation. They also concluded that in most part of reaction diffusion of C in ferrite is rate controlling factor.

2.8 Quantitative Metallography:

Quantitative metallography methods are required to measure the particle size distribution in metallurgical processes such as recrystallization and nucleation, growth of precipitate particles etc. Several analysis have been made for determining spatial size distributions from two dimensional measurements. In general, the analysis are based on the assumption that (a) the particles have spherical shapes, (b) the distribution of particle sizes is broken up in to descrete size groups.

These methods may be classified in to three major categories according to type of planar measurement performed. These categories are based on:

    (a) Distribution of section diameter

    (b) Distribution of section areas

    (c) Distribution of section chord lengths

All the methods are based on the statistical probability of the plane intersecting a sphere of diameter D_j so as to produce a section of size d_i. The probability may be expressed in terms of radii as

$$P_{i,j} = \frac{1}{R_j} \left(\sqrt{R_j^2 - r_{i-1}^2} - \sqrt{R_j^2 - r_i^2} \right) \quad \ldots \ldots (47)$$

Let us now consider a polydispersed system of spheres that has been separated in to five class intervals. The number of spheres per unit volume in each class interval is represented by N_j, $j = 1, 5$ and corresponding radii are R_j, $j = 1.5$.

The total number of circular sections of given size per unit area is n_1, n_2, n_3, n_4, n_5 where the section radii vary from 0 to R_1, R_1 to R_2, R_2 to R_3, R_3 to R_4, R_4 to R_5 respectively.

Spheres of the largest class interval yield sections of all radii when cut by a random plane. Therefore, the observed number of sections of the smallest size per unit area, n_1, is the sum of contributions from spheres of all sizes. So we can write

$$n_1 = \sum_j N_{1,j} = N_{1,1} + N_{1,2} + N_{1,3} + N_{1,4} + N_{1,5} \quad \ldots (48)$$

We want to calculate the number of spheres per unit volume in each class interval. In order to do so the number of sections having the same radius as their spheres $(N_{1,1})$, $(N_{1,2})$ etc. are determined. In this case equation (48) becomes

$$N_{5,5} = n_5$$

$$N_{4,4} = n_4 + N_{4,5}$$

$$N_{3,3} = n_3 - N_{3,5} - N_{3,4} \qquad \dots \dots (49)$$

$$N_{2,2} = n_2 - N_{2,5} - N_{2,4} - N_{2,3}$$

$$N_{1,1} = n_1 - N_{1,5} - N_{1,4} - N_{1,3} - N_{1,2}$$

Since n_5 is measured quantity $N_{5,5}$ is known, $P_{5,5}$ is calculated from equation (47), and D_5 is measured from the plane of polish. We can now calculate N_5 from the equation

$$N_j = \frac{\sum_i \dfrac{N_{i,j}}{P_{i,j}}}{D_j} \frac{1}{D_j} \qquad \dots \dots (50)$$

Knowing N_5 we proceed to calculate N_4. This sequence of calculation is continued down to the smalles particles size.

Let us now discuss a few important methods for transforming two dimensional measurements in to corresponding three dimensional distribution.

Schwartz-Saltykov[50] (diameter) analysis:

The particle size may be broken down in to any number of groups up to 15, depending up on the accuracy required. The number of groups should not be less than 7. If the largest diameter is D_{max}, and K be the total number of groups then,

$$= \frac{D_{max}}{K}$$

Thus the diameter of the particles of the first group is $\triangle$, that of the second group is $2\triangle$ etc. To properly identify the number of sections of a particular class interval both section size and particle size must be specified. Index j indicates the group of particles which form the given sections

on the plane of polish. Index i refers to the size groups of the sections. Thus for example, $N_{3,4}$ indicates the number of sections of the third size group (with diameter between 2 and 3) formed exclusively from 4th size group (with dia equal to 4). With this notation we can write total number of sections of the first size group as

$$n_1 = \sum_{j=1}^{K} N_{1,j} = N_{1,1} + N_{1,2} + N_{1,3} + \dots + N_{1,i} \dots + N_{1,K}$$

Similarly for the second size group

$$n_2 = \sum_{j=2}^{K} N_{2,j} = N_{2,2} + N_{2,3} + N_{2,4} + \dots + N_{2,i} \dots + N_{2,K}$$

and so on.

The total number of particles per unit volume is

$$N = N_1 + N_2 + \dots + N_K$$

The probabilities that a random plane will intersect spheres of the various diameters to give particular sections are calculated as describe before. Equations are then set up for N_j in terms of $N_{i,j}$. The latter terms can be eliminated by substituting n_i values for $N_{i,j}$ values by the calculations as described earlier, leaving N_j expressed as function of n_i values i.e. the measured quantity. The general equation is

$$N_j = \frac{1}{\Delta} \sum_{i=j}^{K} \beta_{j,i} \, n_i \qquad \dots (51)$$

Though N can be calculated by summing N_j, it can be calculated as

$$N = \frac{1}{\Delta} \sum_{i=1}^{K} \beta_{j,i} \, n_i$$

Saltykov[51] (Area) analysis:

This method does not require sequential calculations nor tables of coefficients. Saltykov adopt A/A_{max} to specify size of a section instead of the absolute area. The scale factor used to get class intervals for A/A_{max} is based on a logarithmic scale of diameters with the factor $10^{-0.1}$. The advantage of using A/A_{max} to group the sections lies in the unique relationship of particles shape to the n versus A/A_{max} frequency distribution.

The computations follow along lines described previously. The results of the successive calculations give a general working formula which gives N_j directly for any desired class interval.

$$N_j = \frac{1}{D_j} \left[1.6461\, n_1 - 0.4561\, n_{i-1} - 0.1162\, n_{i-2} - 0.0415\, n_{i-3} \right.$$
$$- 0.0173\, n_{i-4} - 0.0079\, n_{i-5} - 0.0038\, n_{i-6} - 0.0018\, n_{i-7}$$
$$- 0.001\, n_{i-8} - 0.0003\, n_{i-9} - 0.0002\, n_{i-10}$$
$$\left. - 0.0002\, n_{i-11} \right] \quad\quad \ldots\ldots (52)$$

Evidently not more than 12 class intervals should be used. The method is direct and simple. It is applicable not only to polydispersed systems of spherical particles but in principle convex particle as well.

The Spektor[52] (Chord) analysis:

In this analysis a random line is passed through a section plane and chord lengths of the particles cut by the test

line are measured. They are grouped in to number of size classes. The size interval is fixed as in diameter analysis.

The working equation is

$$N_j = \frac{4}{\pi \triangle^2} \left[\frac{(n_L)_j}{2j - 1} - \frac{(n_L)_{j+1}}{2j + 1} \right] \qquad \ldots \ldots (53)$$

where, N_j and $(n_L)_j$ are the number of particles per unit volume and the number of chords per unit length of test line, respectively for the indicated jth size class. The equation is very handy and simple in its use.

Spatial size distribution of non-spherical particles:

It is obvious that computational complexities increase considerably in the analysis of size distribution of non-spherical particles. Wicksell[53] was first to give an analysis for ellipsoidal particles. Wicksell's analysis is very lengthy and mathematically complex.

Recently analysis for ellipsoids have been published by Dehoff[54]. Dehoff's analysis for oblate ellipsoids was used in our investigations and given in detail in chapter 4.

Paulus[55] has analysed a little more difficult case of pentagon and dodicahedron while Cahn and Fullman[56] have analysed the lamellar structure.

2.9 Scope of Present Investigation:

It is clear from above that the results of previous workers on coarsening of cementite in steels are conflicting. Dey and Radford[38] found that coarsening of cementite is grain

boundary diffusion controlled. The investigation of Heckel and Degregorio[41] shows that it is interface controlled process. Vedula and Heckel[39] showed it to be volume diffusion controlled process. Moreover the effect of alloying elements have not been investigated extensively. Particularly of silicon not been investigated except the work of Gokhale[46]. He has done some preliminary work on the effect of silicon in a 0.73%C steel. He carried out his investigations at 690°C only. As no thorough investigation has yet been carried out on the effect of Si in the steel, it was decided to investigate the effect of silicon on the coarsening kinetics of cementite in steel as a function of temperature.

Table 1:   The Coarsening in non-ferrous systems.

System	Technique used to measure r̄	Variation of r̄ with time $\bar{r}^n - \bar{r}_0^n = kt$	Particle size distribution	Conclusion	Remarks	Reference
Co ppt in Cu	Magnetic method	n = 3	Not measured	Diffusion controlled growth	Despite the fact that lattice mismatch between Co and Cu is very large and strain field results from coherency, the variation of r̄ with time seem to be unaffected.	21
Ni-Al in Ni	Transmission electron microscopy	n = 3	Distribution reaches a quasisteady state but cut off tends to be more than 1.5.	Diffusion controlled growth	Agreement of r̄ vs t with WLS theory even when particles are very close together shows dominating effect of concentration gradient near the particle surface.	22, 23
Ni-Ti in Ni	TEM	n = 3	Distribution much broader than that predicted	Diffusion controlled growth	For particles in the Ni alloys there seem to be reasonable correlation between γ'/matrix mismatch of lattice parameter and deviation of experimental size distributions from that predicted by theory. It is found that larger the mismatch, larger is the deviation.	24

System	Method	n value	Distributions / Results	Mechanism	Comments	Ref.
Mg-Si in Fe-Si	Electron microscopy	n = 3	Distributions were much broader than the theoretical one	Diffusion controlled coarsening	Diffusion theory is obeyed only when variable diffusion coefficient is applied	26
Mg-Al in Al-metal	Not known	n = 3	Distributions in best agreement with theory. Cut off at P = 1.5	Diffusion controlled coarsening	$D = D_0(1 + \frac{K}{r})$	25
SiO$_2$ in Al$_2$O$_3$	Transmission electron microscopy	-	-	Decomposition of SiO$_2$ in matrix is rate controlling factor	Though at low times growth rate is relatively high and activation energy for the growth rate approaches that of diffusion rate of solute atoms. At large particle size activation energy f for growth increases and appears to be more nearly dependent solely on the dissociation of Si and O$_2$	27
Si & O in Al-on alloy	Transmission electron microscopy	n = 3 for σ	-	Diffusion controlled growth for σ or short circuit diffusion occurs in case of σ	A trace addition of Ge to Cu reduces coarsening rate of σ probably reduction of interfacial energy	28

Contd...

System	Technique	n		Mechanism	Remarks	Ref.
Cu ppt in Cu	Replica technique electron microscopy	n = 3	*	Diffusion controlled coarsening	The equilibrium shape of the particles is that of rods with hemi-spherical caps and is due to large anisotropy in the copper/ -Fe inter-facial free energy ($\gamma_/\gamma = 4$). The mean calculated radius was found to be smaller than those observed by a factor of about one half.	29
Al₂O₃ in Ni	Electron microscopy	*	*	Mean free path was measured. Mean free path $\sim 1/3$ path Dissolution of Al and O₂ is believed to be rate controlling factor	It was found that shape of the particle changes with time so VLS theory could not be applied	31, 32
Al₂O₃ in Ni	Electron microscopy	n = 3	Not studied	Diffusion controlled	The growth rate of largest particle were measured. It did not agree with VLS equation of growth rate since their expression is for growth average particle size	35
Mn ppt in Mn alloy	Replica technique electron microscopy	Both n = 2 and n = 3	Good agreement with both diffusion and interface controlled models	It is not possible to decide from the data obtained whether the coarsening process is diffusion or interface controlled		90

Contd...

Material	Technique	n	Observations	Conclusion	Ref.
Inter-metallic precipitate in ferrite Fe-Mo-C alloy	Electron microscopy	n = 3	It is seen that for the smaller particle sizes distribution is normal and as the coarsening process progresses the distribution becomes wider. It is also seen that distribution tends to be log normal at long tempering time.	Diffusion controlled	33
δ' PPt in β	Replica technique electron microscopy	n = 3 at high temperature than when matrix is β, n = 4 at 665°C, n = 5 at 590°C when matrix is α	Both broader than that predicted by the theory and no sharp cut off at P = 1.5	Coarsening in the value of n = 4 and 5 suggest that grain boundary diffusion and pipe diffusion play important roles. Nothing can be said about α matrix	34
Al₂O₃ in transmission Ni-Al₂O₃-electron Mg microscopy		n = 3	Not studied	Addition of magnesium initially increases the coarsening rate of Al₂O₃ at 1300°C. After 16 hrs., however, the magnesium almost restricts coarsening	The behaviour of coarsening process at larger times has been attributed to the reduction of the diffusivity of the element moving atom x in matrix species in the matrix	57, 58

Contd...

| Thoria in Ni and 20% Cr Ni | Electron microscopy | n = 3 | Not studied | Diffusion controlled growth | It is observed that rate of particle growth is more in Ni-Cr-Th alloy. This is accounted for by the increased value of the diffusion coeff-icient of thorium in the alloy over the value in pure Ni | 63 |

CHAPTER 3

EXPERIMENTAL WORK

Coarsening of cementite in ferrite matrix was studied in Fe-C-Si alloy at four different temperatures. The temperatures selected were 710°C, 690°C, 660°C and 630°C?

3.1 Materials:

The Fe-C-Si alloy was prepared from 99.9% pure Fe, 99.99% pure C and 99.5% pure Si. Two alloys of approximate composition Fe-0.75%C - 0.4%Si were made by melting appropriate amount of iron, Carbon and silicon. Melting was done in an induction furnace in argon atmosphere. The alloys were melted twice to get a homogeneous button. Each time the alloys were kept in the liquid state for about 15 minutes, for liquid state homogenisation. The alloy buttons were hot forged at about 1000°C to 12.5 mm diameter rod. These were than cold swaged to 10 mm diameter rod. These rods were vacuum sealed in a quartz tube. The sealed rods were homogenised at about 1000°C for four days. A piece was cut from each of the rods and microstructure was examined. No evidence of any seggregation was observed in one of the rods. This rod was further reduced to 6 mm diameter by cold swaging and cut in to small pieces of about 12 mm length.

The samples were chemically analysed and the composition was found to be Fe-0.74%C - 0.37%Si.

3.2 Heat Treatment:

Austenitizing was done in a vertical resistance furnace[46] in nitrogen atmosphere. The nitrogen gas was passed through pyrogalal before entering the furnace. Pyrogalal solution absorbs oxygen from nitrogen. The samples were austenitized for about 15 minutes at 850°C. The sample was then quenched in brine water. Since the M_f temperature of steel with more than 0.6%C is below 0°C, the samples were given subzero treatment. This was done by requenching the samples in liquid nitrogen. Hardness of every quenched sample was measured and microstructure was seen to ensure that all of austenite has been transformed to martensite. The hardness of samples ranged from R_c 62 to R_c 65. It is necessary to start with a martensite matrix, because the nucleation of cementite is very fast and uniform distribution of cementite in ferrite matrix is obtained.

Tempering:

The quenched samples were tempered in lead bath at 630°C, 660°C, 690°C and 710°C from time ranging from 5 hrs. to 15 days. The temperature control was ± 3°C.

To avoid oxidation of the lead bath it was kept covered with charcoal powder all the time.

3.3 Metallography:

The tempered samples were ground, polished and etched with 5% nital and then washed with water and alcohol to avoid formation of stains on the etched surface. The microstructure

3.2 Heat Treatment:

Austenitizing was done in a vertical resistance furnace[46] in nitrogen atmosphere. The nitrogen gas was passed through pyrogalal before entering the furnace. Pyrogalal solution absorbs oxygen from nitrogen. The samples were austenitized for about 15 minutes at 850°C. The sample was then quenched in brine water. Since the M_g temperature of steel with more than 0.6%C is below 0°C, the samples were given subzero treatment. This was done by requenching the samples in liquid nitrogen. Hardness of every quenched sample was measured and microstructure was seen to ensure that all of austenite has been transformed to martensite. The hardness of samples ranged from R_g 62 to R_g 65. It is necessary to start with a matensite matrix, because the nucleation of cementite is very fast and uniform distribution of cementite in ferrite matrix is obtained.

Tempering:

The quenched samples were tempered in lead bath at 630°C, 660°C, 690°C and 710°C from time ranging from 5 hrs. to 15 days. The temperature control was ± 3°C.

To avoid oxidation of the lead bath it was kept covered with charcoal powder all the time.

3.3 Metallography:

The tempered samples were ground, polished and etched with 5% nital and then washed with water and alcohol to avoid formation of stains on the etched surface. The microstructure

was observed under a microscope whose eye piece and objective were kept same through out the investigation. Oil immersion objective was used to get better resolution. Total magnification was kept constant at X1000 to minimize relative errors.

Some of the photographs are given in the next chapter to illustrate the nature and shape etc.

3.4 Particle Size Measurement:

Direct measurement under microscope though possible was not accurate enough because at low times and temperatures the particle size was quite small and at X1000 magnification thickness of the cross wires will be comparable to many of the particle size. Equally difficult was to measure accurately the area of polished plane. Microfilm reader was tried. But though much more accurate, due to very high magnification (X19.6 coupled with X1000 of microscope), it was difficult to measure because all the particles were not exactly circular or elliptical and approximate ellipses had to be made out of particles. That meant to trace the particles on a paper first and then measure. This took as much effort and probably more time than making photographs, and then measuring the particle size. Also due to high magnification the cementite-ferrite grain boundaries got diffused which offset the accuracy obtained by high magnification. Hence photographs were made with 4 times enlargement to get a total magnification of X4000. The particle which were not exactly circular of elliptical were approximated to the best possible ellipses. Major axis of each particle was measured. 350 to 450 particles were measured for each time-temperature

combination. The measurements were done by using a simple linear scale.

3.5 Magnification Calibration:

Actual magnification of photographs may not be necessarily same as obtained by numerical ratings of lenses. There are 5 factors which may cause error. (1) Errors in objective lense, (2) Errors in magnification of eye piece, (3) Error due to camera set up, (4) Film shrinkage after washing, (5) Improper length of microscope tube. To measure this error a standard stage micrometer was used with equally spaced fine lines on it. A photograph of the micrometer was taken with all the conditions as closely simulated to those in micrographs, as possible. The distance between 5 lines was measured at an apparent magnification of X4000. The ratio of this distance to the actual was the magnification. The magnification was found to be X2420. The correction factor due to the use of the apparent magnification m is given as

$$m = \frac{\text{Apparent magnification}}{\text{Actual magnification}} = \frac{4000}{2420} = 1.653.$$

RESULTS

4.1 Calculation of Particle Size Distribution:

The major axis of the best fitting ellipse was measured for 350 to 450 particles for each tempering time. In order to obtain particle size distribution from these data, Dehoff's method[54] of quantitative metallography was used. This method was preferred because it is applicable to oblate spheroidal particles and it is simpler than other methods such as Sheil's[64] method, Skepter's[52] method etc. Moreover most of the other methods are applicable to spherical particles only while in our photomicrographs the particle sections were both circular and elliptical which means that all particles were not spherical.

Dehoff's method[54]:

If D_{max} be the maximum section size observed in a particular section size distribution and we make K section classes, the size interval Δ is defined by the following expression,

$$\Delta = \frac{D_{max}}{K} \qquad \qquad \cdots \cdots (54)$$

The section with their major axis between 0 and Δ are kept in first size class. Sections with major axis between Δ and 2Δ are grouped in the second size class and so on. If i denotes the size class number and n_1, n_2, ... n_i ..... n_K be the number of sections in 1st, 2nd ..... i-th .... and K-th size class respectively, then i-th size class will have particle

sections having major axes between $(i-1)\triangle$. and $i\triangle$. We want
to convert this two dimensional size distribution in to a
3 dimensional size distribution. Let j denote the three
dimensional size class and N_1, N_2, ... N_j .... N_K be the number
of particles per unit volume in 1st, 2nd, ... j-th and K-th
size classes respectively. We want to find values of N_j's from
the values of n_i's.

Dehoff assumed that (1) particles have the shape of an
oblate ellipsoid of revolution and axial ratio of all the
particles is same (2) distribution of particles in the matrix
is random and showed that

$$N_j = \frac{1}{A \triangle K(q)} \sum_{i=j}^{K} n_i \, \beta_{ji} \qquad \cdots\cdots\cdots(55)$$

A = Area of plane of polish in which sections are measured

q = Axial ratio (ratio of minor to major axis)

K(q)= Shape factor (a function of q)

For oblate spheroids

$$K(q) = \frac{q}{2} + \frac{Tan^{-1}\sqrt{(1 - q^2)}/q}{2\sqrt{(1 - q^2)}} \qquad \cdots\cdots(56)$$

β_{ji} = Saltykov's coefficient. These are available in tabulated
form[53,59,60].

Also the volume function of precipitate is given as:

$$V = \sum_{j=1}^{K} N_j \frac{\pi}{6} q(j\triangle)^3 \qquad \cdots\cdots(57)$$

Since we start with a martensitic matrix, distribution of
cementite particles is expected to be random. Most of the

sections were either elliptical or circular but a few were difficult to be imagined as ellipses. Best fitting ellipses were curved out from these particles sections. There was no evidence of cigar shaped particles (plane section of prolate ellipsoids) and hence possibility of ellipsoids with prolate shape was ruled out.

Volume fraction of cementite can be calculated from the composition of the alloy, the densities of ferrite and cementite and the solubility of carbon in ferrite which is obtained from the literature[61]. Densities of ferrite and cementite are also obtained from the literature[62].

The value thus obtained is the actual theoretical volume fraction of cementite. Volume fraction in the alloy used in this investigation was 0.117. Appropriate values of q are obtained by comparing calculated volume fractions from eqn. (56) and eqn. (57) with actual volume fraction.

From N_j values the total number of particles may be obtained by the following equation.

$$N = \sum_{j=1}^{K} N_j \qquad \ldots \ldots (58)$$

The mean particle size for each size class is

$$r_j = \frac{2+1}{6} (j\triangle) \qquad \ldots \ldots (59)$$

and the average particle size is

$$\bar{r} = \sum_{j=1}^{K} N_j r_j / N \qquad \ldots \ldots (60)$$

4.2 A Sample of Calculation:

Let us choose a set of calculations measured on the photomicrographs of a sample tempered for 1.011×10^5 secs, at 690°C. Photomicrographs of this sample are given in Fig. 4(a) and the corresponding section sizes measured on these micrographs are given in table 2. It can be seen that the maximum size is 0.8 cm on the micrographs.

$$D_{max} = \frac{0.8}{2420} = 33.0576 \times 10^{-5} \text{ cm}$$

For convenience section sizes were divided into eight section size classes. So $K = 8$ and $\triangle = 4.132 \times 10^{-5}$. The corresponding section size distribution is given in table 3. Assuming different axial ratios (from 1.0 to 0.5) and using equation (56) and (57) the volume fraction V was calculated for each axial ratio. The values of $K(q)$, V, $\bar{F}$ and N are given in table 4. It is clear that the axial ratio 0.98 gives best agreement with the actual value of 0.117. Once q is known N_j is calculated using equation (55). All calculations were done on IBM 7044 computer. The computer programme is given in Appendix-I.

4.3 Results:

The representative photographs of samples of tempered Fe - 0.74%C - 0.37%Si alloy are given in fig. 2 to 5 for all tempering times. The values of $\triangle$, K, $\bar{F}$, q, V and N are listed in table 6 to 9. The variation of calculated volume fraction with the axial ratio is given in table 5. The calculated volume fractions are compared with the theoretical value and the

selected values of q and V are listed in table 6 to 9. Using
the selected values of q, values of $\bar{F}$ and N are calculated.
These are also listed in table 6 to 9. The values of N_j calcu-
lated after equation (55) are listed in table 10 to 13. The
distribution of particles are presented in the form of
histograms in fig. 6 to 9.

Table 2: The major axes of the best fitting ellipses corresponding to the particles in fig. 4 (tempering temperature 690°C and time 1.011×10^5 sec.). Area on the photomicrographs 297.63 cm². Total number of particles is 390.

Major axis measured on photomicrograph in mm.

3.0	4.0	4.5	5.0	2.0	2.5	0.5	4.0	2.0	1.5	4.0	4.0	5.0
3.0	4.0	2.5	4.0	3.0	3.0	1.0	3.0	2.0	1.0	4.0	4.0	2.5
6.0	3.0	2.0	4.0	4.5	6.0	2.0	1.5	3.5	7.0	3.0	7.0	2.0
1.0	3.0	4.0	5.0	2.0	3.0	4.0	4.5	3.0	4.0	6.0	3.0	1.0
3.0	5.5	3.0	0.5	3.5	2.5	4.5	5.0	1.0	6.0	2.5	3.5	3.5
1.5	7.0	1.0	1.5	4.0	5.0	3.5	3.0	2.0	6.0	2.5	2.5	4.5
1.0	7.0	1.5	5.0	4.0	2.5	1.0	2.0	1.5	1.5	2.5	2.0	
3.5	3.0	2.5	6.0	3.0	3.0	2.0	3.0	2.0	3.5	0.5	1.5	
4.0	3.0	3.0	1.0	6.5	2.0	4.5	3.0	1.0	3.0	2.0	3.0	
2.0	2.5	5.0	2.0	7.0	3.0	3.0	4.5	2.0	2.5	1.0	3.0	
4.0	4.0	7.5	3.5	3.0	3.5	2.0	1.5	1.5	5.0	5.0	4.0	
5.0	1.0	4.0	5.5	3.0	3.5	2.0	6.5	2.0	2.0	4.0	3.0	
6.0	2.0	7.0	4.0	2.0	3.5	5.0	5.0	2.5	2.5	3.5	2.0	
3.5	4.0	2.5	4.5	4.5	1.5	4.5	2.5	3.0	4.5	4.0	3.5	
3.0	2.0	4.5	4.0	3.0	2.0	3.0	3.0	3.5	4.5	2.5	3.5	
5.5	2.0	2.0	1.5	2.5	2.0	1.5	3.0	6.0	5.0	2.0	2.0	
6.5	1.5	2.0	4.5	2.0	3.0	3.5	3.5	1.0	2.5	5.0	2.5	
4.0	2.0	2.0	2.5	3.5	3.0	1.5	7.0	5.0	2.0	5.5	2.0	
5.5	2.0	8.0	2.5	1.5	3.0	3.5	3.0	1.0	2.5	6.0	2.5	
1.5	4.5	2.5	3.5	4.0	2.5	1.0	1.5	1.5	2.0	2.5	2.0	
2.5	4.5	1.0	3.0	4.0	1.5	3.0	5.0	2.0	1.5	2.0	3.0	
2.0	3.5	5.0	3.5	3.5	1.5	3.5	4.5	0.5	1.0	2.0	6.0	
5.0	2.0	6.0	1.0	1.0	5.5	7.5	3.0	1.5	2.5	5.5	3.0	
3.5	0.5	1.0	3.5	1.0	3.0	8.0	2.5	2.0	3.0	3.5	1.5	
3.5	7.0	5.0	2.0	3.0	2.5	1.5	3.5	4.0	3.5	6.0	2.0	
1.0	1.0	4.0	3.0	4.5	1.0	2.0	2.0	2.0	3.0	3.0	6.0	
2.0	4.0	4.5	8.0	3.0	1.5	4.0	1.5	1.5	3.5	4.0	4.0	
3.5	1.5	5.5	3.5	0.5	1.5	5.0	4.0	0.5	4.0	3.5	2.0	
4.0	3.0	4.0	2.0	3.0	1.5	1.0	3.5	2.5	3.0	6.5	3.5	
2.0	4.5	3.5	3.0	2.0	4.5	1.0	2.5	3.5	3.0	7.0	1.5	
2.5	2.5	4.0	3.0	2.0	2.5	0.5	3.5	2.0	4.0	0.5	3.0	
2.0	3.0	1.5	4.0	1.5	1.5	1.0	3.5	2.0	5.0	3.0	3.5	

Table 3: Section size distribution in the sample tempered at 690°C for 1.01×10^5 secs.

Size class interval $\Delta = 4.132 \times 10^{-5}$ cm.

Section size class	Number of sections in i-th group, n_i
1	36
2	95
3	95
4	85
5	44
6	19
7	13
8	5

Table 4: Variation of V, N, $\bar{r}$ and K(q) on a axial ratio for tempering at 690°C for 1.011 x 10^5 secs.

Axial ratio	Shape factor K(q)	Volume fraction V	Average radius $\bar{r}$ cm. 10^{-5}	Total number of particles N per cm^3 10^{10}
0.99	0.9966	0.1183	6.36	6.032
0.98	0.9933	0.1175	6.33	6.052
0.95	0.9835	0.1150	6.27	6.113
0.90	0.9673	0.1108	6.16	6.215
0.85	0.9516	0.1063	6.06	6.318
0.80	0.9362	0.1017	5.95	6.421
0.75	0.9213	0.0969	5.849	6.525
0.70	0.9068	0.0919	5.743	6.629
0.65	0.8929	0.0867	5.636	6.733
0.60	0.8795	0.0812	5.530	6.835

Table 5: Variation of volume fraction with axial ratio

Temperature °C	Time 10^5 secs.	Axial ratio	Volume fraction
630	1.749	0.7	0.136
		0.65	0.128
		0.58	0.117
		0.55	0.112
		0.5	0.103
	4.283	0.75	0.135
		0.70	0.128
		0.63	0.118
		0.6	0.113
		0.55	0.105
	9.15	0.65	0.134
		0.6	0.125
		0.55	0.117
		0.5	0.107
	12.57	0.6	0.139
		0.55	0.130
		0.5	0.119
660	0.435	0.8	0.132
		0.75	0.125
		0.68	0.1167
		0.65	0.112
	1.008	0.85	0.128
		0.80	0.122
		0.75	0.1167
		0.70	0.110
		0.65	0.104
	4.356	0.85	0.131
		0.80	0.125
		0.74	0.118
		0.7	0.113
	8.46	0.8	0.131
		0.75	0.125
		0.70	0.118
		0.65	0.111
		0.6	0.104

690	0.216	0.95	0.121
		0.90	0.117
		0.85	0.112
		0.8	0.107
	0.417	0.9	0.130
		0.85	0.125
		0.78	0.117
		0.70	0.108
		0.65	0.102
	1.011	0.98	0.117
		0.95	0.115
		0.9	0.110
	4.3332	0.6	0.131
		0.55	0.122
		0.52	0.117
710	0.204	0.75	0.131
		0.70	0.124
		0.65	0.117
		0.60	0.109
		0.55	0.102
	0.3984	0.95	0.121
		0.90	0.1168
		0.85	0.112
		0.80	0.102
	0.984	0.85	0.124
		0.80	0.120
		0.78	0.117
		0.7	0.108
		0.65	0.102
	4.313	0.65	0.134
		0.60	0.125
		0.55	0.117
		0.5	0.107

Table 6: Values of K, △, q, V, $\overline{F}$ and N at various tempering times corresponding to the tempering temperature of 630°C

Time (sec.) 10^5	Size class number K	Size class interval △ 10^{-5} cm	Axial ratio q	Calculated volume fraction V	Average radius $\overline{F}$ 10^{-5} cm	Total number of particles per unit volume, N 10^{10}
1.749	10	4.132	0.58	0.117	5.008	13.09
4.283	8	6.198	0.63	0.118	6.56	6.66
9.15	8	6.198	0.55	0.117	7.60	4.70
12.57	8	8.264	0.5	0.119	8.84	2.97

Table 7: Values of K, △, q, V, $\overline{F}$ and N at various tempering times corresponding to the tempering temperature of 660°C

Time (secs.) 10^5	Size class number K	Size class interval △ 10^{-5} cm	Axial ratio q	Calculated volume fraction V	Average radius $\overline{F}$ 10^{-5} cm	Total number of particles per unit volume N 10^{10}
0.435	7	4.132	0.68	0.1167	4.32	20.2
1.008	7	4.132	0.75	0.1167	5.64	10.5
4.356	11	4.132	0.74	0.118	7.73	3.77
8.46	10	6.198	0.7	0.118	9.36	2.26

Table 8: Values of K, $\triangle$, q, V, $\bar{r}$ and N at various tempering times corresponding to the tempering temperature of 690°C

Time (secs.) 10^5	Size class number K	Size class interval $\triangle$ 10^{-5} cm	Axial ratio q	Calculated volume fraction V	Average radius $\bar{r}$ 10^{-5} cm	Total number of particles per unit volume N 10^{10}
0.216	7	4.132	0.9	0.117	4.01	21.27
0.417	7	4.132	0.78	0.117	4.79	11.14
1.011	8	4.132	0.98	0.117	6.33	6.05
4.3332	8	8.264	0.52	0.117	10.49	1.79

Table 9: Values of K, $\triangle$, q, V, $\bar{r}$ and N at various tempering times corresponding to the tempering temperature of 710°C

Time (secs.) 10^5	Size class number K	Size class interval $\triangle$ 10^{-5} cm	Axial ratio q	Calculated volume fraction V	Average radius $\bar{r} \times 10^{-5}$ cm	Total number of particles per unit volume N 10^{10}
0.204	8	4.132	0.65	0.117	5.16	12.45
0.3984	9	4.132	0.9	0.1168	6.33	6.58
0.984	10	4.132	0.78	0.117	7.93	3.99
4.314	9	8.264	0.55	0.117	11.74	1.20

Table 10: Particle size distribution for sample tempered at 630°C for various times.

Size class number, j	1.749 × 10⁵ secs.		4.283 × 10⁵ secs.		9.15 × 10⁵ secs.		12.57 × 10⁶ secs.	
	Major axis, j (10^{-5} cm)	Number of particles in the jth class n_j (10^{10} cm^{-3})	Major axis, j (10^{-5} cm)	Number of particles in the jth class n_j (10^{10} cm^{-3})	Major axis, j (10^{-5} cm)	Number of particles in the jth class n_j (10^{10} cm^{-3})	Major axis, j (10^{-5} cm)	Number of particles in the jth class n_j (10^{10} cm^{-3})
1	4.132	1.562	6.198	0.5712	6.198	0.011	8.262	0.313
2	8.264	4.564	12.396	3.910	12.396	2.178	16.528	1.347
3	12.396	3.693	18.594	1.422	18.594	1.395	24.792	0.834
4	16.528	1.923	24.792	0.505	24.792	0.792	33.056	0.341
5	20.660	0.601	30.990	0.157	30.990	0.185	41.320	0.093
6	24.792	0.285	37.188	0.082	37.188	0.093	49.584	0.017
7	28.924	0.102	43.386	0.020	43.386	0.053	57.848	0.015
8	33.056	0.057	49.584	0.011	49.584	0.019	66.108	0.011
9	37.188	0.081						
10	41.320	0.021						

Table 11: Particle size distribution for the sample tempered at 660°C for various times.

Size class number j	0.495 x 10⁵ secs.		1.008 x 10⁵ secs.		4.35 x 10⁵ secs.		8.46 x 10⁵ secs.	
	Major axis 10^{-5} cm	Number of particles in the jth class n_j 10^{10} cm^{-3}	Major axis 10^{-5} cm	Number of particles in the jth class n_j 10^{10} cm^{-3}	Major axis 10^{-5} cm	Number of particles in the jth class n_j 10^{10} cm^{-3}	Major axis 10^{-5} cm	Number of particles in the jth class n_j 10^{10} cm^{-3}
1	4.132	4.565	4.132	0.459	4.132	0.119	6.198	0.0652
2	8.264	8.300	8.264	3.591	8.264	0.4	12.396	0.5665
3	12.396	4.578	12.396	3.787	12.396	1.055	18.594	0.7640
4	16.528	2.902	16.528	1.596	16.528	1.028	24.792	0.5242
5	20.660	0.573	20.660	0.682	20.660	0.476	30.990	0.1691
6	24.792	0.217	24.792	0.251	24.792	0.307	37.188	0.0951
7	28.924	0.1011	28.924	0.141	28.924	0.199	43.386	0.0585
8					33.056	0.075	49.584	0.0058
9					37.188	0.053	55.782	0.0125
10					41.320	0.025	61.980	0.0044
11					45.452	0.059		

Table 12: Particle size distribution for the sample tempered at 690°C for various times.

Size class number j	0.216 x 10^5 secs.		0.417 x 10^5 secs.		1.011 x 10^5 secs.		4.3332 x 10^5 secs.	
	Major axis, j (10^{-5} cm)	Number of particles in the jth class N_j (10^{10} cm^{-3})	Major axis, j (10^{-5} cm)	Number of particles in the jth class N_j (10^{10} cm^{-3})	Major axis, j (10^{-5} cm)	Number of particles in the jth class N_j (10^{10} cm^{-3})	Major axis, j (10^{-5} cm)	Number of particles in the jth class N_j (10^{10} cm^{-3})
1	4.132	8.257	4.132	4.495	4.132	0.788	8.264	0.084
2	8.264	7.364	8.264	1.575	8.264	1.718	16.528	0.573
3	12.396	3.740	12.396	2.471	12.396	1.377	24.792	0.656
4	16.528	1.254	16.528	1.357	16.528	1.189	33.056	0.269
5	20.660	0.538	20.660	1.015	20.660	0.570	41.320	0.150
6	24.792	0.075	24.792	0.277	24.792	0.198	49.584	0.055
7	28.924	0.060	28.924	0.155	28.924	0.148	57.848	0.009
8					33.056	0.061	66.112	0.134

Table 13: Particle size distribution for the sample tempered at 710°C for various times.

Size class number j	0.984 x 10⁵ secs.		0.3984 x 10⁵ secs.		0.984 x 10⁵ secs.		4.314 x 10⁵ secs.	
	Major axis, j (10^{-5} cm)	Number of particles in the jth class n_j (10^{10} cm^{-3})	Major axis, j (10^{-5} cm)	Number of particles in the jth class n_j (10^{10} cm^{-3})	Major axis, j (10^{-5} cm)	Number of particles in the jth class n_j (10^{10} cm^{-3})	Major axis, j (10^{-5} cm)	Number of particles in the jth class n_j (10^{10} cm^{-3})
1	4.132	0.718	4.132	0.517	4.132	0.104	8.264	0.0011
2	8.264	5.746	8.264	1.741	8.264	0.339	16.528	0.4013
3	12.394	3.017	12.394	2.090	12.394	1.000	24.792	0.5767
4	16.525	1.701	16.525	1.315	16.525	1.058	33.056	0.1724
5	20.657	0.797	20.657	0.549	20.657	0.979	41.320	0.1705
6	24.788	0.189	24.788	0.272	24.788	0.321	49.584	0.0430
7	28.924	0.219	28.924	0.085	28.924	0.186	57.848	0.0202
8	33.056	0.088	33.056	0.007	33.056	0.054	66.112	0.0159
9			57.188	0.051	57.188	0.051	74.576	0.0026
10					41.320	0.018		

Fig. 2(a). Fe-C-Si sample tempered at 630°C for 1.749 x 10^5 secs. Magnification: X2420
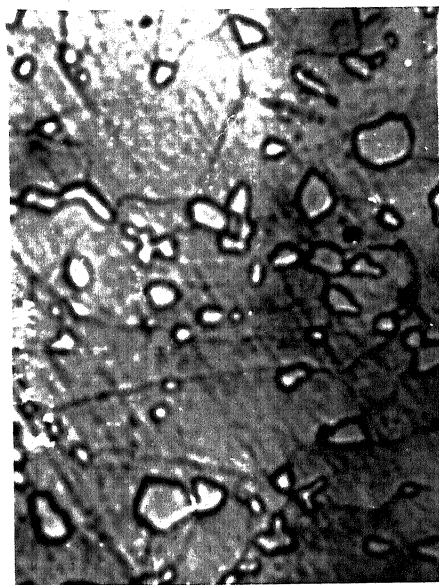
Fig. 2(b). Fe-C-Si sample tempered at 630°C for 4.285 x 10^5 secs. Magnification: X2420
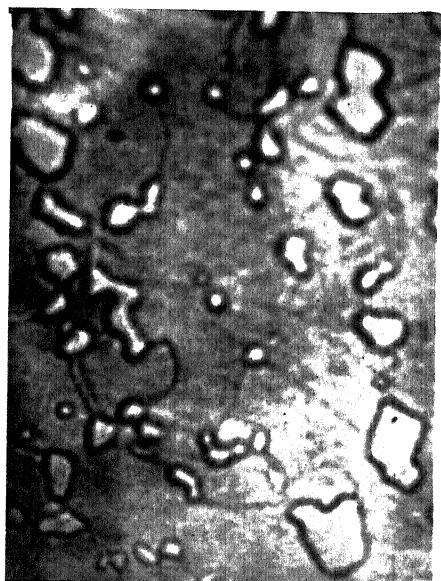
Fig. 2(c). Fe-C-Si sample tempered at 630°C for 9.15 x 10^5 secs. Magnification: X2420

Fig. 2(d). Fe-C-Si sample tempered at 630°C for 12.57 x 10^5 secs. Magnification: X2420
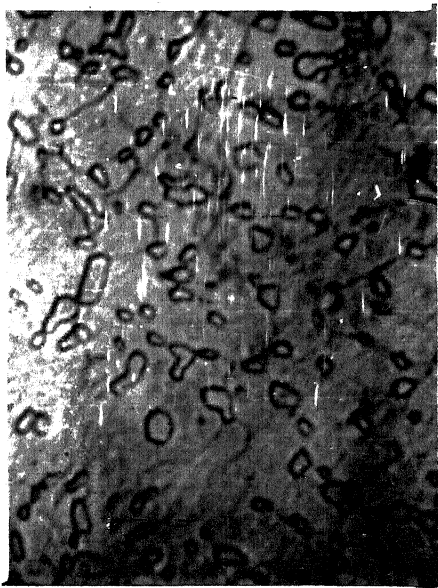
Fig. 3(a). Fe-C-Si sample
tempered at 660°C for 0.435 x
10^5 secs. Magnification: X2420
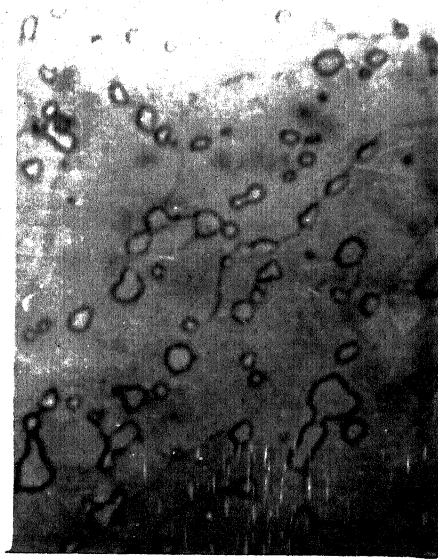
Fig. 3(b). Fe-C-Si sample tempered
at 660°C for 1.008 x 10^5 secs.
Magnification: X2420
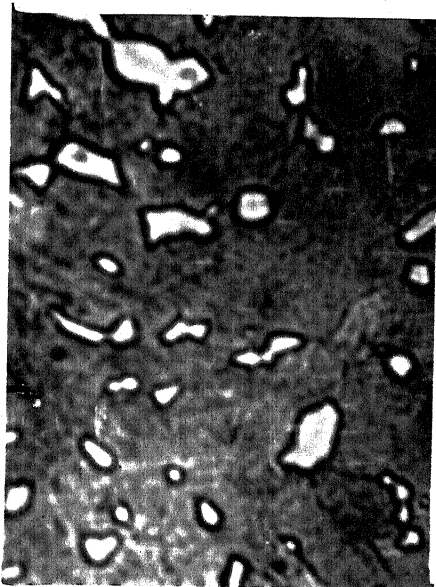
Fig. 3(c). Fe-C-Si sample
tempered at 660°C for 4.356 x
10^5 secs. Magnification: X2420
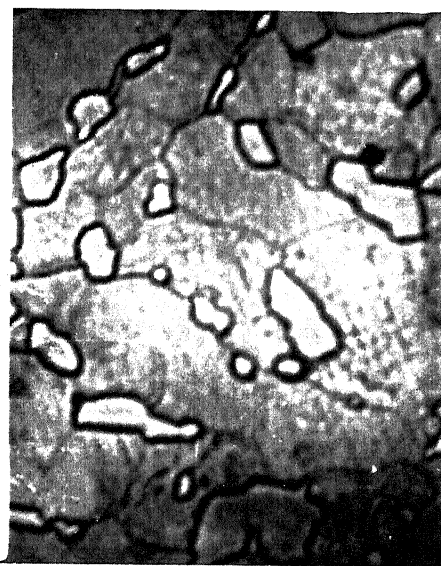
Fig. 3(d). Fe-C-Si sample tempered
at 660°C for 8.46 x 10^5 secs.
Magnification: X2420
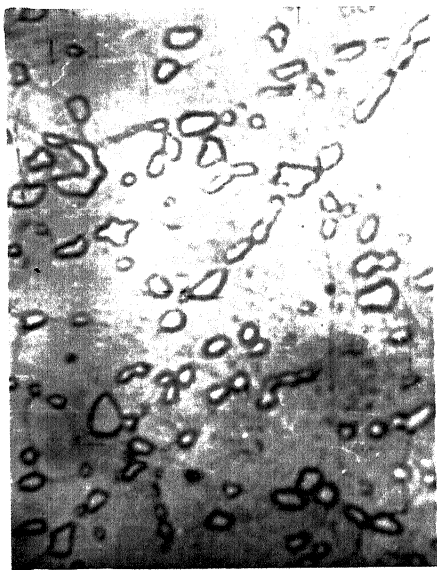
Fig. 4(a). Fe-C-Si sample tempered at 690°C for 0.216 x 10^5 secs. Magnification: X2420

Fig. 4(b). Fe-C-Si sample tempered at 690°C for 0.417 x 10^5 secs. Magnification: X2420
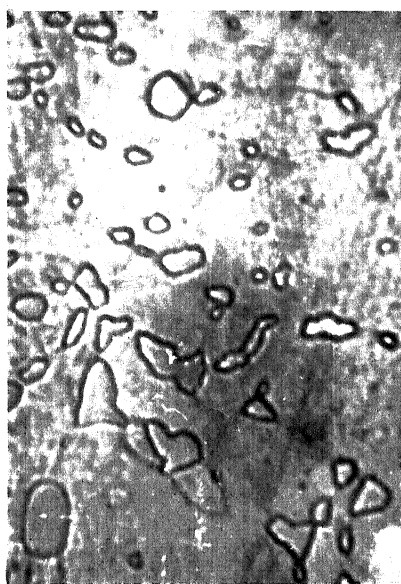
Fig. 4(c). Fe-C-Si sample tempered at 690°C for 1.011 x 10^5 secs. Magnification: X2420
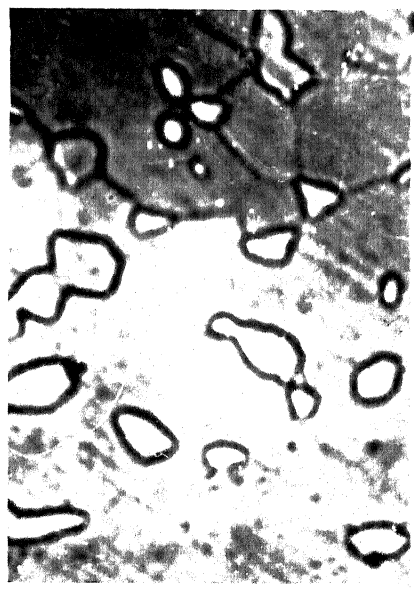
Fig. 4(d). Fe-C-Si sample tempered at 690°C for 4.3332 x 10^5 secs. Magnification: X2420
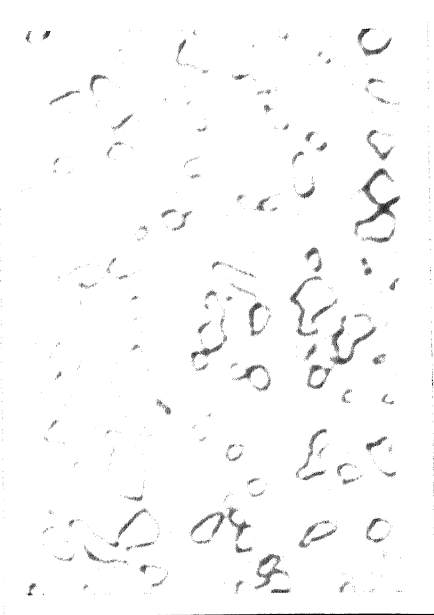
Fig. 5(a). Fe-C-Si sample tempered at 710°C for 0.204 x 10⁵ secs. Magnification: X2420
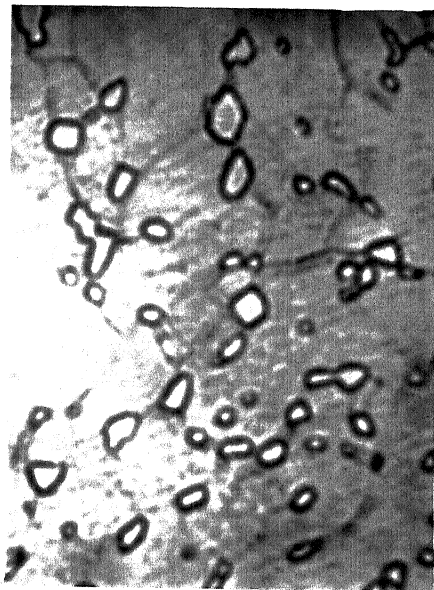
Fig. 5(b). Fe-C-Si sample tempered at 710°C for 0.3984 x 10⁵ secs. Magnification: X2420
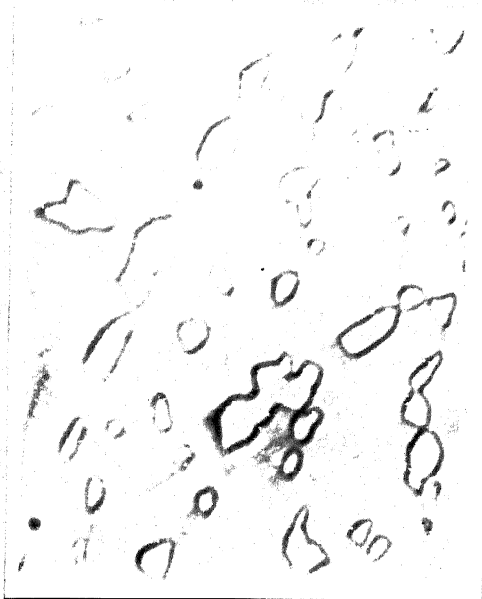
Fig. 5(c). Fe-C-Si sample tempered at 710°C for 0.984 x 10⁵ secs. Magnification: X2420
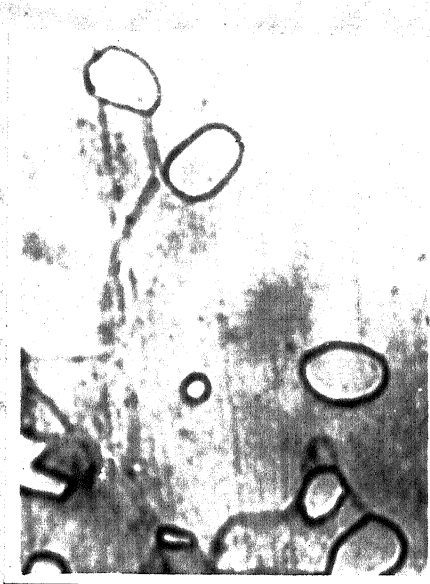
Fig. 5(d). Fe-C-Si sample tempered at 710°C for 4.314 x 10⁵ secs. Magnification: X2420
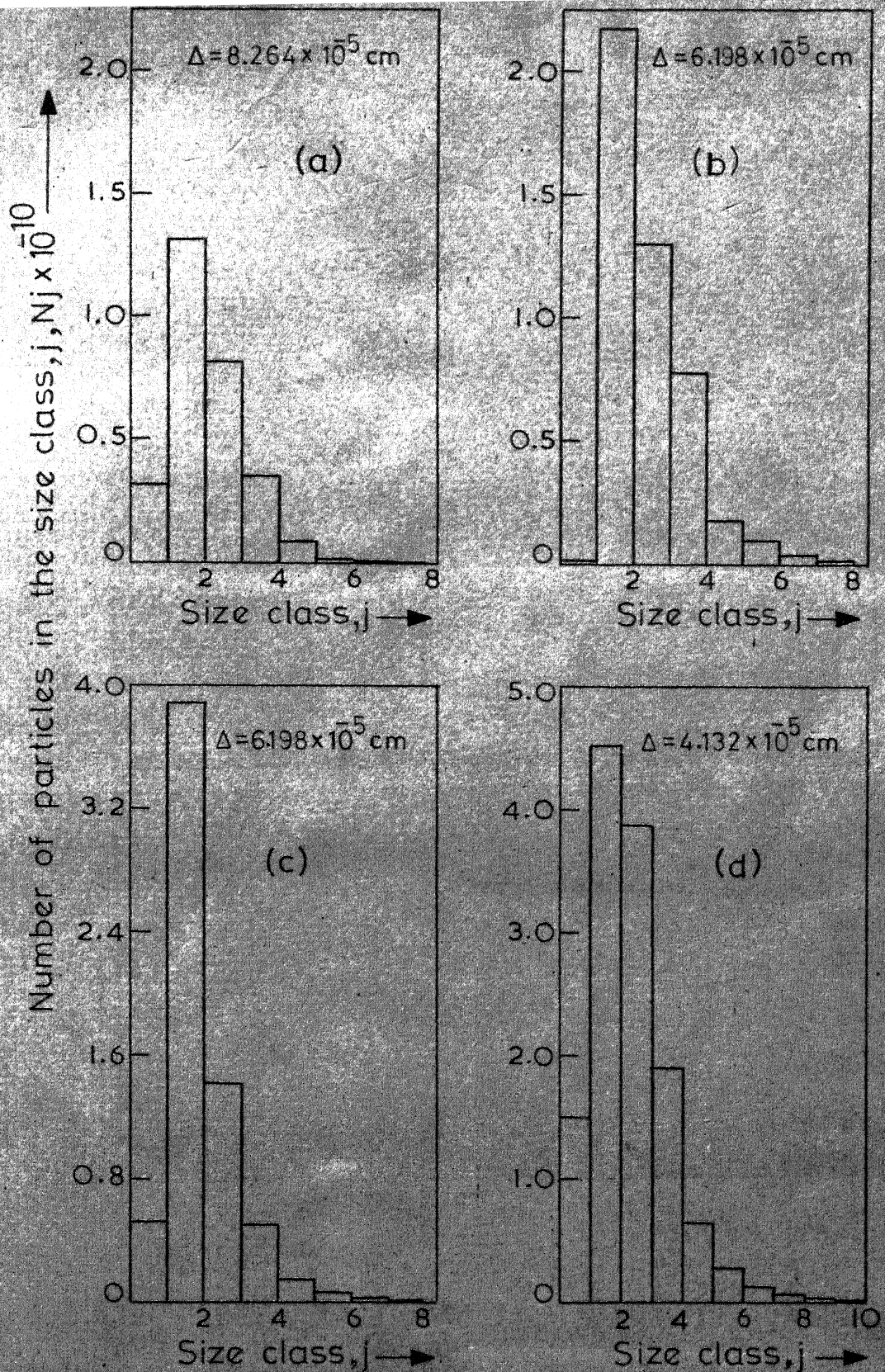
Fig.6 Particle size distribution in the sample tempered at 630°C for (a) 12·57 × 10⁵ secs (b) 9·15 × 10⁵ secs (c) 4.283 × 10⁵ secs (d) 1.749 × 10⁵ secs.
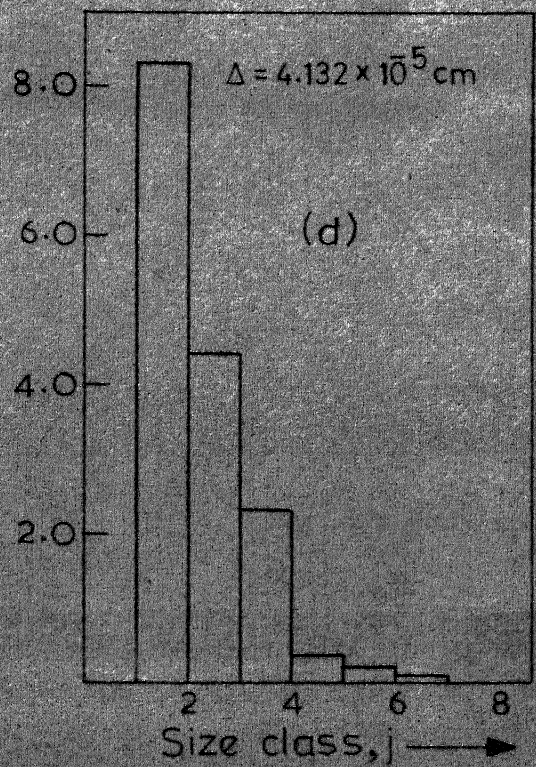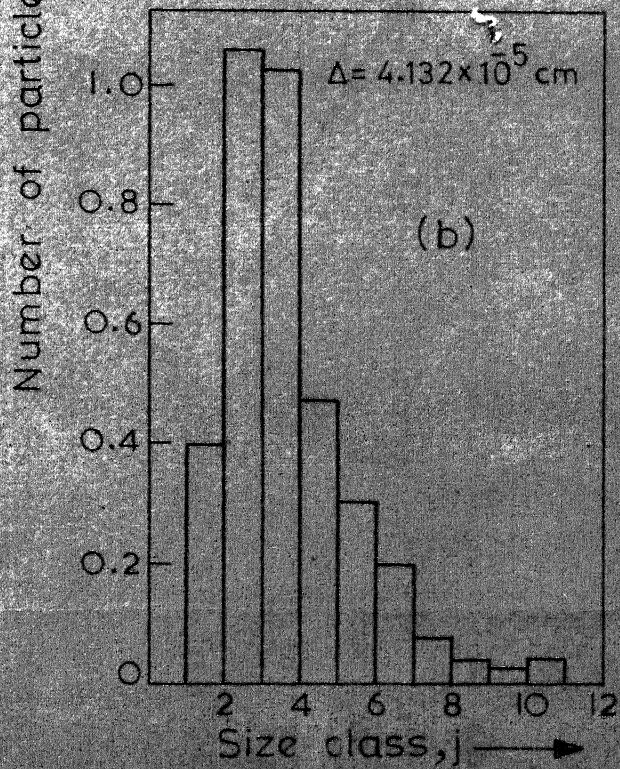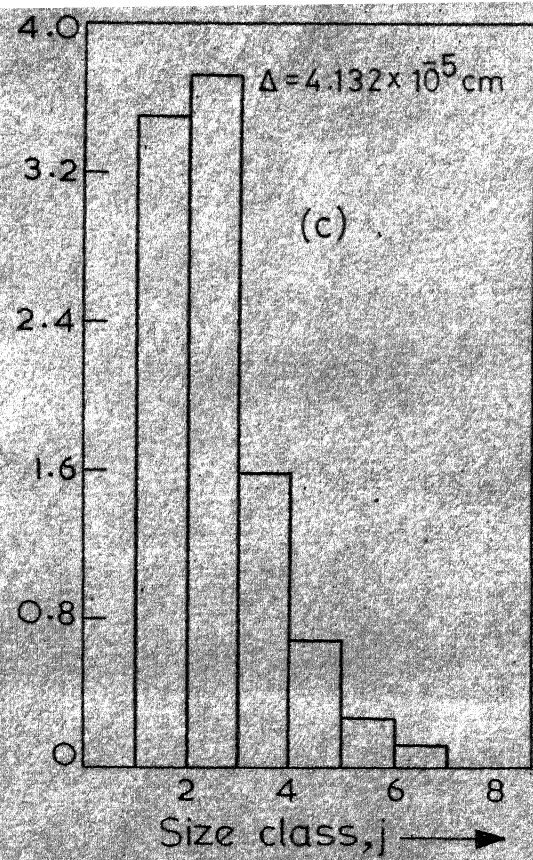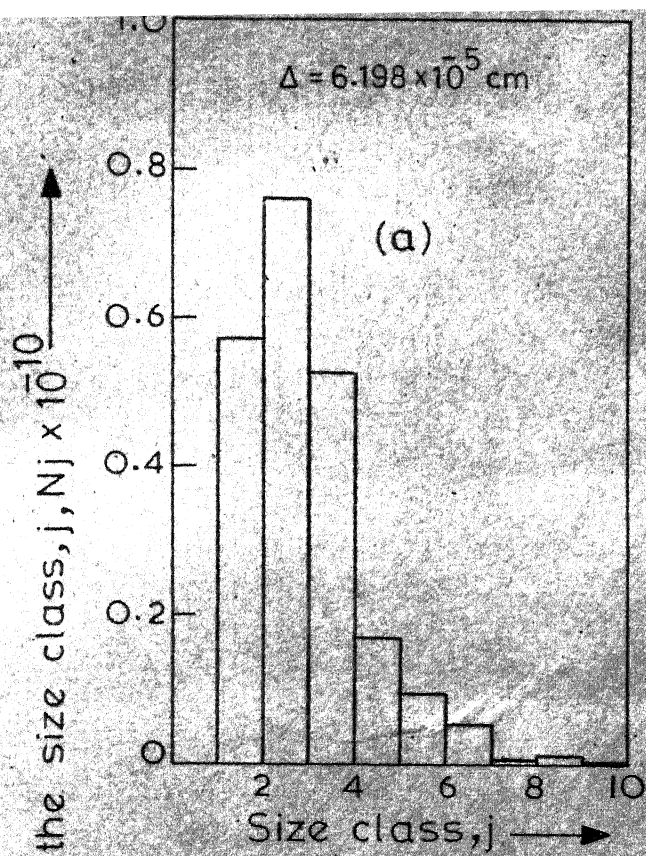
Fig. 7 Particle size distribution in the sample tempered at 660°C for (a) 8.46×10^5 secs (b) 4.356×10^5 secs (c) 1.008×10^5 secs (d) 0.435×10^5 secs.
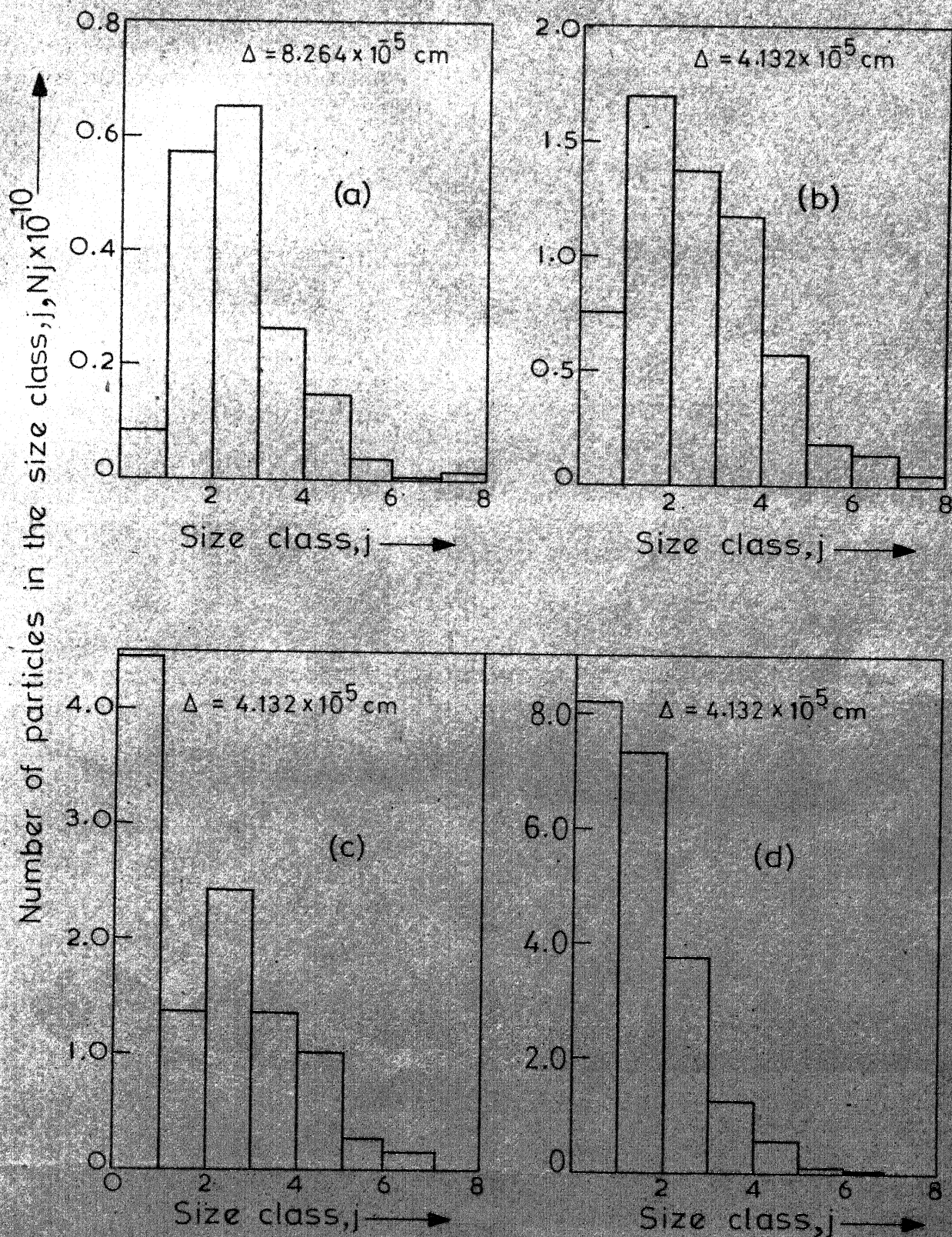
Fig.8 Particle size distribution in the sample tempered at 690°C for (a) 4.3332×10^5 secs (b) 1.011×10^5 secs (c) 0.417×10^5 secs (d) $0.216 \ 10^5$ secs.
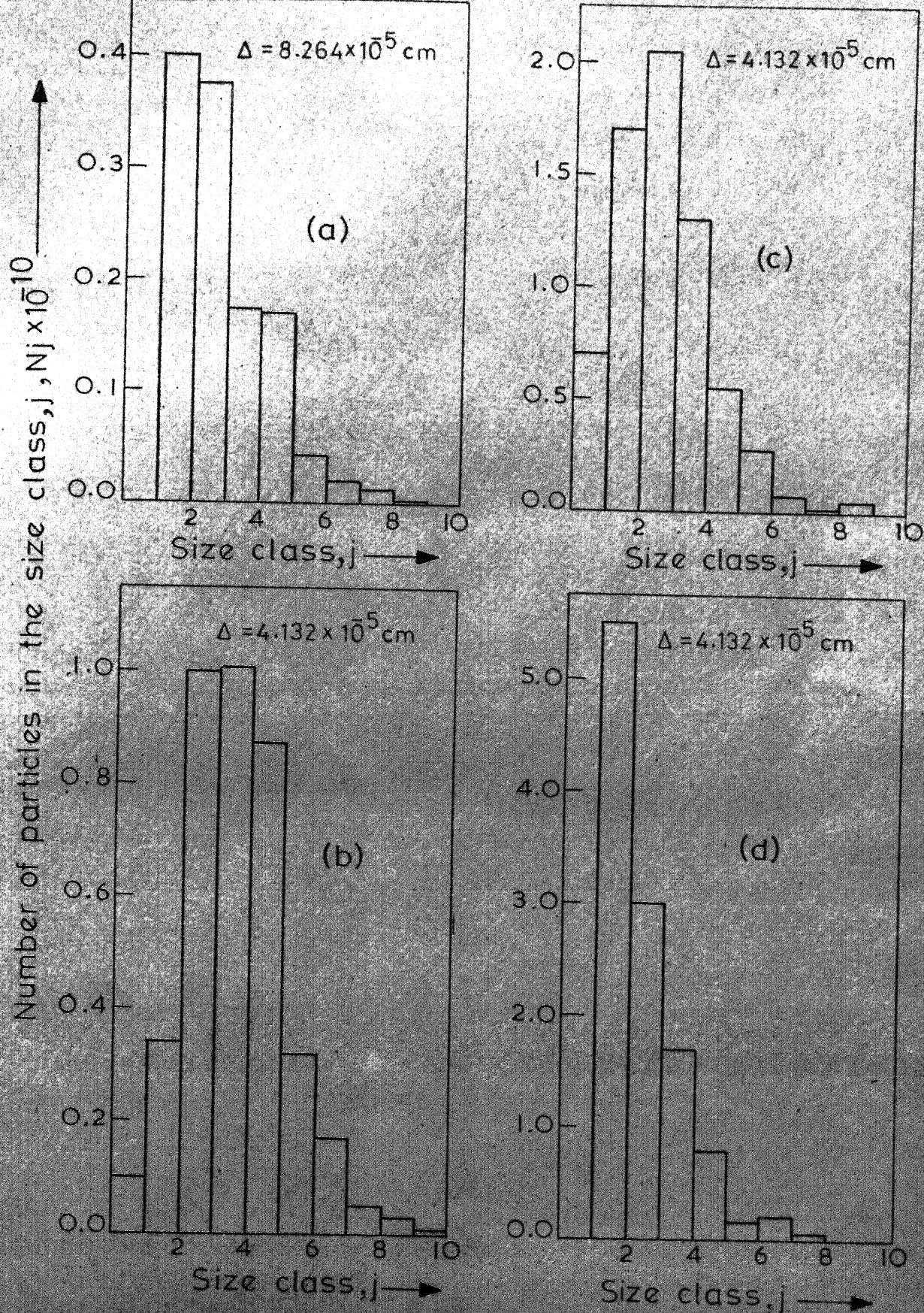
Fig. 9 Particle size distribution in the sample tempered at 710°C for (a) 4.313×10^5 secs (b) 0.948×10^5 secs (c) 0.3984×10^5 secs (d) 0.204×10^5 secs.

CHAPTER 5

DISCUSSION

5.1 Error Analysis:

The scatter in the experimental value may occur due to
the following sources of errors.

Limited resolution of optical microscope: This limitation
puts a restriction on the size of particles which can be observed
under microscope. This will give error in the evaluation of
$\bar{r}$, N, V etc. As is evident, the limited resolution will give
over estimation of $\bar{r}$ and under estimation of N. Because of
partial cancellation of these two opposing factors, the error
in the volume fraction may not be significant. Quantitative
estimation of this error is difficult. For large temperatures
and times however, it may be safely assumed that error due to
this factor is very small.

Magnification error: The actual magnification of the microscope
set up may not be the same as that deduced from the specification
of the lenses. Let,

$$M = \frac{\text{Apparent magnification}}{\text{Actual magnification}}$$

It follows that,

$$\text{Actual} = (\text{observed}) \times M \qquad \qquad \dots \dots (61)$$

$$A_{(\text{actual})} = A_{(\text{observed})} \times M^2 \qquad \dots \dots (62)$$

where observed refers to value obtained using apparent magnification. It is clear that n_i values remain unaffected due to error in the magnification.

From equation (55), (58) and (60)

$$\bar{\bar{F}} = \triangle Z \qquad \dots \dots (63)$$

where

$$Z = \sum_{j=1}^{K} \left[\sum_{i=j}^{K} n_i \, \beta_{j,i} \right] (j) \, \frac{(2+q)}{6} \Big/ \sum_{j=1}^{K} \sum_{i=j}^{K} n_i \, \beta_{j,i}$$

Using equation (61) and (63)

$$\bar{\bar{F}}_{actual} = \bar{\bar{F}}_{observed} \times M \qquad \dots \dots (65)$$

From equation (55) and (56)

$$V = U \frac{\triangle^2}{A} \qquad \dots \dots (66)$$

where

$$U = \frac{\pi}{6 \times K(q)} \, \frac{q}{\,} \sum_{j=1}^{K} \left\{ \sum_{i=j}^{K} n_i \, \beta_{j,i}(j)^3 \right\}$$

Using equations (61), (67) and (66) we get

$$V_{actual} = V_{observed} \qquad \dots \dots (67)$$

Thus the error due to magnification does not change the value of V.

Using a similar procedure it may be shown that,

$$N_{actual} = N_{observed} / M^3 \qquad \dots \dots (68)$$

Using a stage micrometer, it was found that in this work
M = 1.695. Through out this investigation the lenses were kept

same and the same procedure was followed to obtain photograph
of micrometer as was used to obtain micrographs.

Though the absolute values of $\bar{r}$ and N do change with
error in magnification, the slopes of log $\bar{r}$ vs log t and log N
vs log t remain unaffected. The experimental size distribution
will be scaled down due to this error.

Error in measurement of section sizes:

As the particles were measured with ordinary scale it
is but natural that error will be introduced in measurement.
The minimum distance measurable was 0.05 cm. Therefore any
distance below 0.025 can not be measured and hence this is the
maximum error possible. Let us examine how $\bar{r}$, N and V change
with this error. Let $\pm e$ be the maximum error in measurement
of section size. The maximum error in $\bar{r}$, N and V which can
occur due to this factor can be calculated as follows.

First add $+e$ to all the section sizes measured for a
particular sample and find out new section size distribution.
From this, particle size distribution $\bar{r}$, N and V can be calculated
as described before. Let the new values be denoted by $(\bar{r})_+$,
$(V)_+$ and $(N)_+$. Now subtract e from all the section sizes
measured for the sample and calculate $(\bar{r})_-$, $(V)_-$ and $(N)_-$ in a
similar way.

Calculations were done for Fe-C-Si sample tempered at
690°C for 26 hrs. with $e = \pm 0.025$ cm. on micrograph. It was
found that maximum error found in $\bar{r}$ was 11.5% while that for V
and N was $\pm 12.4\%$ and 14% respectively. The errors are not very

large when see that an error of $\pm$ 20% has been reported in literature.

Error due to shrinkage of film:

For this the error analysis is exactly same as that for the error due to magnification due to micrographs. If,

$$S = \frac{\text{Apparent length of film}}{\text{Actual length of film}}$$

5.2 Coarsening Kinetics:

A general equation for the variation of average particle with time can be written as

$$\bar{r}^n - \bar{r}_o^n = K^* t \qquad \qquad \ldots \ldots (69)$$

where n is a coefficient and K^* is a constant. It has been shown that under certain conditions

n = 2 for interface controlled coarsening[2]

n = 3 for diffusion controlled coarsening[2,3]

n = 4 for grain boundary controlled coarsening[13,16]

The constant K^* is different for three cases. If $\bar{r} \gg \bar{r}_o$ we can approximate equation (69) by the following expression.

$$\log \bar{r} = \frac{1}{n} \log K^* + \frac{1}{n} \log t \qquad \ldots \ldots (70)$$

Thus from the slope of $\log \bar{r}$ vs $\log t$ one can obtain   information on the coarsening mechanism. The results of the present investigations were plotted as $\log \bar{r}$ vs $\log t$ (Fig. 10) and the best fitting straight lines were drawn through the points. The

with time[51]. The distribution function $f(r,t)$ may be written as

$$f(r,t) = P^2 h_1(P) \, g(t)$$

where $P^2 h_1(P)$ is a function of P only, $P = r/\bar{r}$, $g(t)$ is a function of t only and $f(r,t)$ is such that at a given time

$$\int_0^\infty f(r,t) \, dr = N.$$

Hence

$$N = \int_0^\infty f(r,t) \, dr = \int_0^\infty P^2 h_1(P) \, g(t) \, dr$$

$$= g(t) \, \bar{r} \int_0^\infty P^2 h_1(P) \, dP$$

But according to the theory (see chapter II)

$$\int_0^\infty P^2 h_1(P) \, dP = \frac{9}{4}$$

Hence

$$g(t) = \frac{N}{\bar{r}} \times \frac{4}{9}$$

and

$$f(r,t) = \frac{N}{\bar{r}} \times \frac{4}{9} \, P^2 h_1(P) \qquad \bullet \ \bullet \ \bullet \ \bullet \ (72)$$

Also

$$N_j = f(r,t) \, dr \simeq f(r,t) \, \frac{(2+a)}{6} \qquad \bullet \ \bullet \ \bullet \ (73)$$

Combining equations (72) and (73)

$$r^2 h_1(P) = \frac{9}{4} \frac{\bar{r}}{(q+2)\,\triangle\,/6} \frac{N_1}{N} \qquad \dots \dots (74)$$

Under steady state condition the function $r^2 h_1(P)$ should have a maximum at $P = 1.13$ and should have a sharp cut off at $P = 1.5$.

In order to compare the experimental size distribution with that predicted by the theory the function $r^2 h_1(P)$ was evaluated using equation (74) and plotted against $r_j/\bar{r}$ for tempering temperatures 630°C, 660°C, 690°C and 710°C in figures 12, 13, 14 and 15 respectively. r_j is calculated using equation (59).

The distribution curves show that the maxima do not occur at $P = 1.13$ although these are very close to $P = 1.13$ and tend to shift towards higher values of p with increase in time at a given tempering temperature. Also the curves do not show any sharp cut off at $P = 1.5$. Each curve has a long tail. The tail becomes more prominent as the temperature is decreased. However at a given tempering temperature, the curves for different tempering times lie very close to each other. Thus the curves do not appear to have reached a steady state.

5.4 Determination of activation energy for the coarsening process

The constant K^* in the general empirical equation (69) can be represented as the rate constant for the coarsening process. The empirical rate constants obtained from fig. 10 are listed in Table 14.

The activation energy for the process can not be determined

Table 14

Intercepts with statistical straight lines and straight
line with slope 1/3 at various temperatures.

Temperature °C	Statistical intercept	Intercept with slope 1/3	Coarsening rate constant K*
630	-5.88	-6.07	6.166×10^{-19}
660	-5.88	-5.95	1.413×10^{-18}
690	-5.47	-5.85	2.818×10^{-18}
710	-5.59	-5.75	5.623×10^{-18}

from the values of empirical K* as the coefficient n appears to
change with temperature. In order to obtain information about
mechanism of this coarsening process, it is assumed on the basis
of the results of the section 5.2 that the coarsening in the
Fe-C-Si system is diffusion controlled. Hence after equation
(15), $\bar{r}^3 = K^*t$, the value of K* therefore can be obtained by
plotting log r vs log t and then forcing the best straight line
with a slope of 1/3. The intercept of this plot corresponds to
1/3 log K*. Such plots are shown in fig. 16 and the K* values
are listed in table 14. A plot of log K* vs $\frac{1}{T}$ in fig. 17 gives
the average empirical activation energy of 51.03 kcal/gm-atom.
The constant K* after equation (15) is given by

$$K^* = \frac{8}{9} \frac{D_{eff.} \, \gamma \, C_e \, V_m^2}{RT} .$$

The effective diffusion coefficient D_{eff} for the Fe-C-Si
system after equation (23) is

$$D_{eff} = \frac{C_{Fe}}{C_C} \frac{v_{Fe}^2}{v_C^2} D_{Fe}$$

Hence

$$K^* = \frac{8 \gamma v_m^2 C_e C_{Fe}}{9 RT C_C} \cdot \frac{v_{Fe}^2}{v_C^2} \cdot D_{Fe} \qquad \dots (75)$$

In this expression C_C the average concentration of carbon in the matrix is close to C_γ which is again close to C_e. Hence $C_C \approx C_e$ and these two terms may be cancelled from equation (75). The equation (75) becomes

$$K^* = \frac{8}{9} \frac{\gamma}{R} \frac{C_{Fe} v_m^2 v_{Fe}^2}{v_C^2} \frac{D_{Fe}}{T} \qquad \dots (76)$$

Since the temperature dependence of the term in square bracket in eqn. (76) is negligible from 710°C to 630°C a plot of log K^*T vs $1/T$ should give a value for activation energy diffusion of iron in ferrite. Such a plot shown in fig. 17 yields a value of 53.305 Kcal/gm-atom which may be compared with a published value of 60.0 Kcal/mole[67] for the self diffusion of Fe in -iron[66]. Considering the assumptions involved the agreement is considered to be reasonable.

5.5 Growth of individual particle

Dehoff[65] has recently suggested a method for obtaining the growth rate of individual particles from a size distribution of these particles in the system. If $N(r,t)$ be the number of particles per unit volume of size r, at time we can define a quantity $N(> r,t)$ which gives the number of particles of size

greater than r at time t in the following manner.

$$N(> r, t) = \int_{r}^{r_{max}} N(r, t) \, dr \qquad \qquad \ldots \ldots (77)$$

where r is the size of the particle and r_{max} is the maximum size at time t. If it is assumed that the growth path of individual particles do not cross the value of function $N(> r, t)$ will be same for a given particle at all times. This suggests a method for graphically obtaining the growth rate of any particle.

In the iron-carbon-silicon system considered here the growth path of individual particles during coarsening are unlikely to cross each other. Hence above procedure may be applied. In terms of particle size distribution N_j, the equation (77) may be written the following manner.

$$N(> r_j, t) = \sum_{j+1}^{K} N_j$$

where K represents the size class containing particles of maximum size r and $r_j = \frac{(2+a)}{K^a} (j\triangle)$. Figs. 19 to 26 show the plots of $N(> r, t)$ i.e. $\sum_{j+1} N_j$ against r_j, for the Fe – 0.74%C – 0.37%Si alloy tempered at 630°C, 660°C, 690°C and 710°C for various times. Cross cuts were taken from these curves at constant $N(> r, t)$ in several positions. These cross cuts are indicated in the figs. 19 to 26. They give the values of r of a given particle at different times at a given temperature. The change in the value of r with time obtained in the cross cuts are shown in the figs. 27 to 34. It is to be noted that figs.

19, 21, 23, 25, 28, 29, 31 and 32 show the decrease in size of small particles where as figs. 20, 22, 24, 26, 27, 30, 33 and 34 show that larger particles increase with time and the growth rate is large when time is small and decreases with increase in time. The growth rate of particles at the tempering times of 4.283×10^5 secs., 4.356×10⁵ secs ₁.011 $\times 10^5$ secs. and 0.984×10^5 secs. at temperature of 630°C, 660°C, 690°C and 710°C respectively are obtained from gfigs. 27, 28, 29, 30, 31, 32, 33, and 34. The growth rates thus obtained are plotted against r for the above mentioned time and temperature. These are shown in fig. 35, 36, 37 and 38. These figures show that the growth rate is negative at smaller sizes, becomes positive at larger sizes and tends to approach a maximum. The maximum in growth rate occurs approximately at $r = 2\bar{r}$ at 630°C and 710°C (Fig. 35 and 38) and the growth rate is zero at about $r = \bar{r}$.

The above result is consistent with Greenwood's theory. This theory suggests that $r \frac{dr}{dt}$ vs $\frac{1}{r}$ is linear. Such plots are shown in figs. 39, 40, 41 and 42. The slope of these lines at 630°C, 660°C, 690°C and 710°C are 5.6×10^{-17} cm^3/sec., 15.9×10^{-17} cm^3/sec., 1.06×10^{-17} cm^3/sec. and 0.5×10^{-17} cm^3/sec. respectively. These values may be compared with values of 6.75×10^{-17}, 10.49×10^{-17}, 18.25×10^{-17} and 23×10^{-17} cm^3/sec. calculated from equation (9) using values of $\gamma = 700$ ergs/cm^2,[67], the diffusion coefficient ofcarbon $D = 0.02$ exp $(-\frac{20100}{RT})$,[68] the molar volume of cementite, $V_m = 24.3$ cm^3/mole,[67] equilibrium solubility of cementite in α-Fe, $\%C_e = 2.55$ exp $(-\frac{9700}{RT})$,[61] The values of $\bar{r}$ calculated from these plots are 9.7×10^{-5} cm, 10.5×10^{-5} cm, 9.5×10^{-5} cm and 6.6×10^{-5} cm,

710°C, 690°C, 660°C and 630°C respectively. These values may be compared with the experimental values of 7.93×10^{-5} cm, 6.33×10^{-5} cm, 7.73×10^{-5} cm and 6.56×10^{-5} cm at 710°C, 690°C, 660°C and 630°C respectively. The agreement is considered good because the accuracy is not expected to be high. It was possible to have only limited number of points on the graph. Thus inspite of its simplicity, Greenwood's theory of diffusion controlled coarsening seems to be in reasonable agreement with our experimental results. This analysis also supports our earlier conclusion that the coarsening process in Fe – 0.74%C – 0.37%Si alloy at 630°C, 660°C, 690°C and 710°C is diffusion controlled.

5.6 Determination of surface energy

Surface energy γ can be evaluated from equation (75) by substituting the values of all other terms. However, Ardell[13] has pointed out that equation (75) for 'K^*' is strictly valid when the volume fraction of cementite is nearly zero. The volume fraction of cementite in the Fe-C-Si alloy used in this investigation is 0.117. The equation (75) may be written after Ardell[13] as

$$= \frac{9K^* \ RT \ V_C^2}{8C_{Fe} \ V_m^2 \ V_{Fe}^2 \ D_{Fe}} \left(\frac{4}{27 \ \nu} \right) \quad \cdots \cdot (76)$$

where ν is a function of volume fraction of cementite. The value of ν calculated from Ardell's[13] expression for the volume fraction 0.117 of cementite is 0.86. The value of V_C, the difference in the volume of one mole of Fe_3C and 3 mole of Fe in ferrite is

2.1 cm^3/mole.[67] The other values are given below:

Concentration of iron in ferrite, C_{Fe} = 0.14 mole/cm^3

Volume of cementite per mole of carbon, V_m = 24.3 cm^3/mole.[67]

Molar volume of iron in ferrite, V_{Fe} = 7.09 cm^3/mole.[67]

Diffusivity of iron in ferrite, D_{Fe} = 2.0 exp $(-\frac{60000}{RT})$.[66]

Substituting these values in equation (78) surface energies of 874, 800, 1130, and 1110 ergs/cm^2 are found at 710°C, 690°C, 660°C and 630°C respectively. Thus it is seen that these results are in very good agreement with expected value of about 700 ergs/cm^2.

5.7 Effect of silicon on coarsening kinetics

Fortunately the results of an investigation carried out in this laboratory on the coarsening kinetics of cementite in an Fe - 0.79%C alloy at 630, 660, 688 and 712°C are available. These results show that in this temperature range the coarsening is diffusioncontrolled but the particle size distribution does not approach a steady state. A similar behaviour was observed in this investigation in the Fe-C-Si alloy. The empirical activation energy of coarsening of 52.17 Kcal /gm-atom found in the iron carbon alloy is close to the value of 51.03 Kcal /gm-atom found in the Fe-C-Si alloy. However, the values of coarsening rate constant K° found in the Fe-C-Si alloy are only about 40% of the values of K° found in the Fe-C alloy. Thus the presence of silicon considerably reduces the rate of coarsening. The surface energy of cementite found in the Fe-C-Si alloy 874, 800, 1130 and 1110 ergs/cm^2 are also much less than the values of 2290, 1850, 2020

and 2700 ergs/cm^2 in the Fe-C alloy. It is thus clear that the presence of silicon considerably reduces the interfacial energies between cementite and ferrite which in turn is responsible for slower coarsening rate of cementite particles.

CHAPTER 6

SUMMARY AND CONCLUSIONS

Samples of steel containing 0.74%C and 0.37%Si were hardened and tempered at 710°C for 5 hrs, 11 hrs, 27 hrs and 120 hrs, at 690°C for 6 hrs, 12 hrs, 28 hrs and 120 hrs, at 660°C for 12 hrs, 28 hrs, 120 hrs and 240 hrs and at 630°C for 48 hrs, 120 hrs, 240 hrs and 350 hrs. The particle size distribution in these samples was determined and the results were analysed in terms of theories of coarsening. The following conclusions were drawn:

(i)   log $\bar{r}$ vs log t plots were straight lines with slopes of about 0.29 to 0.32

(ii) log N vs log t plots were straight lines with a slope of 0.80 to 0.87

(iii) Although the above results suggest that the coarsening is diffusion controlled, the particle size distribution did not reach a steady state.

(iv) Activation energy calculated from coarsening rate constant is 53.3 Kcal/gm-atom, which is close to that of diffusion of iron in   -iron.

(v)   The coarsening rate constants K° in the presence of the silicon are about 40% of those in the pure iron carbon.

(vi) Interfacial energy of cementite-ferrite interface was found to be around 950 ergs/cm^2. Thus silicon appears to decrease the interfacial energy.

(vii) The growth rate of individual particles was determined by applying a new method. The results obtained also indicate coarsening to be diffusion controlled.
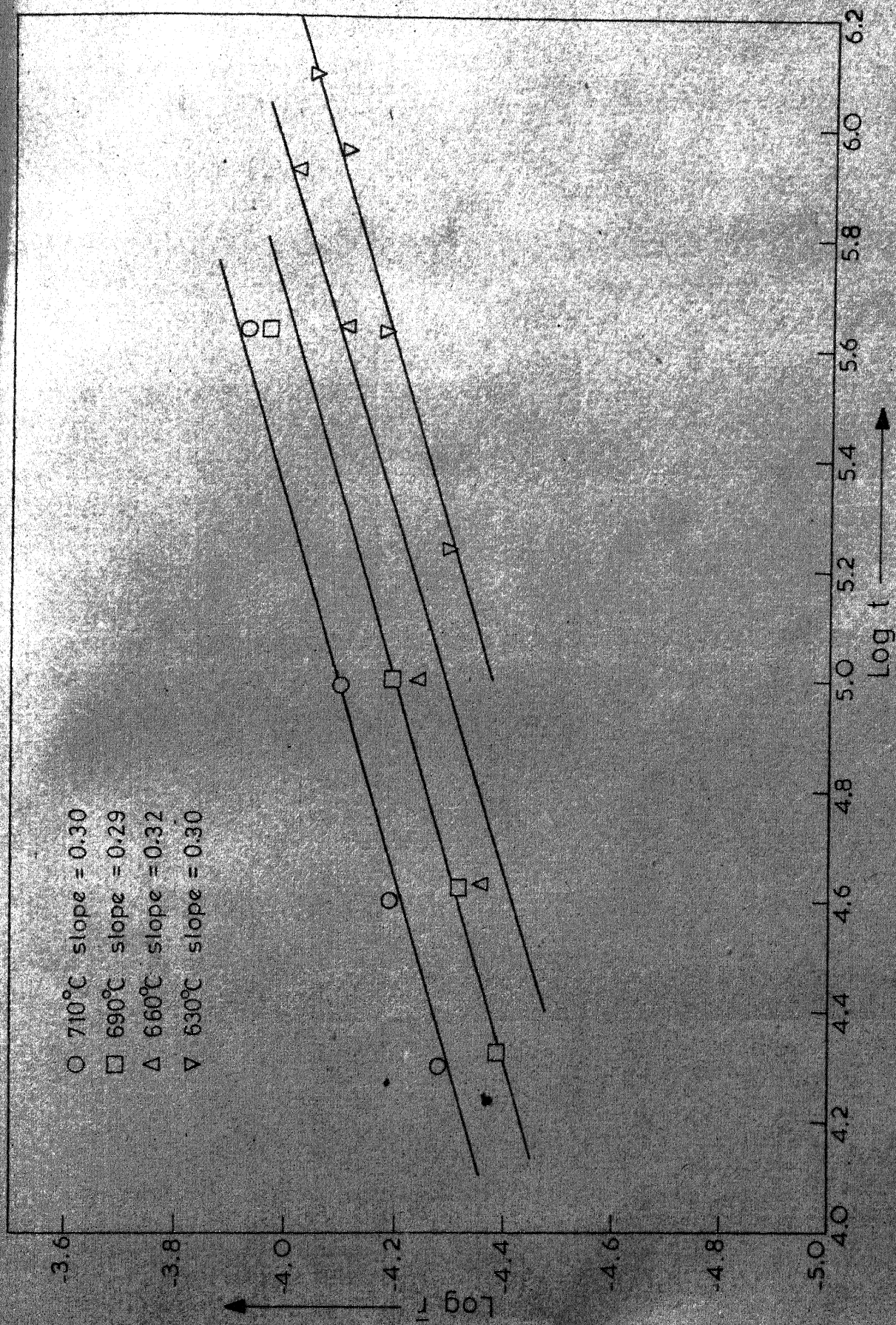
Fig. 10 Plot of log $\bar{r}$ vs. log t for Fe – 0.74% C – 0.37% Si hardened and tempered at at various temperature.
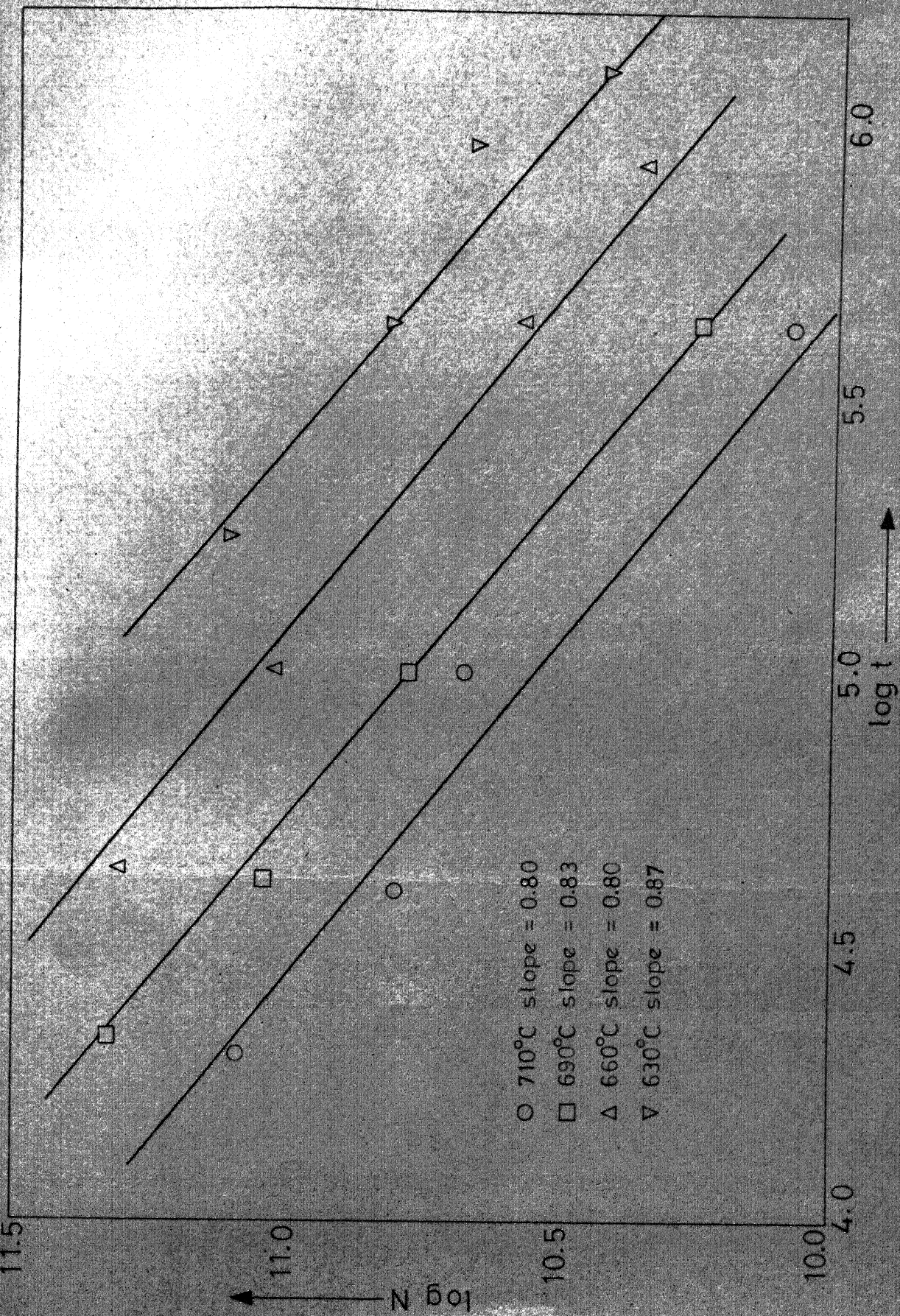
Fig.11 Log N vs. log t plot for the Fe–0.74% C–0.37% Si sample tempered at various temperatures.

O 710°C slope = 0.80
□ 690°C slope = 0.83
△ 660°C slope = 0.80
▽ 630°C slope = 0.87

log t

log N

The graph axes are labelled:

Vertical axis: $\dfrac{9}{4} \dfrac{\bar{r}}{(2+q)\,\Delta/6} \dfrac{N_j}{N}$ with gridlines at 1.0, 2.0, 3.0, 4.0, 5.0

Horizontal axis: $r_j/\bar{r}$ with gridlines at 1.0, 2.0, 3.0

Curve labels:

- Theoretical
- 4.283 × 10^5 secs.
- 9.15 × 10^5 secs.
- 12.57 × 10^5 secs.
- 1.749 × 10^5 secs.
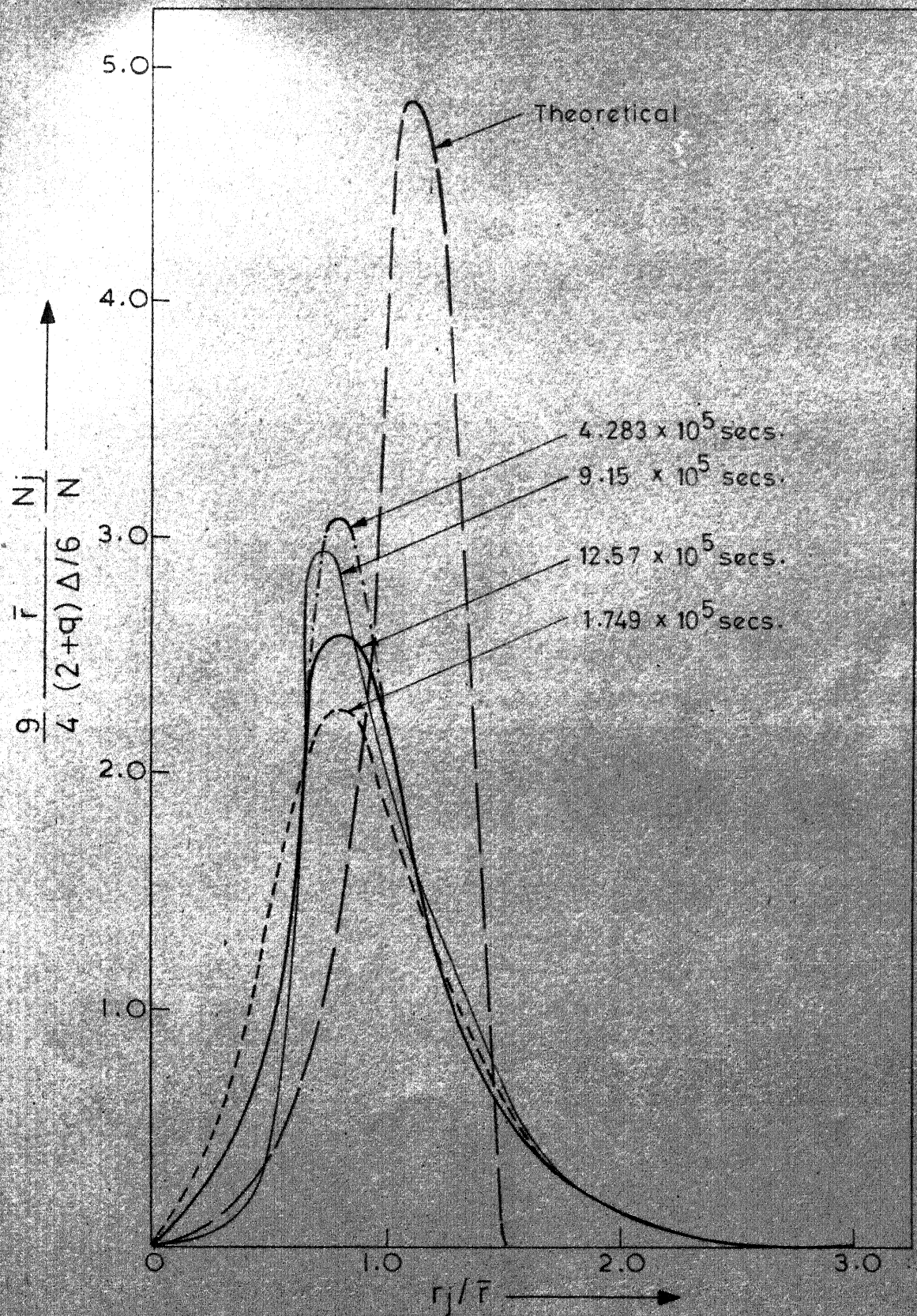
Fig.12 The normalised size distribution curve for the sample tempered at 630°C.
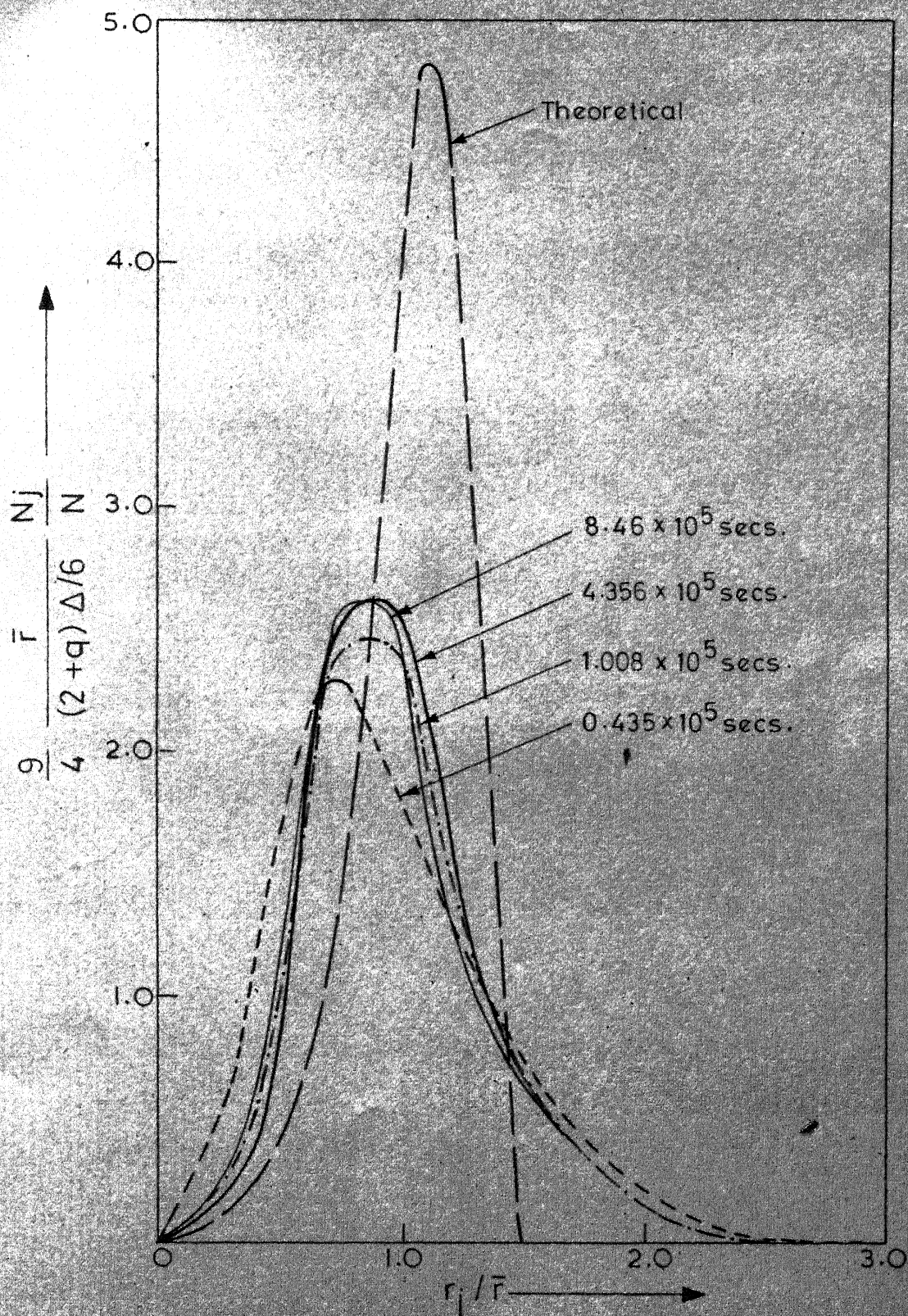
Fig.13 The normalised size distribution curve
for the sample tempered at 660°C.

Axis labels:
- Y-axis: $\dfrac{9}{4} \dfrac{\bar{r}}{(2+q)\,\Delta/6} \dfrac{N_j}{N}$
- X-axis: $r_j/\bar{r}$

Curve labels:
- Theoretical
- 8.46×10^5 secs.
- 4.356×10^5 secs.
- 1.008×10^5 secs.
- 0.435×10^5 secs.
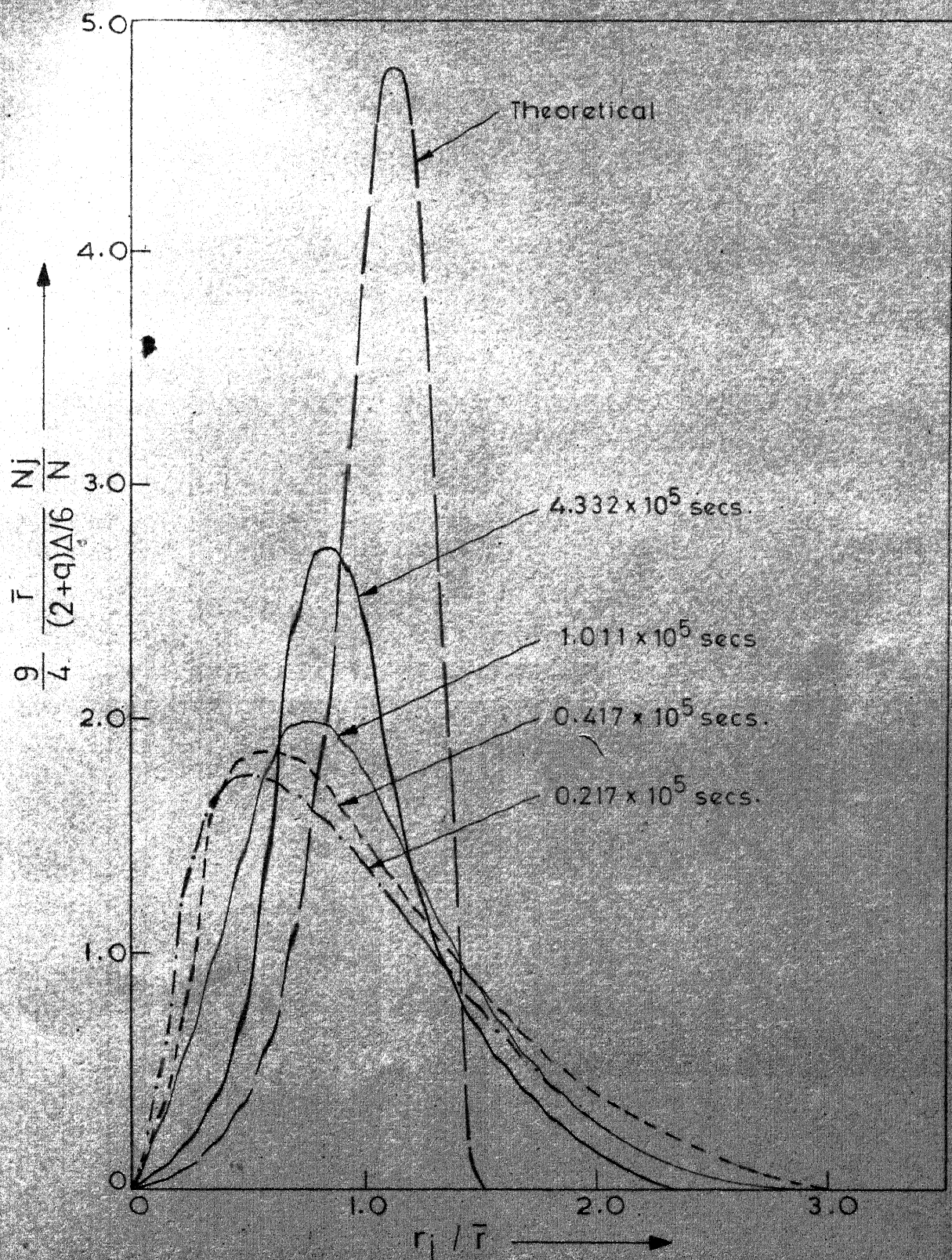
Fig.14 The normalised size distribution curve for the sample tempered at 690°C.
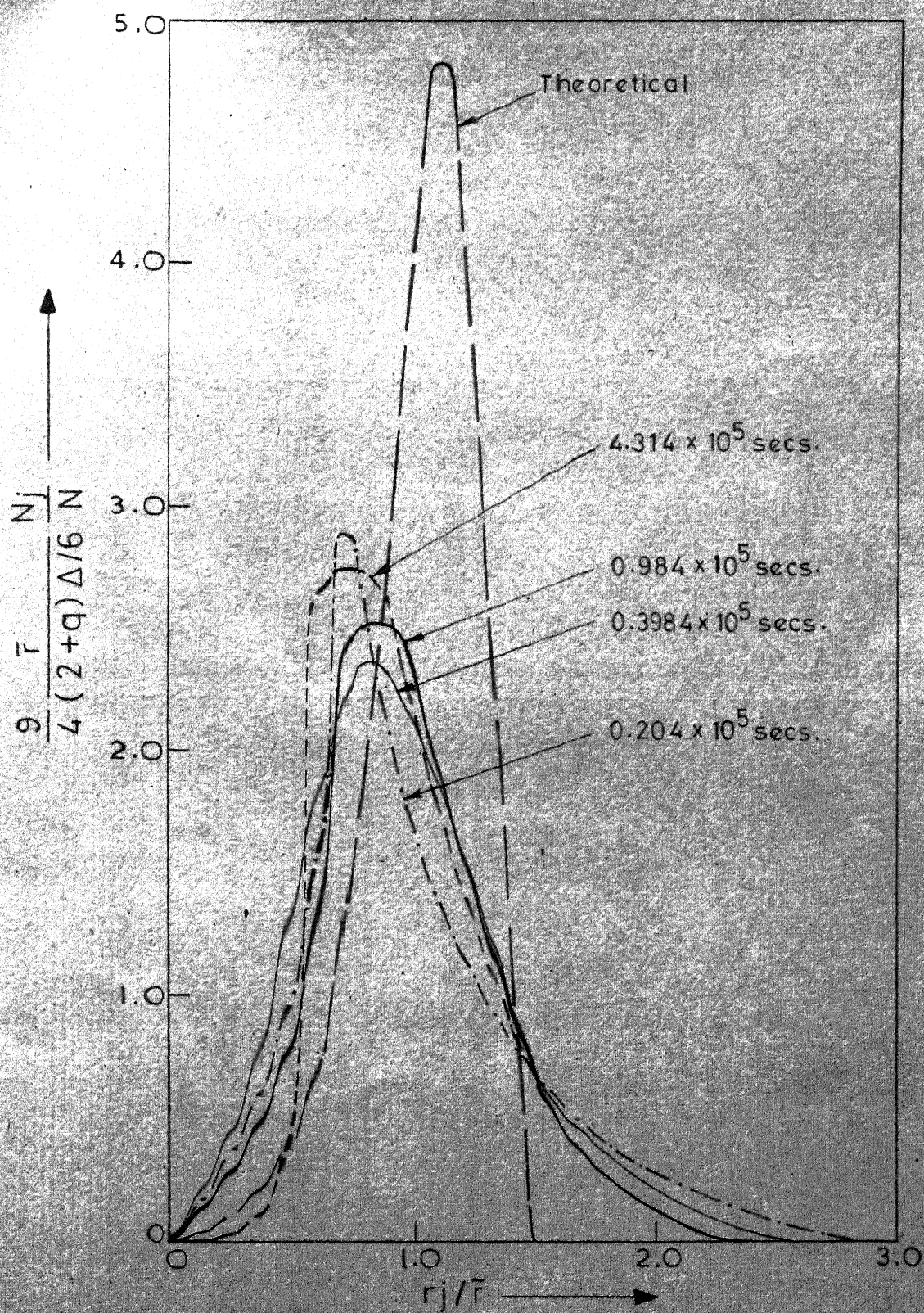
Fig. 15   The normalised size distribution curve
for the sample tempered at 710°C
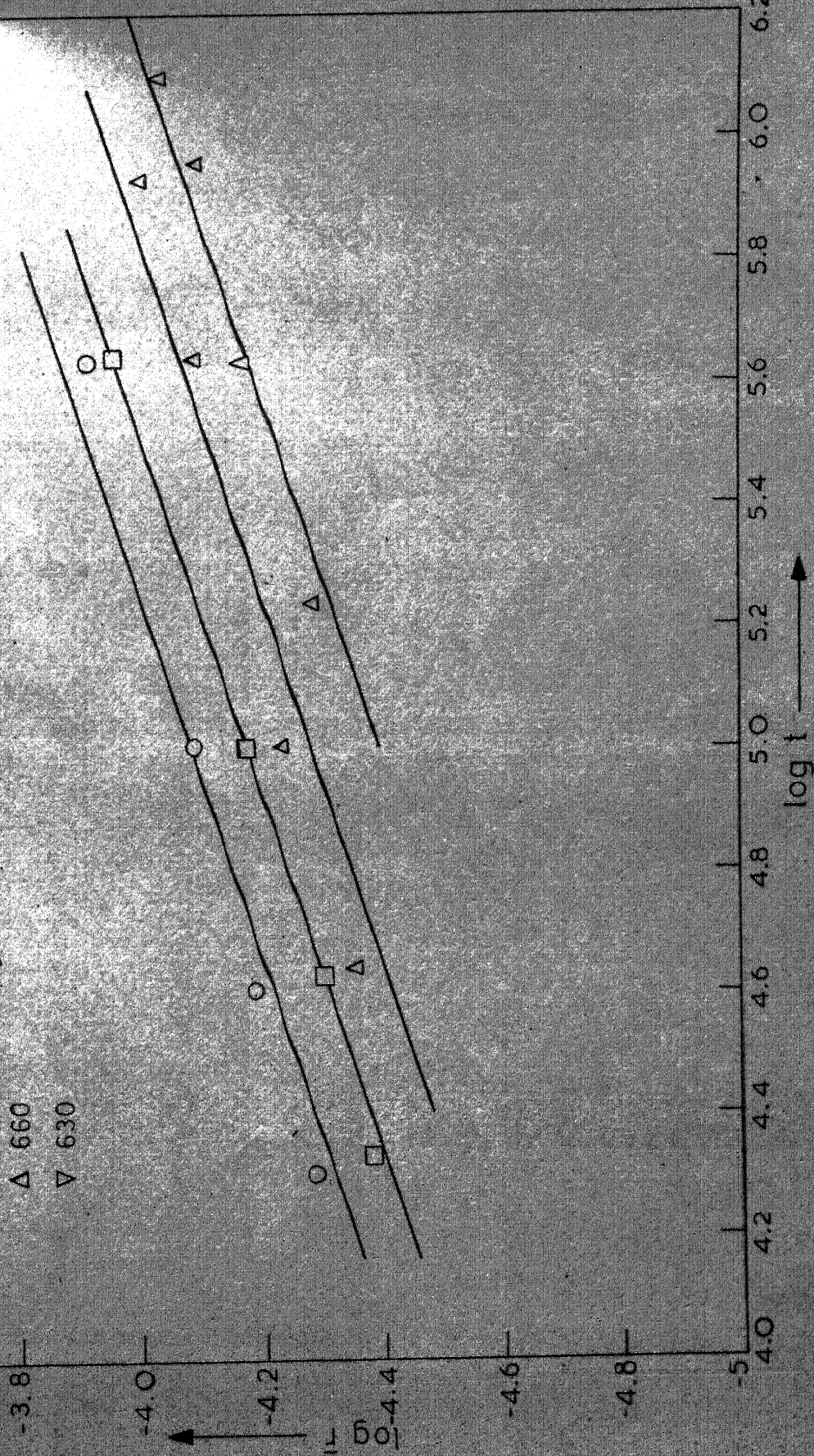
Fig. 16 Plot of log $\bar{r}$ vs. log t for Fe-0·74% C-0·37% Si sample tempered at various temperatures.
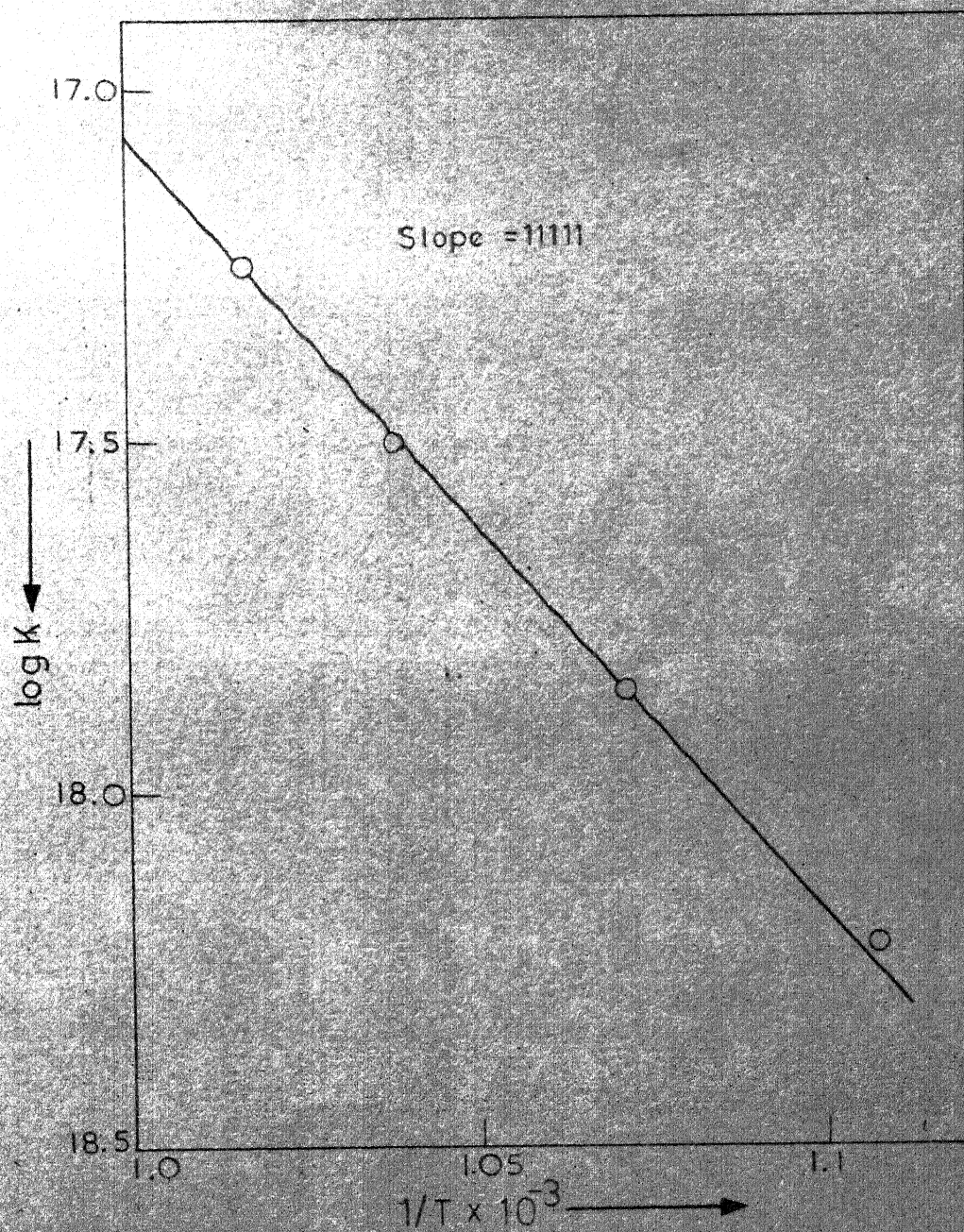
Fig.17 Plot of log K vs. 1/T
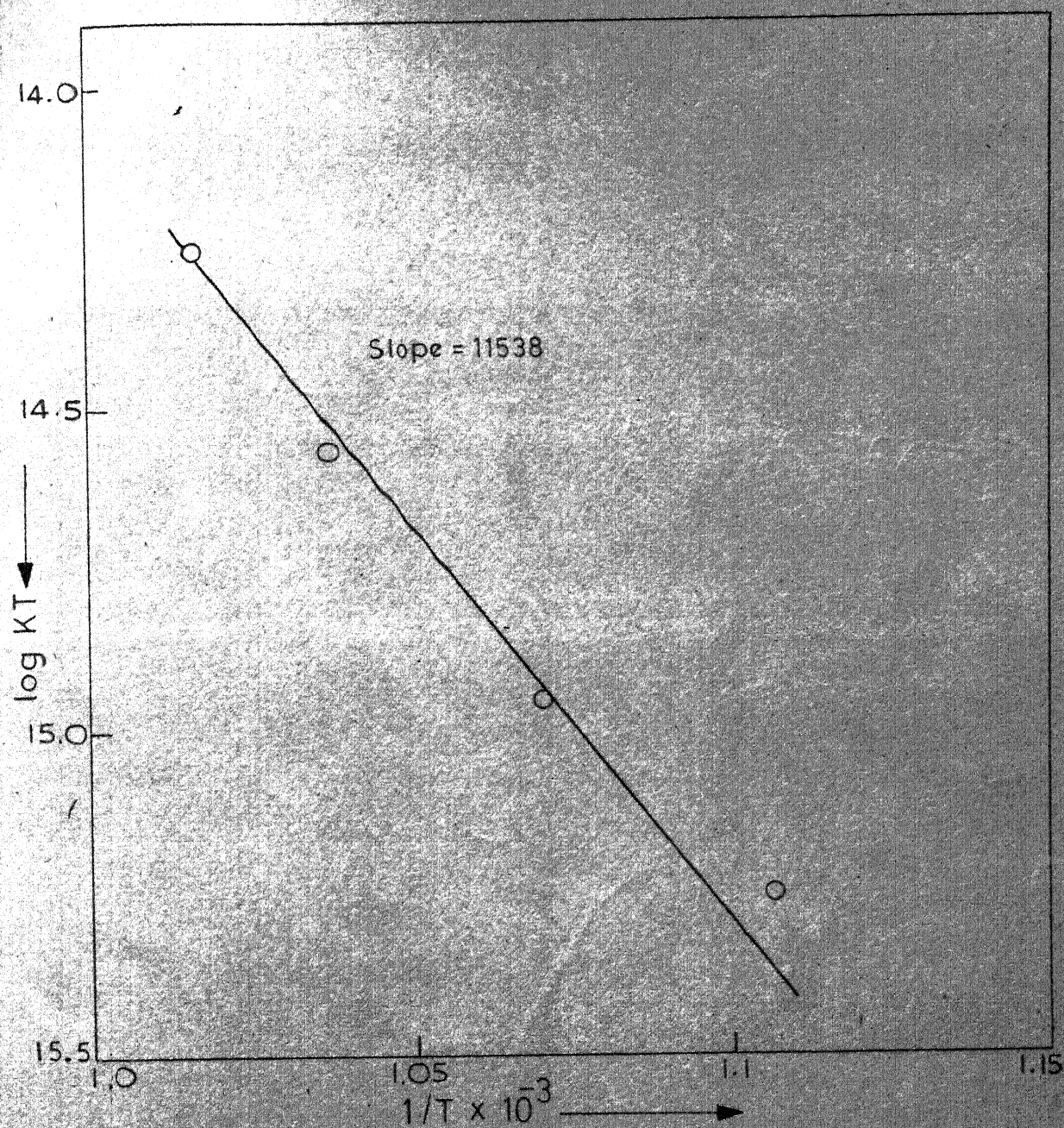
Fig. 18 Plot of log KT vs. 1/T
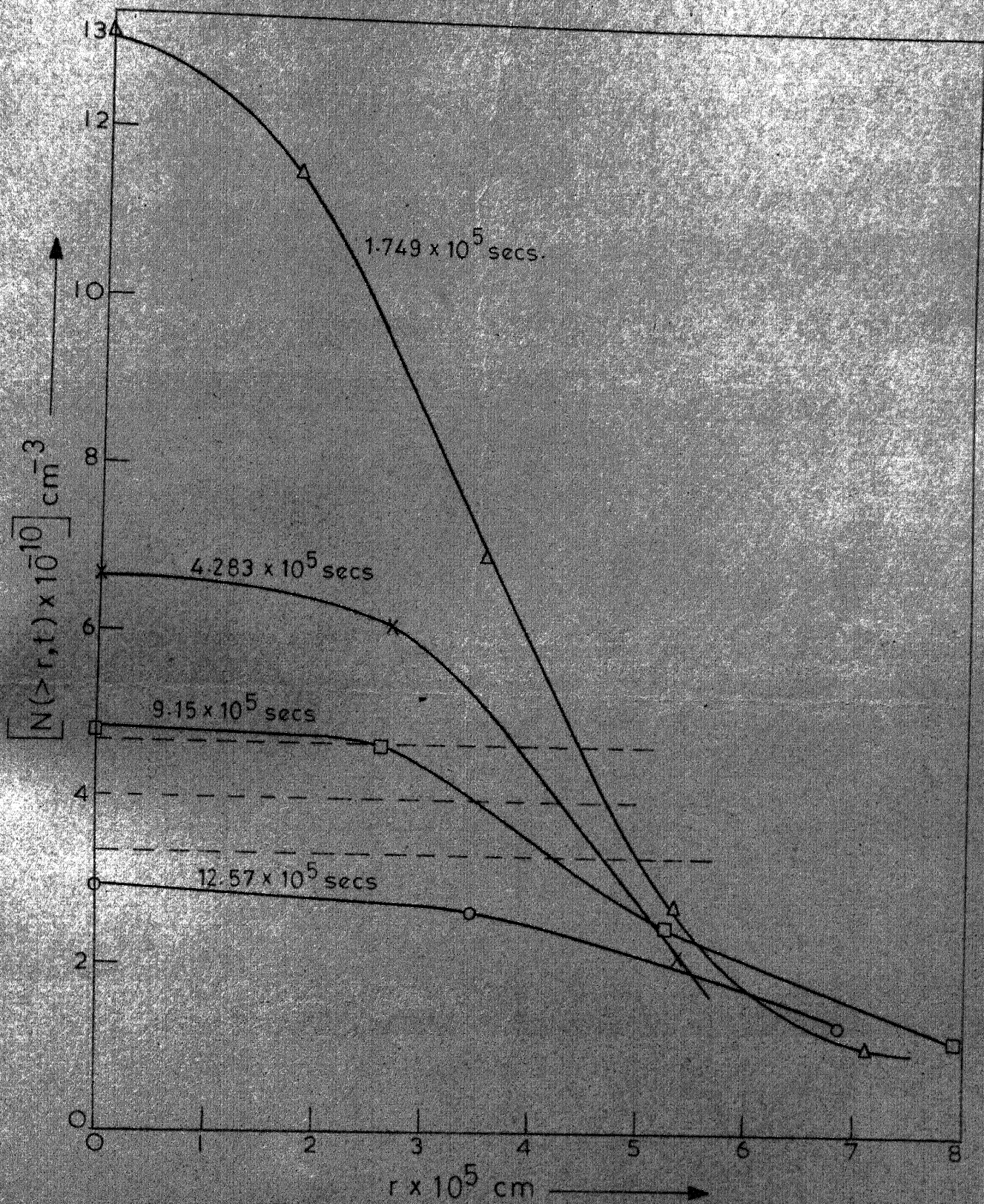
Fig. 19 Plot of $[N(>r,t)]$ vs. r for Fe-C-Si sample tempered at 630°C.

The vertical axis is labeled $[N(>r,t)] \times 10^{-10}$ cm^{-3} with values 2, 4, 6, 8, 10, 12, 13 marked.

The horizontal axis is labeled $r \times 10^5$ cm with values 1 through 8 marked.

Curves labeled:
1.749 $\times 10^5$ secs.
4.283 $\times 10^5$ secs
9.15 $\times 10^5$ secs
12.57 $\times 10^5$ secs
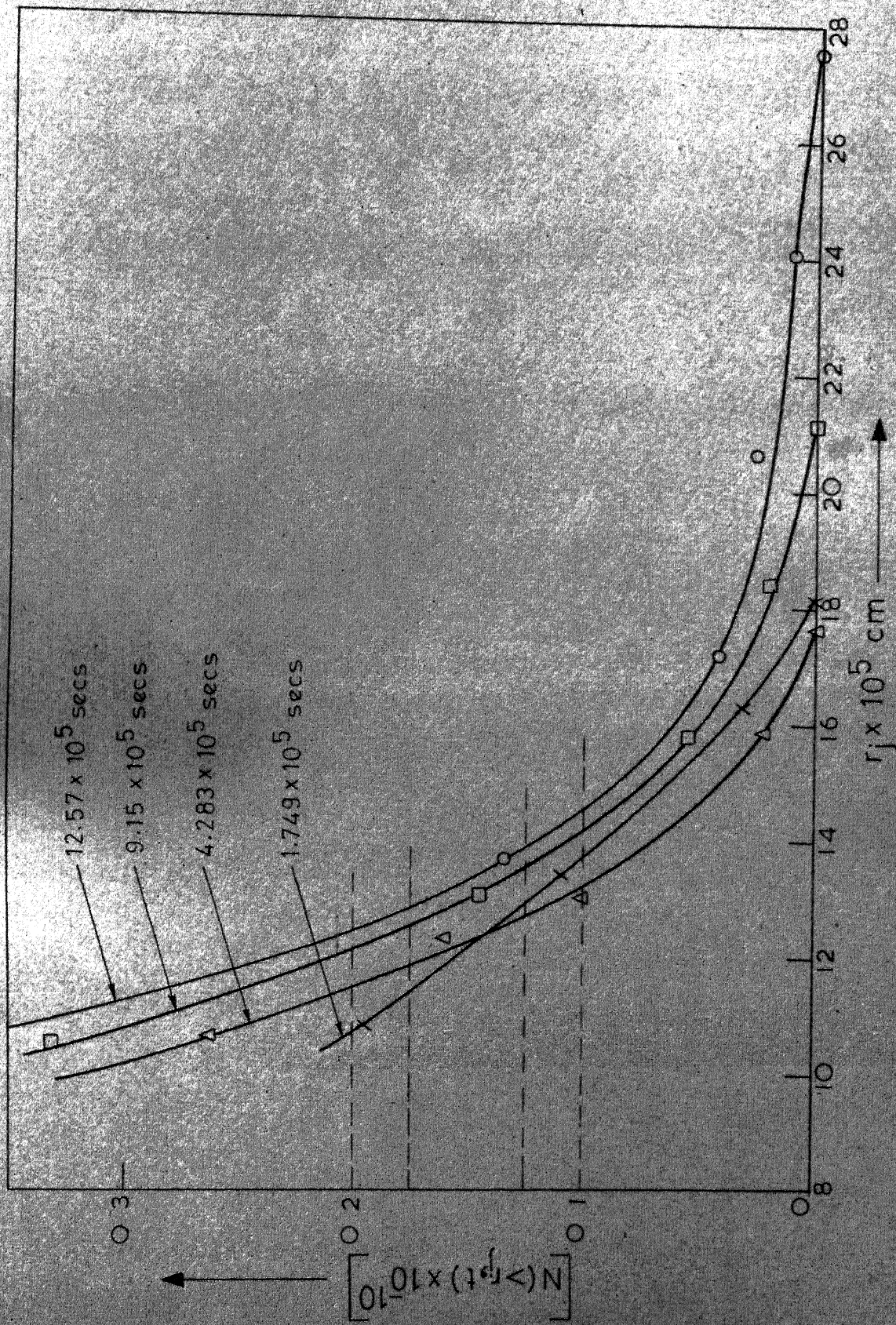
Fig. 20. Plot of $N(>r_j,t)$ vs.r for Fe-C-Si alloy at 630°C.
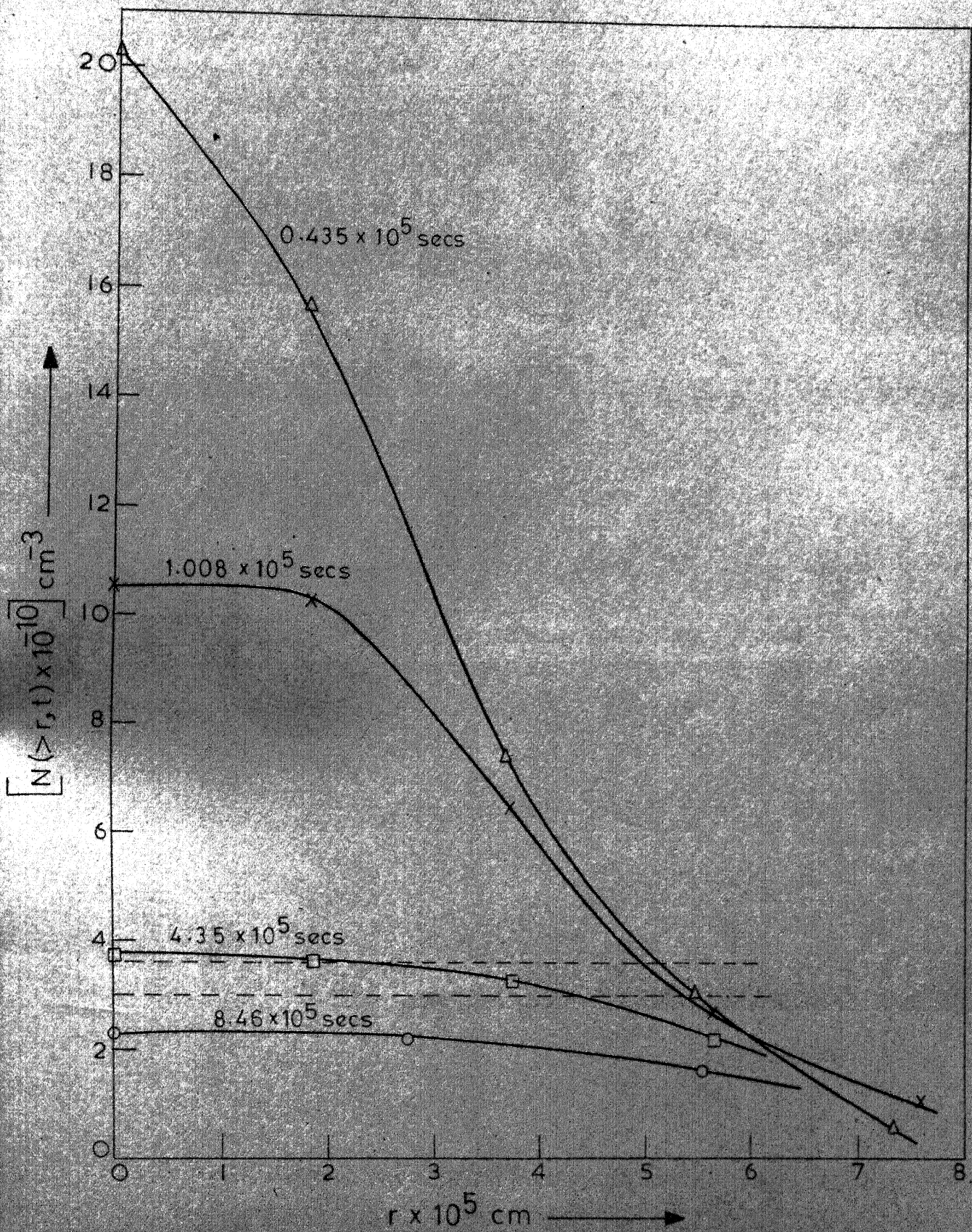
Fig.21 Plot of N(>r,t) vs r for Fe-C-Si alloy tempered at 660°C.

Fig. 22 Plot of $[N(>r,t)]$ vs. r for Fe–C–Si alloy tempered at 660°C

Axis labels and curve annotations:

x-axis: $r \times 10^5$ cm

y-axis: $[N(>r,t)] \times 10^{-10}$

Curve labels: 8.46×10^5 secs, 4.35×10^5 secs, 1.008×10^5 secs, 0.435×10^5 secs
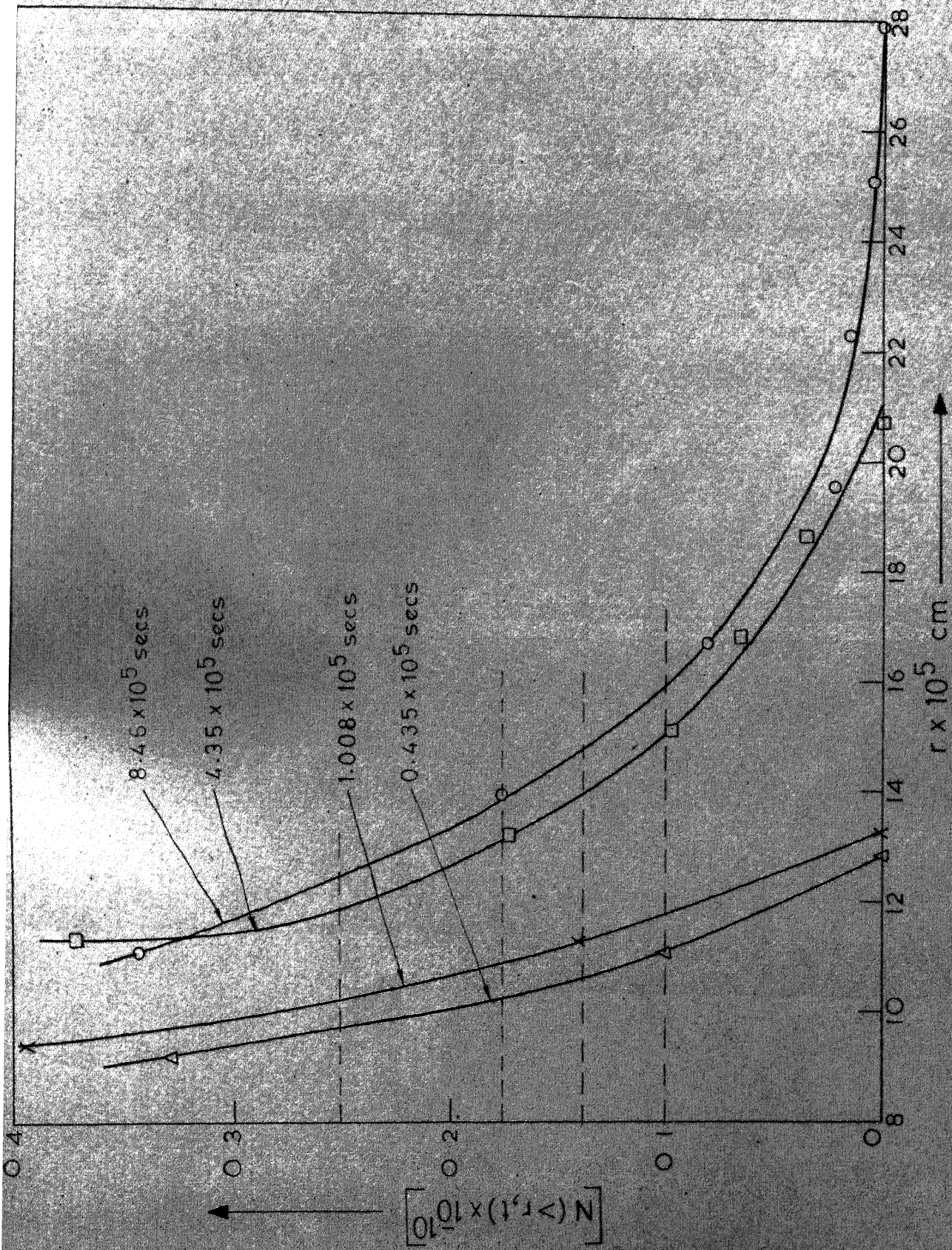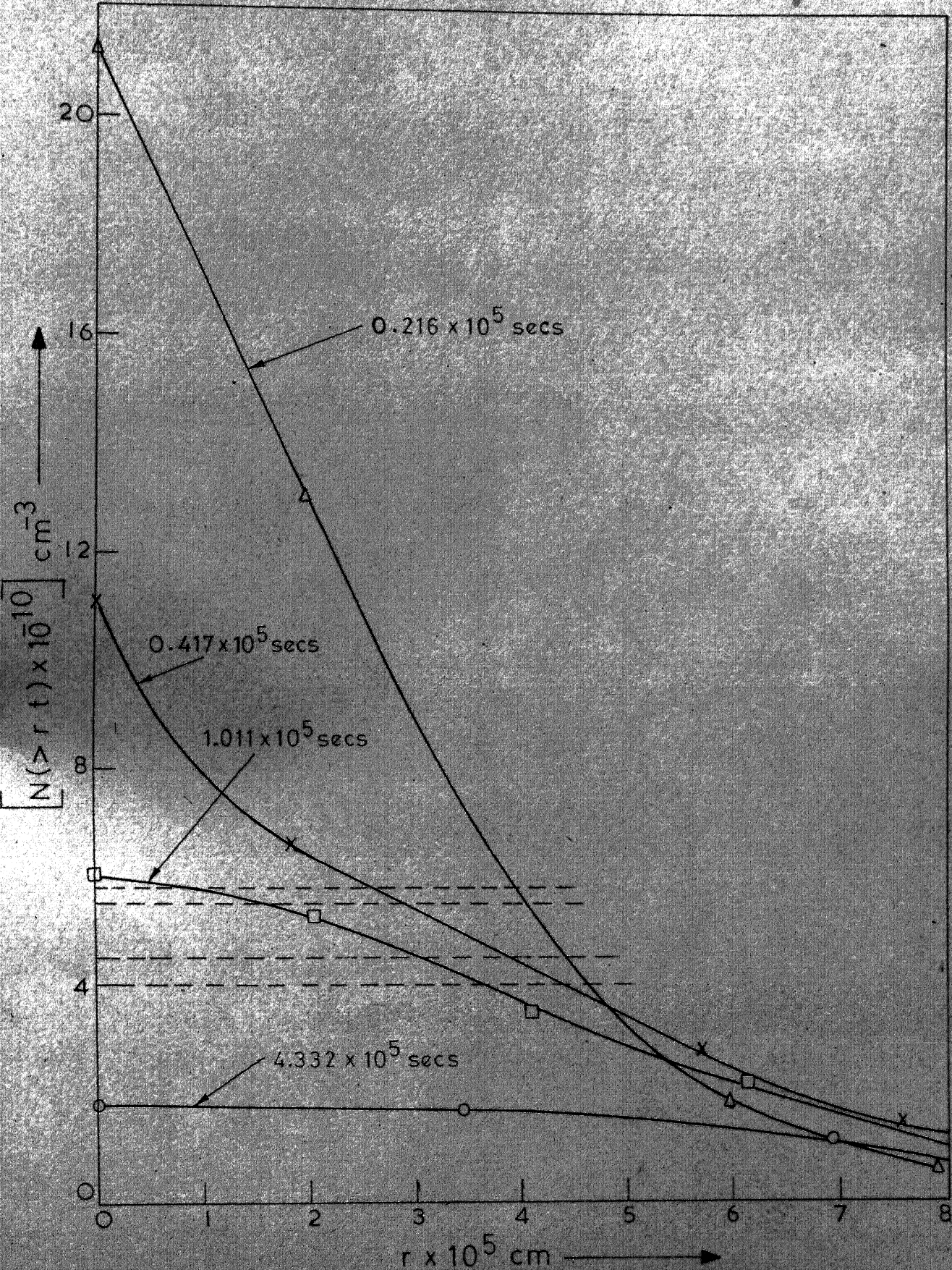
Fig.23 Plot of N(>r,t) vs. r for the Fe-C-Si alloy tempered at 690°C.
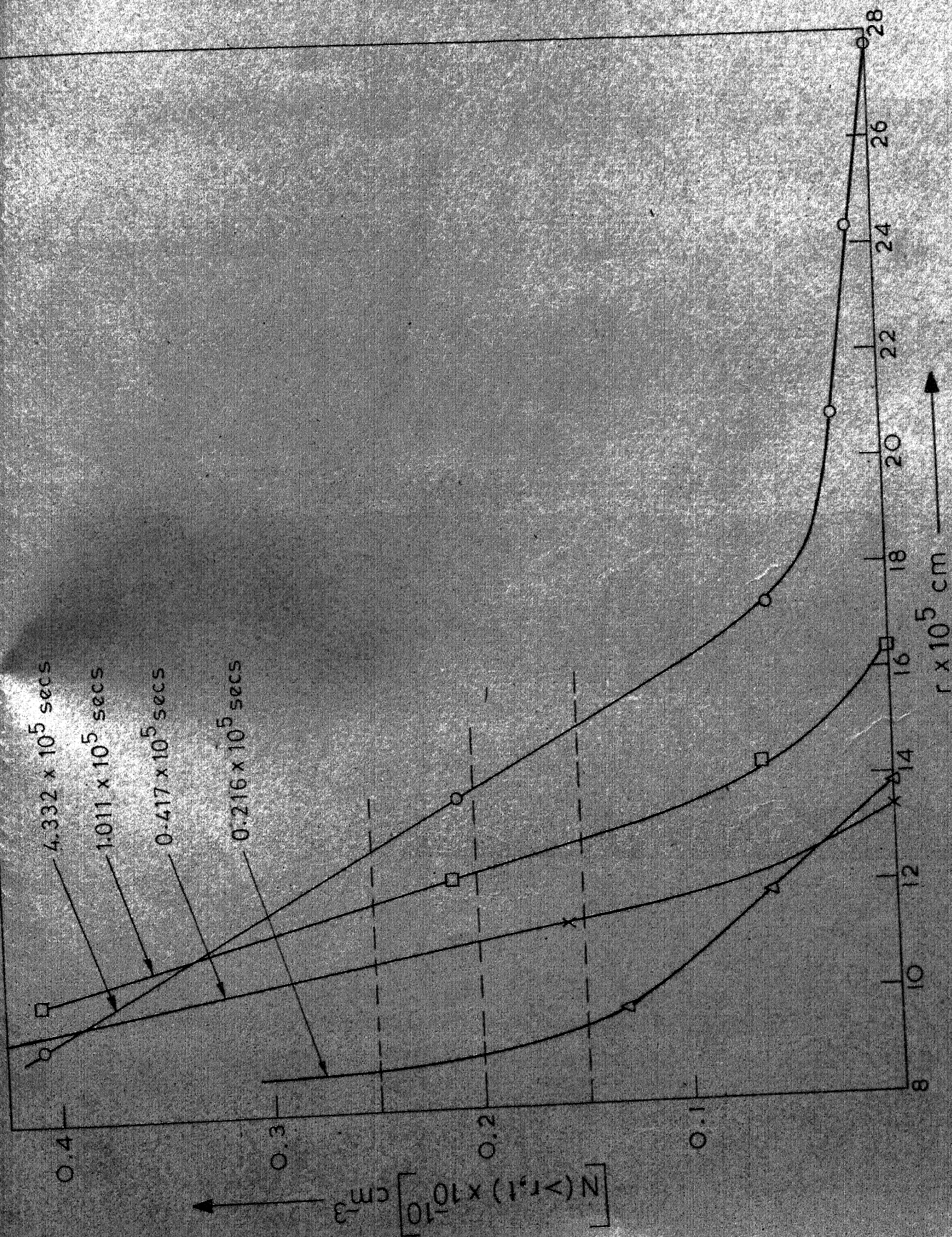
Fig.24 Plot of $N(>r,t)$ vs. r for Fe-C-Si alloy tempered at 690°C.
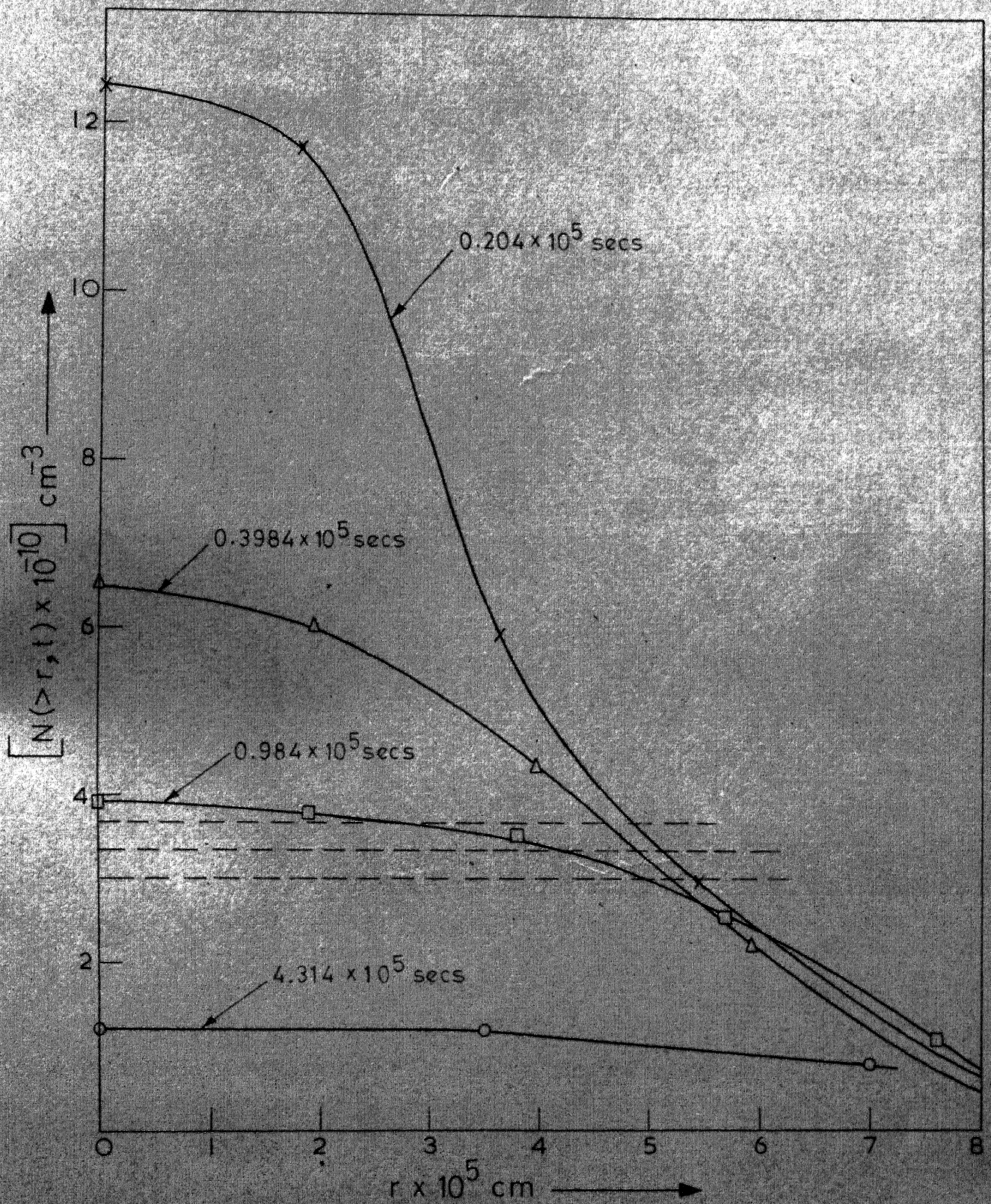
Fig.25 Plot of N(>r,t) vs r for Fe-C-Si alloy tempered at 710°C
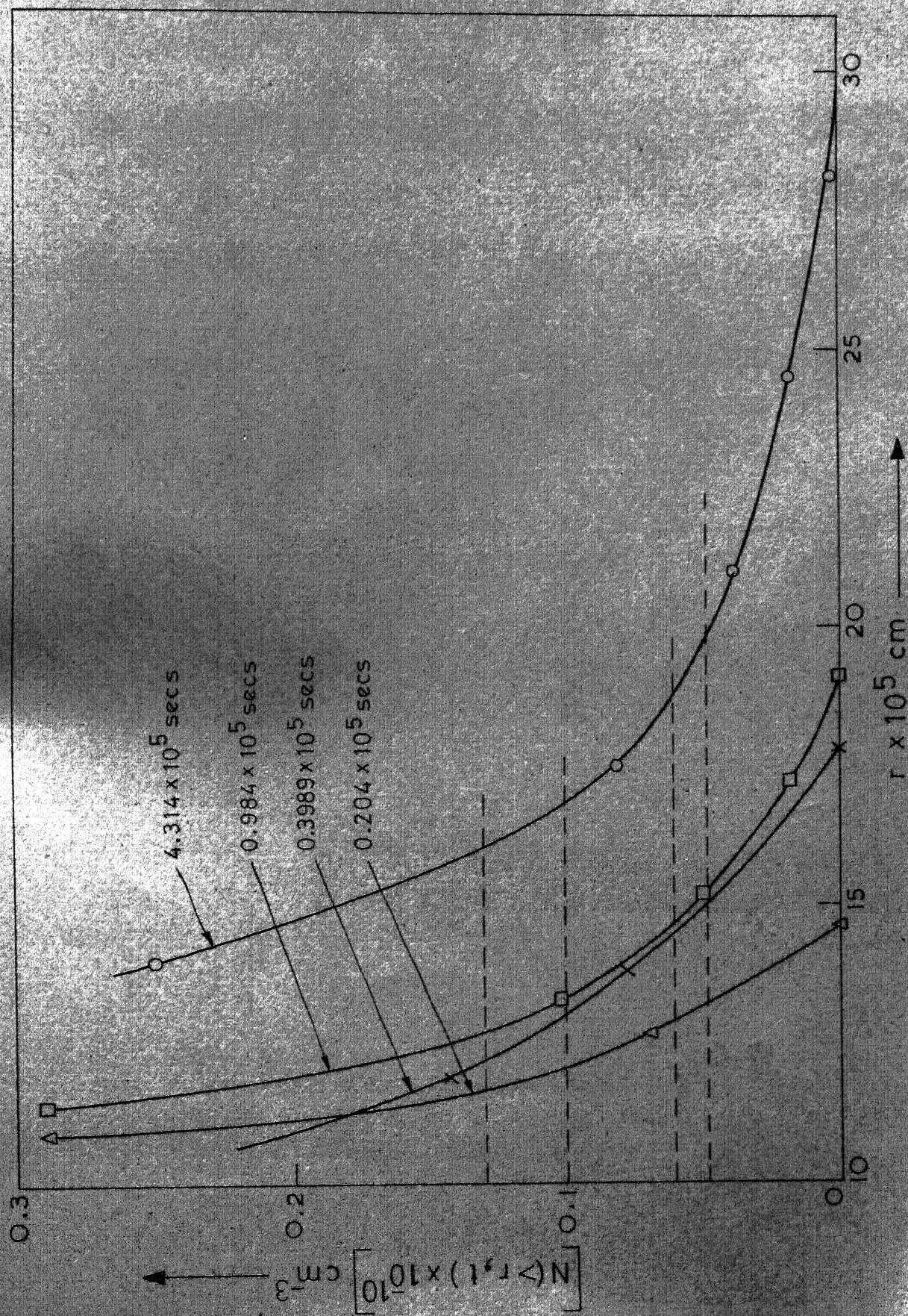
Fig. 26 Plot of N(>r, t) vs. r for the Fe-C-Si sample tempered at 710°C.
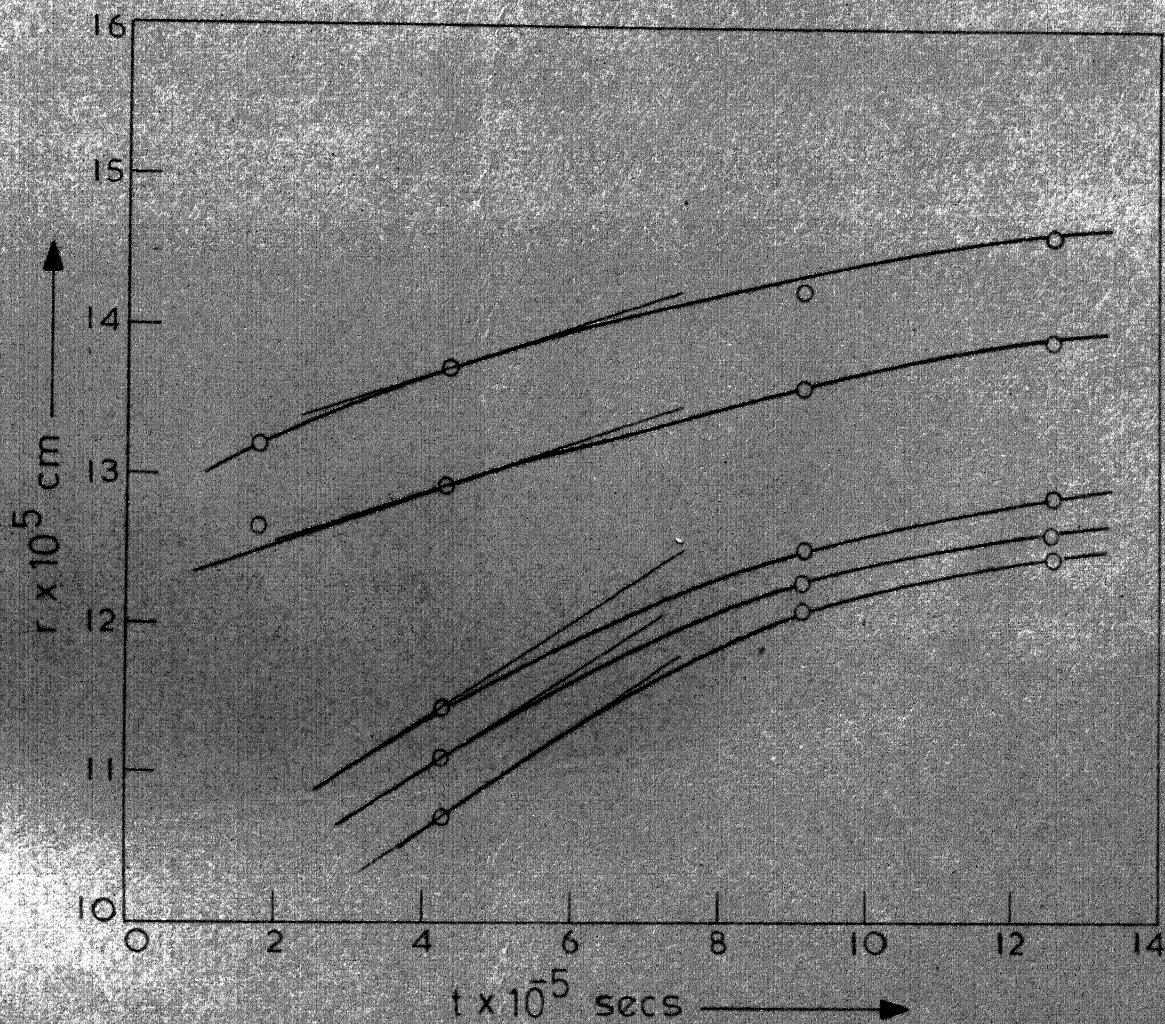
Fig. 27 Plot of r vs. t for the sample tempered at 630° C.

95

Fig.29 Plot of r vs. t for the sample tempered at 660°C.
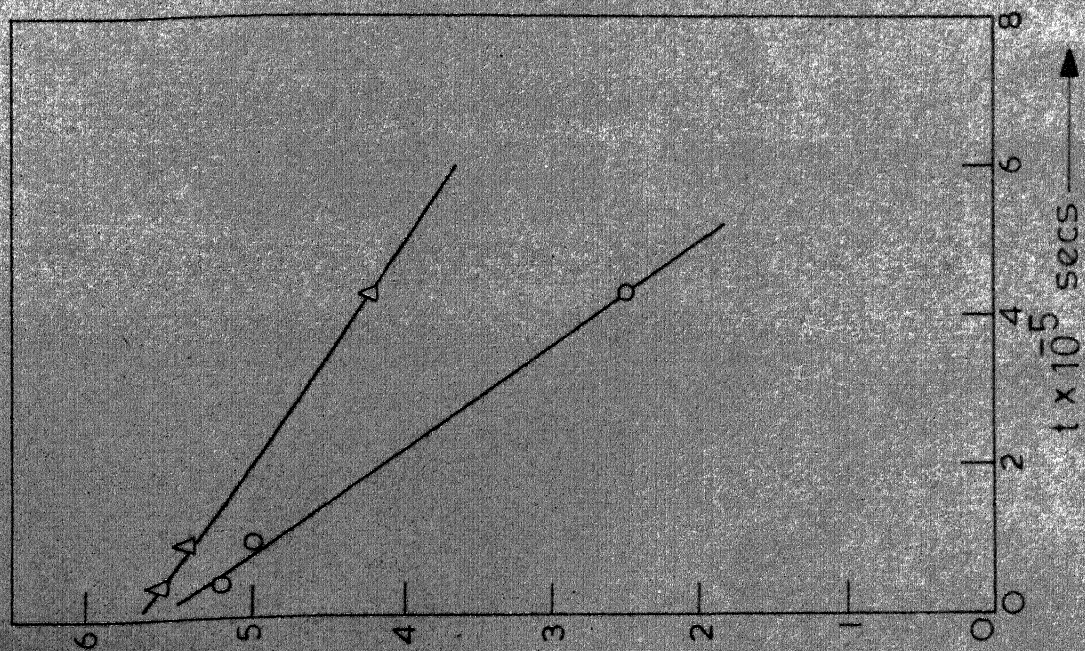
Fig.28 Plot of r vs. t for the sample tempered at 630°C.

t x 10⁵ secs

r x 10⁵ cm
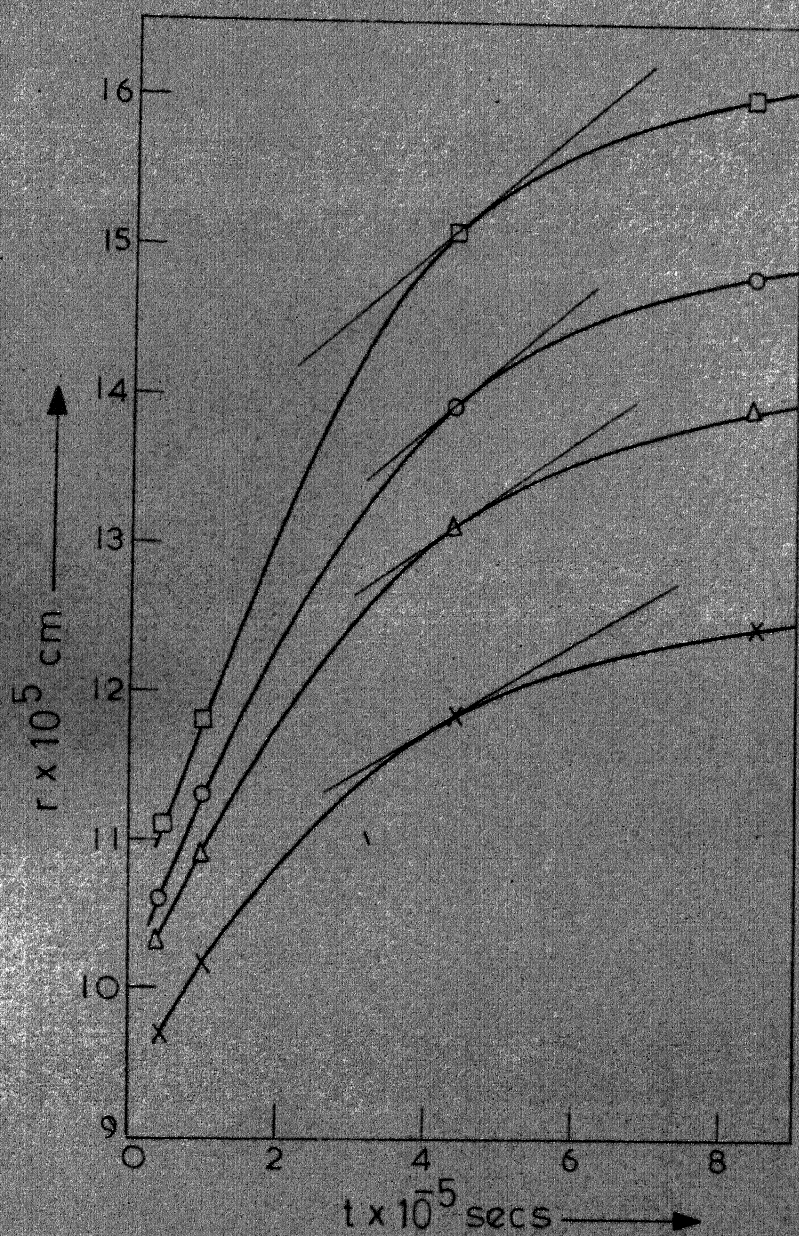
Fig.30 Plot of r vs. t for the sample
tempered at 660°C.

Fig.32 Plot of r vs. t for the sample tempered at 710°C.
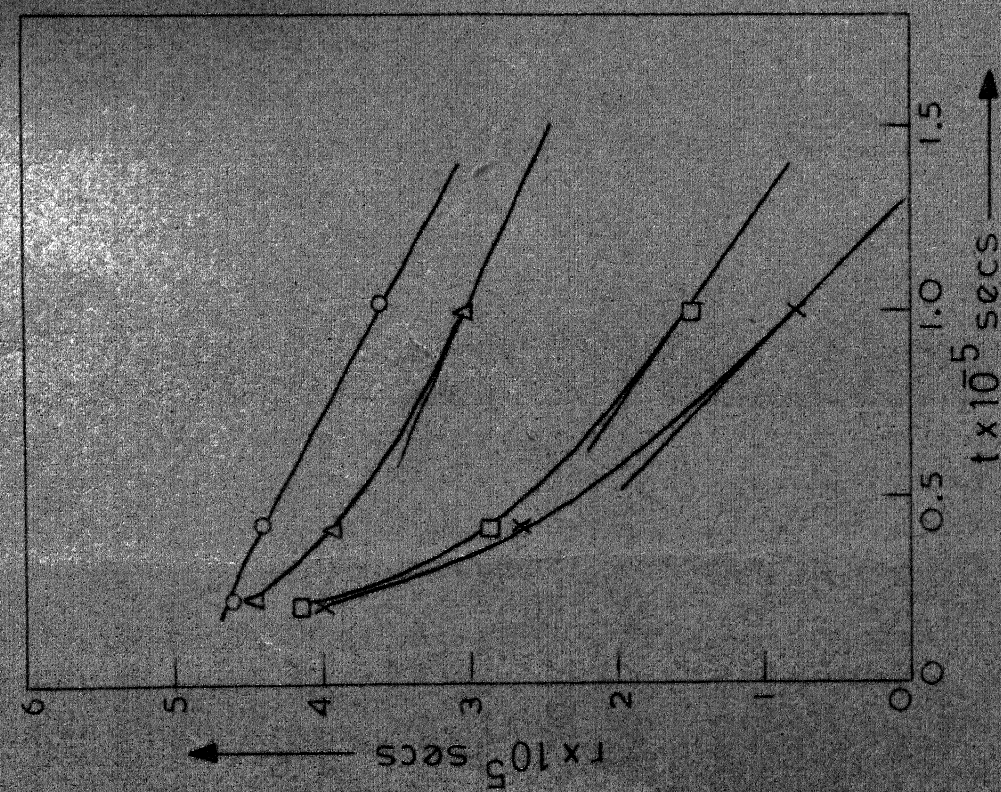
Fig.31 Plot of r vs. t for the sample tempered at 690°C.
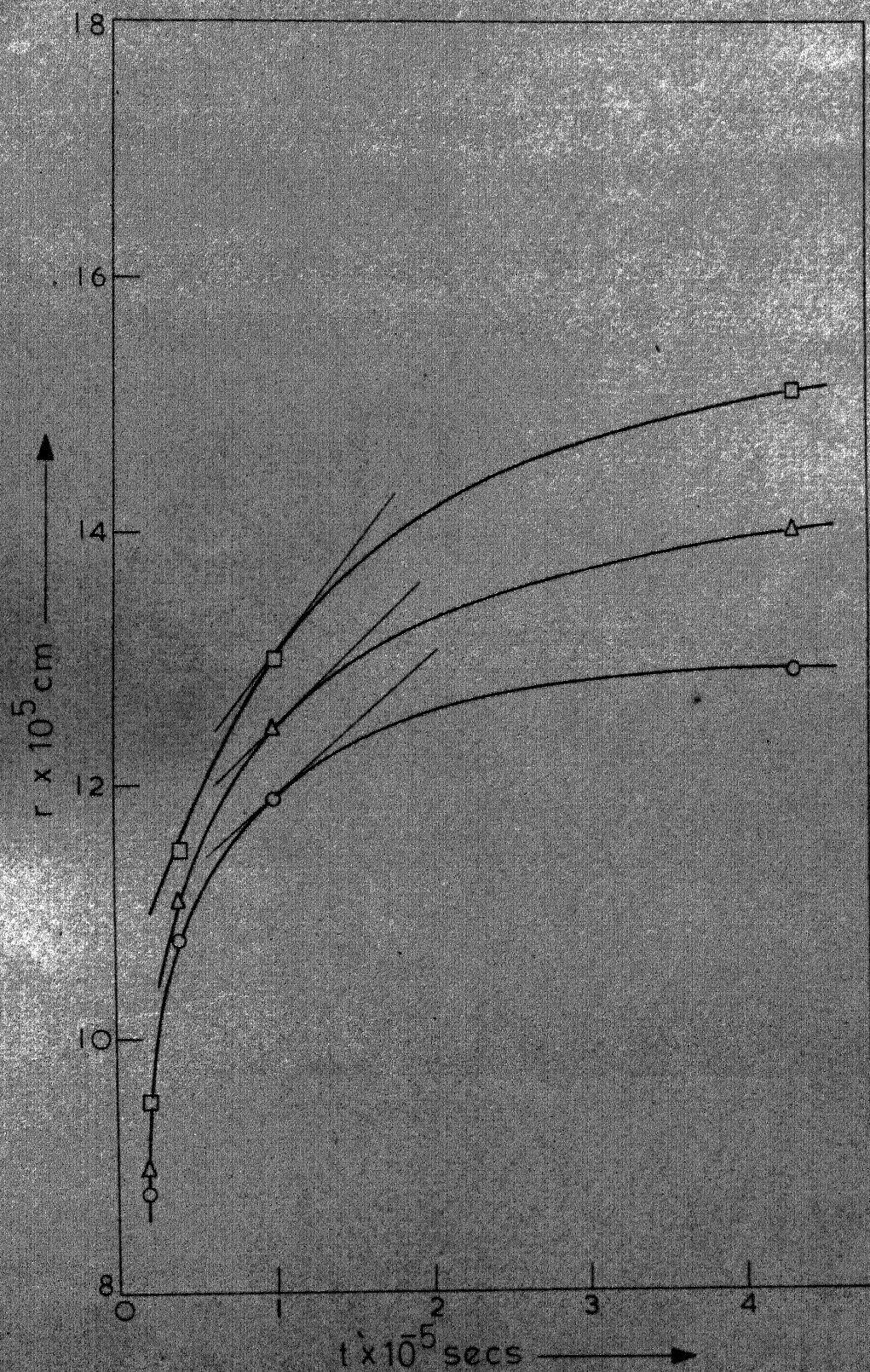
Fig. 33 Plot of r vs. t for the sample tempered at 690°C.
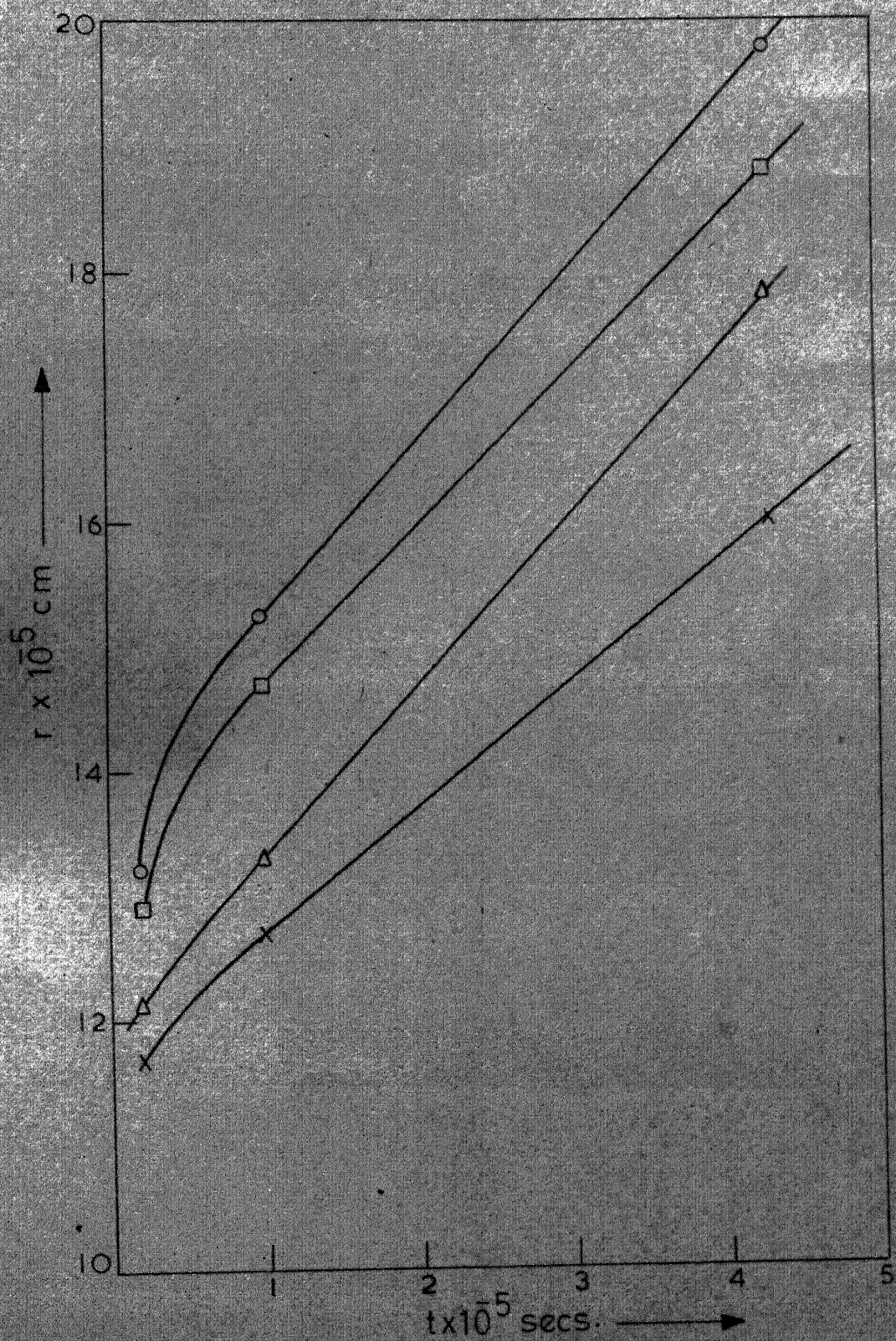
Fig. 34 Plot of r vs. t for the sample tempered at 710°C.
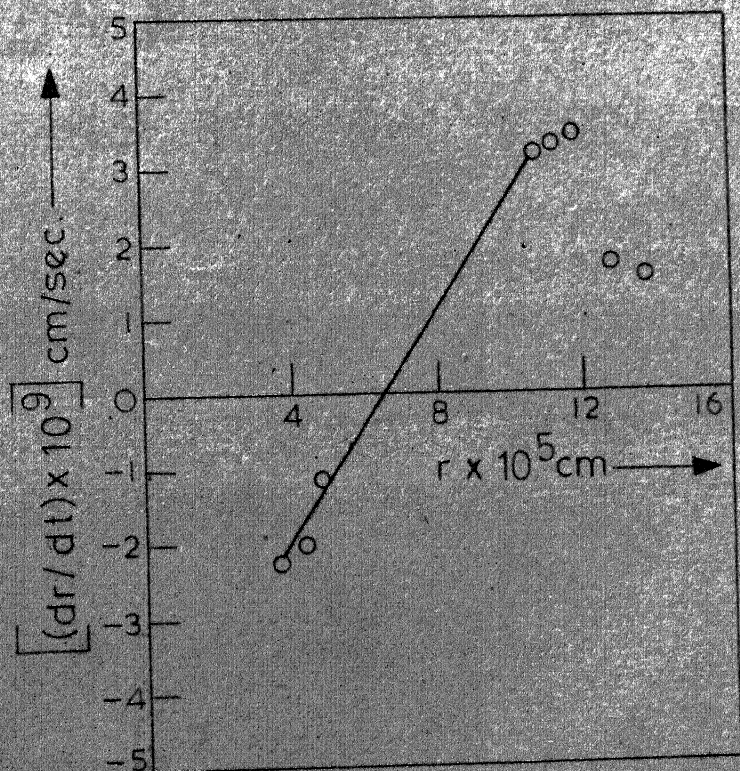
Fig. 35 Plot of dr/dt vs. r for the sample tempered at 630°C.
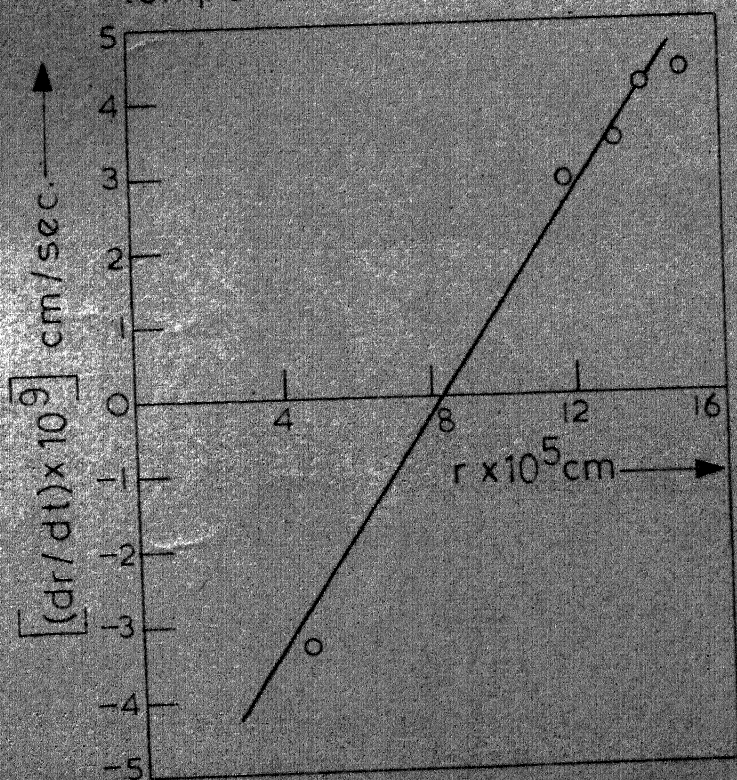
Fig. 36 Plot of dr/dt vs. r for the sample tempered at 660°C.
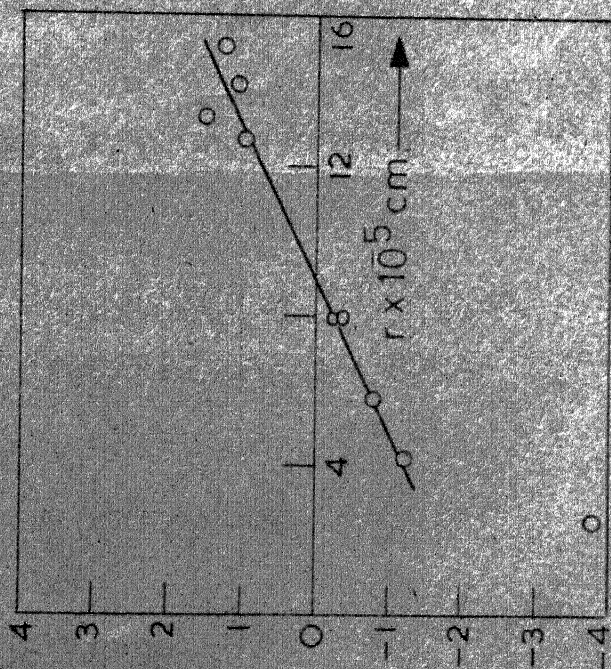
Fig.38 Plot of dr/dt vs r for the sample tempered at 710°C.
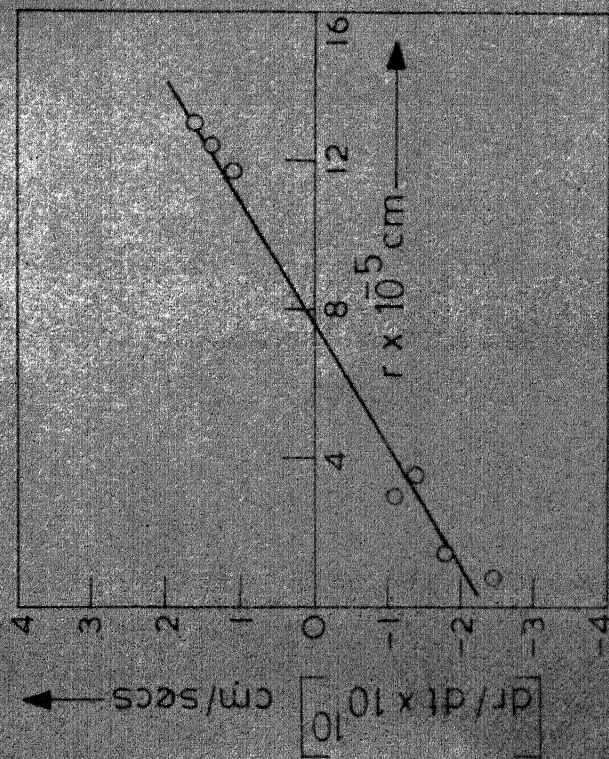
Fig 37 Plot of dr/dt vs r for the sample tempered at 690°C.

Fig. 40 Plot of $r\frac{dr}{dt}$ vs. $\frac{1}{r}$

Fig. 39 Plot of $r\frac{dr}{dt}$ vs. $\frac{1}{r}$

temp=710°C

temp = 690°C

$\frac{1}{r} \times 10^5 \ cm^{-1} \longrightarrow$

$\frac{1}{r} \times 10^5 \ cm^{-1} \longrightarrow$

30

20

10

0.05

0.1

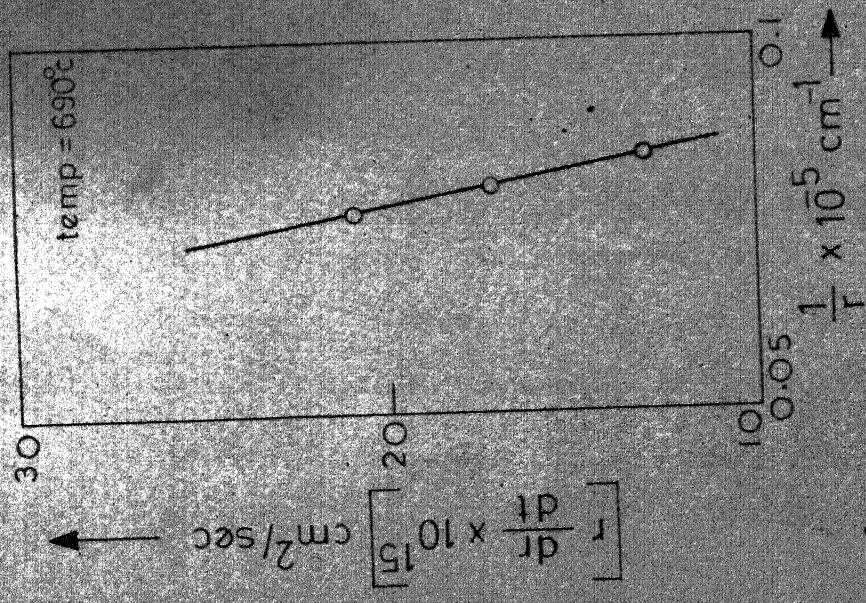$\left[r \frac{dr}{dt} \times 10^{15} \right] cm^2/sec \longleftarrow$
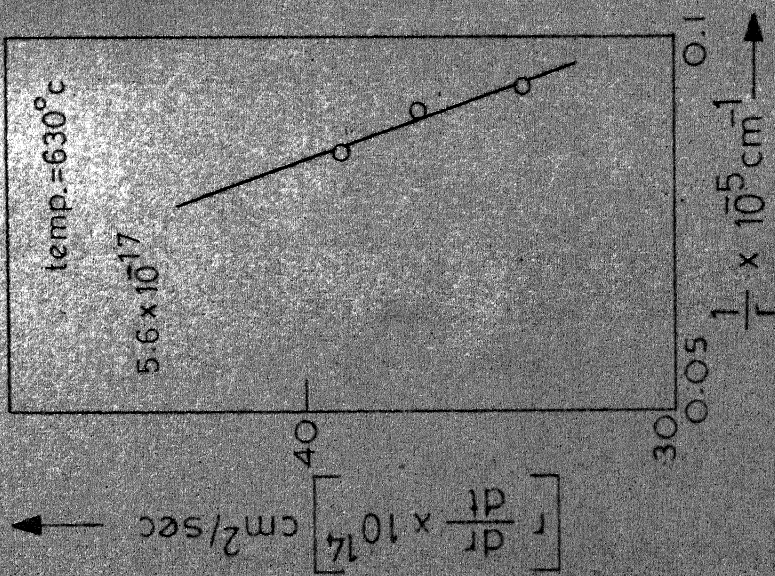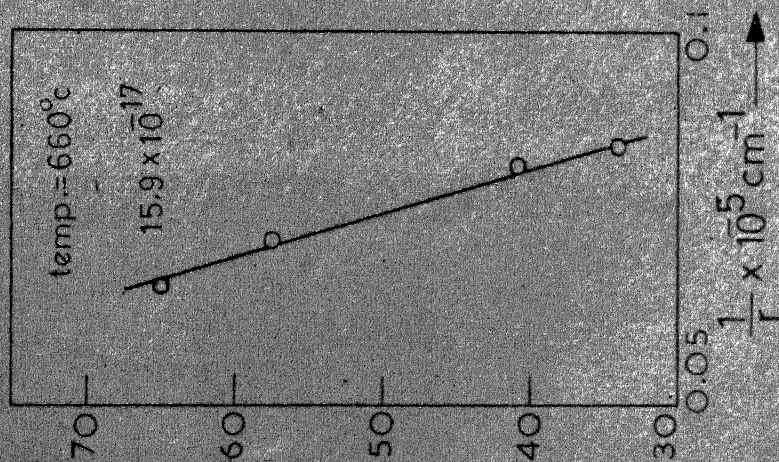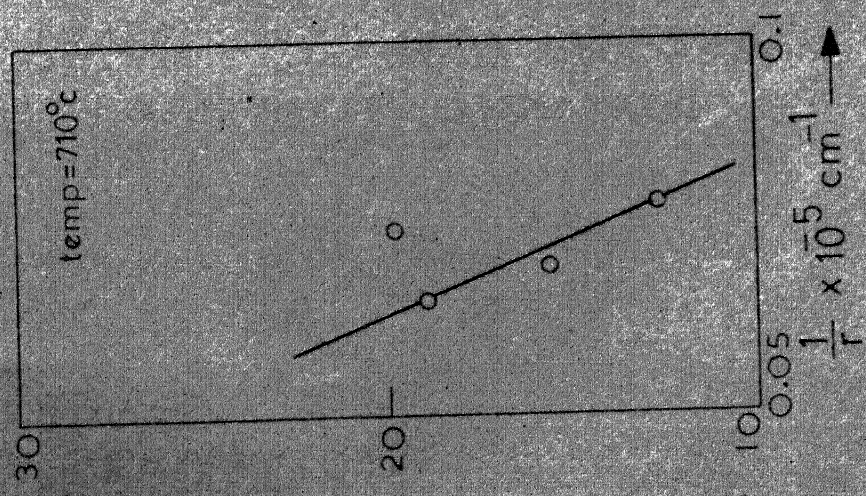
Fig.41 Plot of $r \frac{dr}{dt}$ vs. $\frac{1}{r}$

Fig.42 Plot of $r \frac{dr}{dt}$ vs. $\frac{1}{r}$

24. A.J. Ardell, 1970, Met. Trans., 1, p 525.

25. E. Hornbogen and M. Roth, 1967, Z. Metallkunde, 58, p 842.

26. A.J. Ardell and P.K. Rastogi, 1971, Acta Met., 19, p 329.

27. Noboru Komatsu and N.J. Grant, 1964, Trans., A.I.M.E., 230, p 1090.

28. J.D. Boyd and R.B. Nicholson, 1971, Acta Met., 19, p 1370.

29. R.A. Oriani and G.R. Speich, 1965, Trans. A.I.M.E., 233, p 623.

30. A.F. Smith, 1967, Acta. Met., 15, p 1867.

31. J.A. Dromsky, F.V. Lavel and G.S. Anrel, 1962, Trans. A.I.M.E., 224, p 236.

32. M.H. Lewis, R.H. Seebohm and J.W. Martin, 1962, Powder Metallurgy, 10, p 87.

33. B.H. Bower and J. Whiteman, 1968, Mechanism of phase transformation in crystalline solids (Manchester conference), p 119.

34. A.F. Smith, 1965, J. Less Common Metals, 19, p 233.

35. A. Gatti, 1962, Powder Metallurgy, 10, p 77.

36. O. Bannby, H. Modin and S. Modin, 1962, Jernkontorets, Ann., 146, p 744.

37. G.W. Greenwood, 1968, Mechanism of phase transformation, (Manchester conference), p 103.

38. R.V. Day and J. Barford, 1968, Nature, 217, p 1145.

39. K.M. Vedula and R.W. Heckel, 1970, Met. Trans., 1, p 9.

40. R.W. Heckel, 1965, Trans. A.I.M.E., 233, p 1994.

41. R.W. Heckel and R.L. Degregoria, 1965, Trans. A.I.M.E., 233, p 2001.

42. G.P. Airey, T.A. Hughs and R.F. Mehl, 1968, Trans. Met. Soc. A.I.M.E., 242, p 1853.

43. F.V. Nolfi, Jr. Paul G. Shewmon and James S. Foster, 1970, Met. Trans., 1, p 789.

44. J.B. Harris, J.A. Whiteman and A.G. Quarell, 1965, Trans. A.I.M.E., 233, p 168.

45. R.G. Speich, 1969, Met. Trans. A.I.M.E., 245, p 2553.

46. A.M. Gokhale, 1972, M. Tech Thesis, Met. Engg. Dept. IIT Kanpur.

47. K.P.S. Verma, 1972, M. Tech Thesis, Met. Engg. Dept. IIT Kanpur.

48. P.S. Dirn-feld, 1972, Script. Met., 6, p 985.

49. T.A. Mukherjee, W.E. Stumpf, C.M. Sellers and J. Megtegart, 1969, J.I.S.I., 207, p 621.

50. S.A. Saltykov, 1958, Steriometric Metallography

51. S.A. Saltykov, Steriology, Ed. by H. Ellias, Proc. second Int. Cong. for Steriology.

52. A.G. Spektor, 1950, Zavod Lab., 16, p 173.

53. S.D. Wicksell, 1926, Biometrics, 18, p 151.

54. R.T. Dehoff, 1962, Trans. A.I.M.E., 224, p 474.

55. M. Paulus, 1962, Metaux Corrosion Industries, 37, p 448.

56. J.W. Cahn and R.L. Fullman, 1956, Trans. A.I.M.E., 206, p 610.

57. R.G. Faulkner, 1971, Script. Met., Vol. 5, p 717.

58. B. Parny and R.E. Smallman, 1972, Script. Met., Vol. 6, p 149.

59. R.T. Dehoff and F.N. Rhines, 1961, Quantitative Microscopy, McGraw Hill, p 167.

60. E. Underwood, 1970, 'Quantitative Steriology', Addison and Wesley, p 122.

61. R.W. Gurry and L.S. Darken, 1953, Physical Chemistry of Metals, McGraw Hill, p 399.

62. R.E. Reedhill, 'Physical Metallurgy Principles', De Van Nostrand, p 444.

63. P.K. Footner and C.B. Alcock, 1972, Met. Trans., 13, p 2633.

64. E. Scheil and M. Werat, 1956, Metall Kunde, p 340.

65. R.T. Dehoff, 1971, Met. Trans., 2, p 521.

66. F.S. Buffington, K. Hirano and M. Cohen, 1961, Acta. Met., 9, p 434.

67. R.A. Oriani, 1964, Acta. Met., 12, p 1399.